Final report

Effect of pressure maintenance by fluid injection on seismic risk

Simulation of reservoir depletion and injection induced seismic events using hydro-mechanical coupled Particle Flow Code 2D modelling on Groningen reservoir geological fault model, including external review

DynaFrax UG (haftungsbeschränkt)

Fugro

30 September 2022

Contents

Executive summary

This numerical modelling study aimed at investigating and quantify the effect of fluid injection on the seismicity in the depleted Groningen gas reservoir. The objective is to assess whether the fluid injection has a positive effect in mitigating the seismic events that have occurred due to pressure decline and to give recommendations for pressure maintenance.

Previous studies by TNO and NAM concluded that injection can maintain reservoir pressure in depleting reservoirs, such as the Groningen gas field, and the fluid injection is technically feasible. However, the overall net effect of large-scale fluid injection on the seismic risk profile was not quantified and the seismic risk associated with different fluid injection scenarios was only studied in a qualitative way. Therefore, it is unknown whether fluid injection can be used to minimize the risk of induced seismicity in depleting gas fields.

The modelling code used in this study is PFC2D (Particle Flow Code 2D), a commercial code of ITASCA, with in-house developed hydro-mechanical coupled and seismicity computing models. We modelled the entire field of Groningen gas reservoir with 40 km by 50 km in size with the complex reservoir faults. The model is in 2D which we considered valid due to its long horizontal extent compared to the net thickness of the reservoir. The model contains highly complex geometry of the reservoir fault using the smooth joint contact model in PFC2D. Model parameters used were taken from various literatures related to the Groningen reservoir and seismicity studies.

First, we simulated the past 60 years of depletion induced seismicity occurred in Groningen gas field. Second, we simulated future seismicity, assuming that the gas production stopped in year 2020 (or in year 2010). Third, we simulated future seismicity after year 2020, assuming that injection took place in east central region with CO_2 and N_2. Fourth, we simulated future seismicity after year 2020, when N_2 injection took place in east central region while all other clusters were shut-in or were in continued production.

Following results were obtained.

The simulated evolution of reservoir pressure for the past 60 years of depletion did not match well with the field observed pressure distribution. However, in terms of seismicity, comparison between the simulated and the observed (KNMI seismicity) matched fairly well, for the time period between 1990 and 2020 for the seismic events with ML larger than 2.0

Two hypothetical shut-in scenarios were tested assuming that gas production ended in year 2020 and in year 2010, to see how the reservoir pressure redistributes over time and if additional seismicity would occur. The results confirmed that the seismicity rate decreased

significantly during the shut-in period, implying that the very first measure to take to lower the level of seismic hazard is to stop gas production and to let the reservoir pressure go into equilibrium.

We tested two hypothetical injection scenarios for two different gases, CO2 and N2, into a depleted reservoir with partly saturated with CH4 and water. We used TOUGH3 code to simulate mixture of different gases that are in two phases. With same mass amount of gas injection, the results indicated that the reservoir pressure increase is limited when CO2 is injected, as CO2 dissolves more into the water that is remaining in the reservoir. The results indicated that the reservoir pressure increases as intended for pressure maintenance purpose when N2 is injected, as N2 does not dissolve in the remaining water. The key results in Section 7 is the pressure increase over time monitored at the center of the reservoir, which we formulated mathematically and programmed for inputs in the PFC2D modelling.

We tested two hypothetical injection scenarios for two different gases, CO2 and N2, injected at central cluster, while all other clusters were shut-in. The results demonstrated that, in case of CO2 injection the pressure rise is negligible, and the injection did not generate overpressure zone at east central region. In case of N2 injection, the pressure rise is relatively fast, and resulted in overpressure zone at east central region, and triggered seismic events at Loppersum region. This implies that overpressure zone formed by N2 injection could trigger unwanted seismic events at regions of stress criticality, e.g. Loppersum region. This finding also implies that N2 injection seems to be an effective measure to increase the reservoir pressure, but one has to be careful in choosing the location and the rate of injection, as not to trigger seismic events at far-field due to poro-elastic stress triggering mechanism.

We tested four hypothetical injection (what-if) injection scenarios, combining shut-in and injection (what-if injection scenarios 1 and 3) and combining shut-in, depletion and injection (what-if injection scenarios 2 and 4). In all tested what-if injection scenarios, the largest magnitude seismic event occurred at Loppersum region. This implies that the fault stability at Loppersum region is very sensitive and injection at east central clusters easily triggers seismicity of the faults at Loppersum region. This implies that production/injection at or near Loppersum region should be avoided as they may easily trigger seismicity at Loppersum region. Continuing depletion at all well clusters except for east central cluster while applying injection at the east central cluster resulted in inhomogeneous pressure distribution (what-if injection scenarios 2 and 4). The overpressure at east central cluster region resulted in triggering of seismic events at Loppersum region. When compared with shut-in scenarios, the comparison demonstrates that homogeneously distributed reservoir pressure did not generate seismic events at Loppersum. This supports the hypothesis that increased homogeneity in pressure distribution throughout the reservoir may help to mitigate seismic hazard through

decreasing seismicity rates, and emphasizes that the goal of an injection scenario should be to reduce spatially inhomogeneous pressure distribution. The modelling results also indicate that combining injection in depleting reservoir may have negative effect on mitigating seismicity, as stresses on faults may have increased due to pressure depletion, leading to higher level of stress criticality, and injection may trigger fault failure, leading to higher seismic magnitude.

We make the following recommendations for mitigating depletion induced seismicity and for pressure maintenance purpose by fluid injection in Groningen gas field.

1) The first measure to take to lower the seismicity rate is to stop gas production and to shut-in the wells.

2) During significant production in the Groningen gas field, no injection should be carried out in the Loppersum region because of critical stresses and fault locations.

3) To compensate for the pressure loss at those regions, the rate and duration of injection should be low and long, respectively, to prevent instability of near-field faults by pressure increase effect and to prevent instability of far-field faults due to the poro-elastic triggering effect.

4) Based on the increased rate of modelled pressure increase, without a substantial increase in the number or magnitude of simulated seismic events, injection should be carried out using N2 instead of CO2, as CO2 dissolves more effectively in water than N2.

5) Combining injection in a depleting reservoir may have negative effect on mitigating seismicity, as stresses on faults may have increased due to pressure depletion, leading to higher level of stress criticality, and injection may trigger fault failure, leading to higher seismic magnitude.

As of now, there is no conclusive evidence that the injection rate can be adapted to result in minimal seismicity. In the case of significant additional production within the Groningen gas field, additional study, including sensitivity tests, will be necessary in order to determine whether fluid injection is beneficial and/or necessary.

1. Introduction

1.1. Background and the key questions

TNO and NAM have extensively studied the feasibility of pressure maintenance by large-scale fluid injection (Bourne & Oates, 2019; van den Bogert, 2018; Hofmann et al., 2016; Guises et al., 2015; van Thienen-Visser et al., 2015, 2016). Overall, they concluded that injection can maintain reservoir pressure in depleting reservoirs and that fluid injection is technically feasible.

However, the overall net effect of large-scale fluid and gas injection on the seismic risk profile was not quantified, as the seismic risk associated with various fluid and gas injection scenarios was only studied qualitatively.

Therefore, the question of whether fluid and gas injection can be used to minimize the risk of induced seismicity in depleting reservoirs remains unanswered, as TNO and NAM studies did not involve simulation of dynamic fault ruptures induced by fluid and gas injection, and the subsequent generation of earthquake magnitudes from the resulting seismicity.

In this study, we focus on modelling the pressure depletion of the Groningen reservoir through applying 2D discrete element modelling using Particle Flow Code 2D software. Following the depletion stage, we test numerous injection scenarios where fluid and gas injection is applied to areas where the pressure depletion is large, in order to compensate for the pressure decline.

The research questions of the study are as follows:

1) What are possible injection scenarios for pressure maintenance during and after production and for minimizing the pressure difference across the field?

2) What are the reservoir stresses and pressures for various fluid and gas injection scenarios (defined in question 1) around wells and over the entire gas field?

3) How can the Groningen seismic module be adapted for injection to increase or decrease pressure?

4) What is the effect of fluid and gas injection on the overall seismic risk?

5) What is the effect of fluid and gas injection on seismicity near injection wells?

6) What is the most optimal configuration of injection wells?

7) What is the overall effect of fluid and gas injection on seismicity and what are the recommendations for the Groningen HRA model?

1.2. Design of the study

The steps of this project were divided into six work packages, as shown in **Figure 1-1**. They outline the workflow, from the generation of 2D Groningen gas field geological models to seismic hazard map generation for the largest simulated earthquakes.

WP0: Review of past studies and compilation of input data/parameters for Groningen gas field modelling (Section 4)

WP0 will be the preparation stage where earlier studies pertaining to the Groningen gas field are comprehensively reviewed in order to prepare data sets that are needed to generate the numerical model of the Groningen reservoir (see attachment D, *KEM-24 WP0 Literature review and compilation of input data/parameters for Groningen gas field modelling*, primary author Fugro).

WP1: Modelling of depletion-induced seismicity in Groningen gas field using 2D hydro-mechanical coupled discrete element modelling (Section 5 and Section 6)

In the first phase of this project, 2D hydro-mechanical coupled discrete element modelling (Yoon et al., 2014) will be used to simulate the seismicity by pressure depletion within the Groningen gas field. Using the PFC2D software, a detailed 2D geological model will be built, with the complex fault structure represented by using a smooth joint contact model. Production history will be closely simulated in order to monitor changes in the geomechanical processes of the fault system, in particular focusing on fault system stress paths associated with gas production, and their correlation with seismic events. Depletion modelling will generate seismicity catalogs, the resulting seismicity will be compared to observed earthquakes, as reported by KNMI, to further refine the geological model and fault parameters. The resulting spatial distribution in pressure decline will be used to design injection scenarios in the next work package of the project, with the goal of compensating major areas of pressure loss and mitigating resulting seismicity.

WP2: Modelling of various fluid injection scenarios in the Groningen gas field and induced seismicity using 2D hydro-mechanical coupled discrete element modelling (Section 8 and Section 9)

After modelling the depletion-induced seismicity history, multiple fluid injection scenarios will be designed and simulated using PFC2D, to understand how the fault system would respond to injection. These scenarios are designed with the intention of recovering pressure in areas with the large observed decline, as observed in the depletion scenarios from the previous work package. The depleted state at the end of production will be used as an initial condition of the injection model, along with the current in-situ stress state.

WP3: Modelling of multiphase/gas-mixture injection using TOUGH3 (Section 7)

In this work package, modelling of injection of N_2 and CO_2, in a reservoir with mixture of CH_4 and water, will be performed using the TOUGH3 software. The aforementioned injection gas and their mixture with CH_4 and water in the reservoir are then tested, providing temporal evolution of the reservoir pressure change, which will then be used back in the PFC2D modelling.

WP4: Modelling of fluid injection induced fault activation using 3D hydro-mechanical coupled discrete element model

Fault activation by fluid injection will be simulated using 3D hydro-mechanical coupled discrete element modelling. The HM coupled 3D modelling is developed in-house by DynaFrax, based on the PFC3D software.

WP5: Induced seismic hazard assessment

The numerical seismicity catalogs generated from WP2 will be collected and analyzed comprehensively to develop, jointly with Fugro, an induced seismic hazard model of the Groningen gas field.

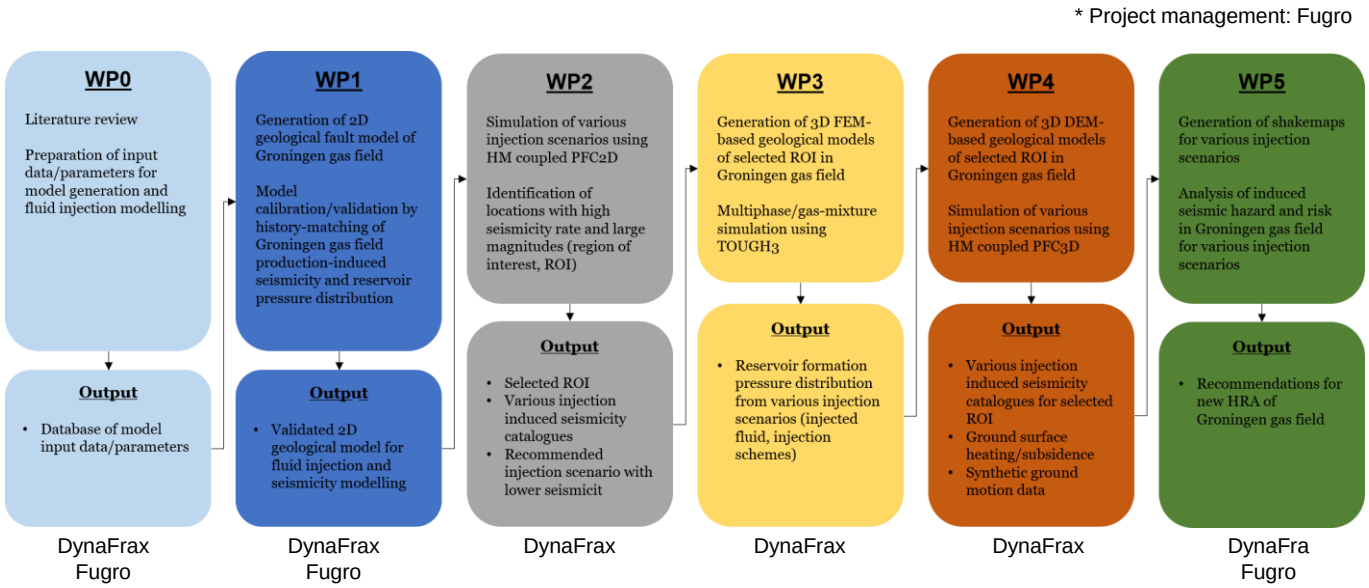

Figure 1-1: Structure of the study and the work packages.

2. Background

2.1. Geology of Groningen gas field

The Groningen gas field is the largest gas field in Western Europe, 40 by 50 km wide and ranges from 100-300 m thick, with thickness increasing from south to north. The total recoverable natural gas volume is approximately 2800 billion cubic meters, of which 83% has been produced by about 300 wells. It is situated in the Rotliegend reservoir at a depth of 3 km, in the northeastern region of the Netherlands (Bourne et al., 2018). The region comprises a dense network of pre-existing normal faults, highly varying in orientation and dimension. Fault dip tends to be near-vertical, ranging from 65-90° (Wentinck, 2015), and three major fault trends are commonly observed: NNW–SSE, E–W and WNW–ESE. The longest faults tend to trend NNW–SSE and display the largest amount of offset (de Jager & Visser, 2017).

Figure 2-1 displays the stratigraphy of the reservoir in the northwestern region of the Groningen field. The reservoir rock itself is primarily the Slochteren Formation, composed of a “sequence of fluvial and aeolian sandstones intercalated with silty claystones which belongs to the late Permian Upper Rotliegend Group”. Porosity of these sediments typically ranges from 10-24%, while permeability tends to range from 1-1000 mD, though greater variability has been observed (de Jager & Visser, 2017). Breccias and conglomerates are also observed toward the top of the reservoir. The reservoir thickness increases to the north due to the Base Permian Unconformity. Ten Boer claystone, of the Silverpit Formation, overlays the Slochteren formation, with a thickness of approximately 20-80 m, increasing southeast to northwest within the Groningen gas field. Above this layer, the Zechstein group forms a low-permeability seal, consisting predominantly of hundreds of meters of halite (Hettema, 2020). The source rock, or Carboniferous Limburg Group, lies directly below the Slochteren Formation, composed of “siliciclastics intercalated with coal seams”, with a thickness ranging from 700 to more than 1500 m within the Groningen field. Direct shear experiments reveal variations in the geomechanical properties of these strata; Hunfeld et al. (2017) determined that the maximum friction coefficients of the Basal Zechstein, Ten Boer claystone, reservoir sandstone, and Carboniferous layers are approximately 0.66, 0.37, 0.6 and 0.5, respectively.

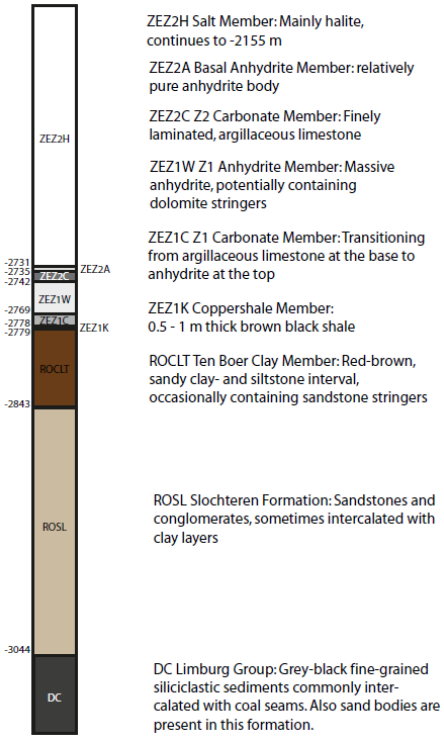

Figure 2-1: Stratigraphy in the northwestern part of the Groningen field (Fig.3 in Buijze et al., 2017).

2.2. Reservoir compaction and induced seismicity in Groningen

Production within the Groningen gas field has caused substantial pressure depletion, accompanied by subsurface deformation and ground subsidence. From 1995 to 2017, pressure has reduced from 25 to 12 MPa, at a mean rate of approximately 0.2 MPa/year (Bourne et al., 2018). Depletion of the porous gas field causes compaction, accompanied by stress changes within the reservoir and surrounding area (Buijze et al., 2017; 2019; Nepveu et al., 2016). Given the coupling of the reservoir to the surrounding rock volume, the decreased reservoir volume results in reduced total horizontal stress, increasing the differential stress within the reservoir and possibly activating faults.

Since 1995, KNMI has operated a near-surface seismic monitoring network in the northeastern region of the Netherlands, which has reported all ML ≥ 1.5 earthquakes since the time of operation (Dost et al., 2012). Most induced seismicity tends to occur in the northwest part of the Groningen gas field, and to some extent in the southwest. In particular, faults that incorporate Basal Zechstein anhydrite-carbonate material from the top of the reservoir are expected to have a higher seismogenic potential (Hunfeld et al., 2017). As of 2017, more than 1000 M > 1.0 earthquakes had been recorded, most notably the Mw 3.6 Huizinge earthquake (Buijze et al., 2017), which occurred on 16 August 2012. This earthquake was the largest recorded induced earthquake in the Netherlands and caused substantial damage to infrastructure and housing, rendering several homes uninhabitable. More recently, on 22 May 2019, the ML 3.4 Westerwijtwerd earthquake occurred in the northwestern area of the gas field (van Elk & Doornhof, 2019). This earthquake was the third largest to occur in Groningen, with a similar magnitude to the Zeerijp earthquake of 8 January 2018. The maximum recorded PGV was 1.0 cm/s, exceeding the “vigilance level” threshold of the MRP and causing DS1 damage to nearby buildings.

Figure 2-2 shows the temporal evolution of gas production, overlain by the evolution of earthquake occurrence (number of earthquakes and their magnitude distribution). From 1990-2020, during which time the production and seismicity histories are displayed, there is a clear correlation between increased production levels and increased earthquake rates and magnitudes. From 2010, a sharp increase in seismicity rates is observed, which persists into 2017 and decreases afterwards, though rates remain elevated compared to those prior to 2010. The continuously-elevated earthquake rates show a delay in seismicity with respect to production times, as the production rate decreases sharply from 2013. By contrast, the magnitudes of the induced earthquakes are more closely correlated in time to production rate; the rates of ML ≥ 1.5 earthquakes reach a maximum at the same time as production rate. Overall, these results indicate that earthquake rates can be lowered through stopping production;

however, the effect is not immediate and a substantial reduction in induced seismicity would only have been possible through stopping production before 2020, or even 2010.

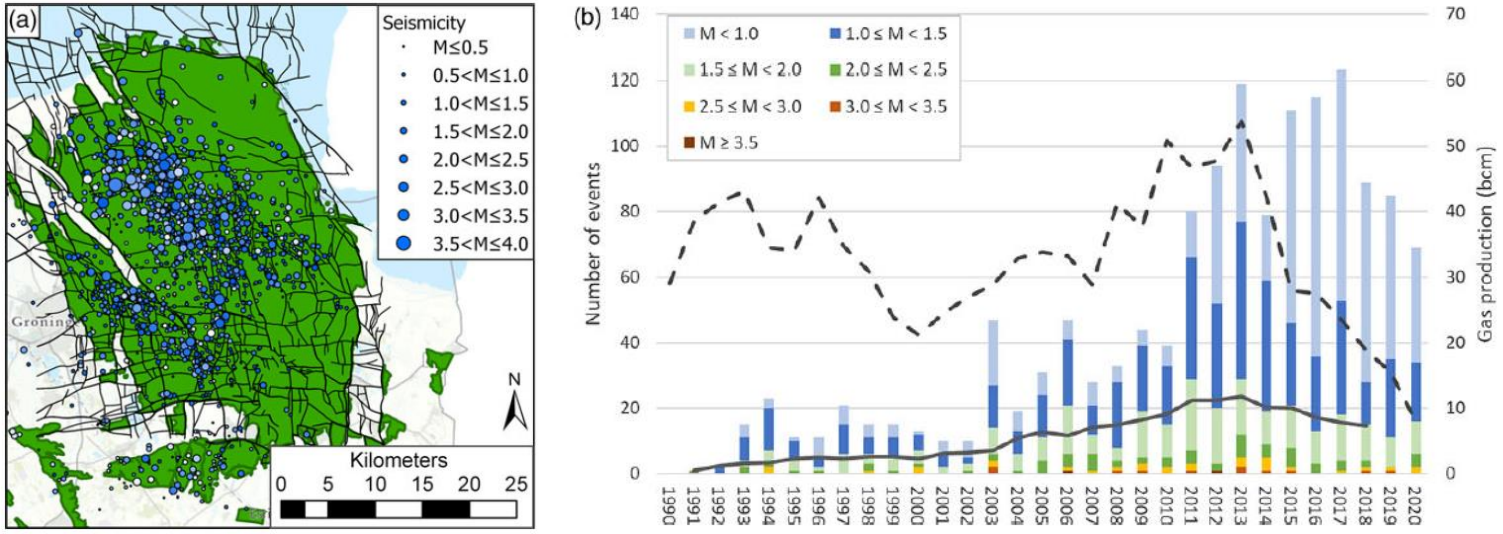

Figure 2-2: (Left) Map of earthquakes recorded by KNMI from 1960-2020, with marker size scaled to magnitude; (Right) Plots of production history (production volume) and numbers of earthquakes during each year from 1990-2020.

2.3. Pressure maintenance

A consequence of gas production in the Groningen field is reservoir subsidence. As the pore pressure decreases during depletion, the reservoir compacts, stresses along pre-existing faults increase. This in turn increases the instability of some faults, triggering induced earthquakes (Hofmann et al., 2016).

During the past decades, pressure maintenance has been investigated as a method to counteract the pressure depletion caused by gas production, thereby reducing the number and magnitude of earthquakes. Through injection of fluids such as N_2, CO_2 or water, the effects of depletion can potentially be offset, maintaining pressures throughout the reservoir. Through injection at specific sites with high depletion levels, pressure levels can also be redistributed, thus reducing spatial imbalances that can trigger earthquakes.

Within the Groningen field, the first plans to introduce pressure maintenance were outlined in the Technical Addendum to the Winningsplan 2013 (NAM, 2013). In this study, N_2 would be injected in new wells throughout the study region, returned via production, and recycled for further injection at existing production clusters. Ultimately the injection plans were deemed infeasible due to cost, loss of production and scale of required infrastructure. Furthermore, the 2013 NAM report acknowledged that geomechanical modelling should be applied to better understand the impact of pressure maintenance through fluid and gas injection on seismic risk mitigation, as injection itself may induce seismic events.

3. Numerical modelling method

3.1. Numerical modelling code: Particle Flow Code 2D (PFC2D)

PFC2D is a two-dimensional distinct element geomechanical modelling software (Itasca, 2008). The material simulated, in this case a reservoir rock mass, is modelled as an aggregate of circular particles bonded at their contacting points with finite thickness of cementing around the contact with the Mohr-Coulomb strength parameters (Itasca, 2012—enhanced parallel bond model). Under an applied load, the bonds can break in Mode I (tensile) or Mode II (shear). The calculation cycle in PFC2D is a time stepping algorithm that requires repeated application of the law of motion applied to each particle and a linear force displacement law applied to each contact (**Figure 3-1**). For more detail, we refer to Potyondy and Cundall (2004).

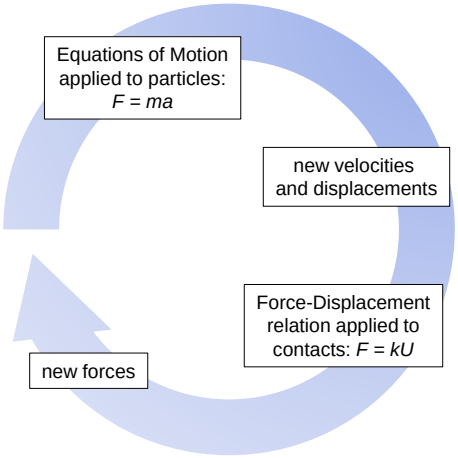

Figure 3-1: Calculation cycle in PFC2D (m: particle mass, a: acceleration, k: stiffness at contacts, U: particle overlap, F: force applied to particles).

3.2. Hydro-mechanical coupling: fluid flow algorithm in PFC2D

Flow of viscous fluid in bonded particle assembly and fluid pressure and volume driven breakages of bonds in Mode I and Mode II are simulated. The original concept of the fluid flow algorithm was proposed by Cundall (unpublished technical note 2000), which was later modified by Hazzard et al. (2002).

Fluid flow is simulated by assuming that each particle-bonded contact is a flow channel (**Figure 3-2**, blue lines) and these channels connect pore spaces (**Figure 3-2**, polygons) that can store pressure. Pressure-driven flow of viscous fluid between the two pore spaces is governed by the Cubic law, assuming that the flow is laminar between two smooth parallel plates:

$$q = \frac{e^3 \Delta P_f}{12 \eta L} \qquad (1)$$

where e is hydraulic aperture, ΔP_f is the fluid pressure difference between the two neighboring pores, L is the flow channel length, and η is the fluid dynamic viscosity.

The hydraulic aperture, e, of the flow channel at a particle contact (**Figure 3-2**, blue lines) was programmed to change as a function of normal stress, σ_n. We used the experimentally derived $e\ vs.\ \sigma_n$ relation from Hökmark et al. (2010):

$$e = e_{inf} + (e_0 - e_{inf}) \exp(-0.15\sigma_n) \qquad (2)$$

where e_{inf} is the hydraulic aperture at infinite normal stress, e_0 is the hydraulic aperture at zero normal stress, and σ_n is the effective normal stress at the particle contact.

Fluid pressure increase per time step in a pore space (ΔP_f in **Figure 3-2**) is computed from the fluid bulk modulus (K_f), pore space volume (V_d), sum of flow volume $\sum q$ (entering and leaving the pore space) and volume change of pore space (ΔV_d) due to mechanical loading, which is neglected in this study due to its minor effect. The equation used is shown below.

$$\Delta P_f = \frac{K_f}{V_d}(\sum q \Delta t - \Delta V_d) \qquad (3)$$

The fluid exerts pressure on the surrounding particles, causing deformations. This force term (F) is a production of fluid pressure (P_f), the length d (Figure 3-2) and unit thickness in the out-of-plane direction. The resulting force term (F) is then applied to the particles from which, applying the law of motion, the particle velocity and displacement are computed. This subsequently changes the stress states at the surrounding contacts, which in turn changes the hydraulic aperture and thereby the flow field.

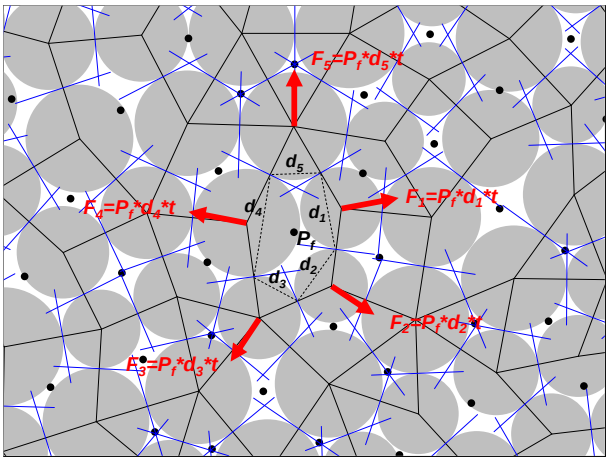

Figure 3-2: Pore network model. Flow channels (blue lines at the particle contacts) connect two neighboring pore spaces bounded by polygons. Black dots at the polygon centers are virtual pores where pressure (Pf) is stored. Red arrows are resultant forces applied to the particles surrounding the pore space due to the pore fluid pressure Pf (Fig.2 in Yoon et al. 2014).

To simulate fluid injection and migration in the reservoir, the fluid flow algorithm was implemented via the FISH coding script of PFC2D (Yoon et al., 2014). The methodology in this study is basically the same as in UDEC (Universal Distinct Element Code) (Itasca, 1999). UDEC models progressive failure associated with crack propagation and fault slip by simulating breakage of pre-existing contacts between the predefined joint-bounded deformable but intact blocks. It is also capable of modeling fluid flow through the defined fracture network. Both UDEC and PFC can handle coupled hydro-mechanical processes, in which fracture conductivity is dependent on mechanical deformation of joint apertures and, conversely, joint fluid pressures can affect the mechanical computations of joint aperture. Unlike in UDEC, however, where fluid flow formulation is restricted to the

fracture flow model, PFC allows not only fluid flow through fractures but also fluid leak-off into the rock matrix. Furthermore, in the UDEC model, fluid flows into the joint only when a joint contact is broken, whereas fluid flow occurs in the PFC model if a pressure gradient exists between neighboring pores. The difference in the two models is that the blocks in the UDEC model are deformable and can generate different normal stress and normal closure or shear dilation of fractures. Particle rigidity in the PFC model therefore can generate different behaviors to those in the UDEC model.

3.3. Seismicity modelling in PFC2D

Each bond breakage in the bonded particle assembly is assumed to be a fracture process associated with seismic energy radiation. PFC runs in dynamic mode with low levels of numerical damping where a realistic level of energy attenuation in rock is simulated.

Upon a bond breakage by Mode I or Mode II, part of accumulated strain energy at the broken bond is released to the surrounding in a form of seismic wave. A numerical technique for calculating the seismic source information in PFC2D has been proposed by Hazzard and Young (2002, 2004) and used in Hazzard et al. (2002), Al-Busaidi et al. (2005) and Zhao and Young (2011).

In this study, a link was made in the algorithm to compute seismic source parameters of the Mode I (tensile) and Mode II (shear) failures at the pre-existing joints, i.e., breakages of smooth joint bonds. Currently, seismic source parameters are obtained only for bond breakage by Mode I and Mode II and not for the subsequent sliding after shear bond breakage, i.e., silent slip (**Figure 3-3**). Ongoing research aims at computing the seismic moment and moment magnitude of the frictional sliding event at the smooth joint contact that is broken by shear. This is necessary as energy can also be released by slip (Marone, 1998). Large numbers of relatively lower magnitude events caused by slipping can result in a more exponential distribution of the magnitude-frequency relation, similar to the Gutenberg-Richter law.

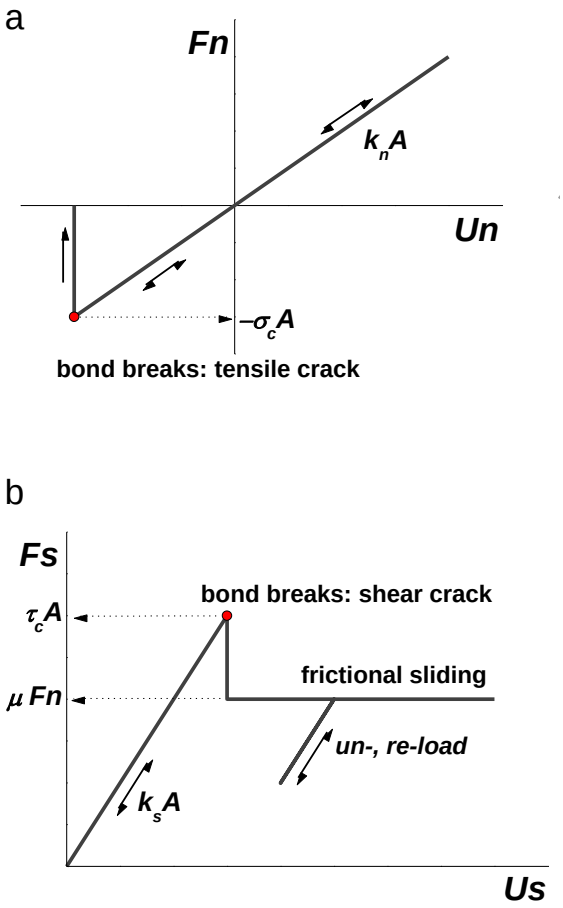

Figure 3-3: Force-displacement law for smooth joint bonded contacts: (a) normal force (Fn) vs. normal displacement (Un), (b) shear force (Fs) vs. shear displacement (Us) (kn: normal stiffness, ks: shear stiffness, σc: tensile strength, τc: shear strength, A: area of smooth joint cross section, μ: coefficient of friction against sliding).

For each bond breakage, the moment tensor is calculated for each time step over the duration of the event. If another crack forms adjacent to the active crack such that the source area overlaps within the duration of the event, then the cracks are considered part of the same event, i.e., two cracks but one event. This approach is thought to be a realistic assumption as it is known that most seismic events in the field are made up of many smaller scale ruptures and shearing of asperities (Scholz, 1990) and that fractures generally grow at some finite velocity (Madariaga, 1976).

For computing numerical seismicity, a simple yet fairly robust method is used. The method uses the change in contact forces around bond breakages to calculate the moment tensor. This is illustrated in **Figure 3-4**. It can be assumed that each bond breakage in PFC represents a single microcrack. When a bond breaks, the two

particles on either side of the crack (the source particles) will move and contacts surrounding the source particles will suffer some deformation. There will be a force change at the surrounding contacts due to the formation of the crack. We can then perform an ‘‘integration’’ around the contacts surrounding the crack to calculate components of the moment tensor from the contact locations and force changes. For a discrete medium, the integration is a sum so the moment tensor can be calculated by:

$$M_{ij} = \sum_S \Delta F_i R_j \qquad (4)$$

Where, ΔF_i is the i-th component of the change in contact force, and R_j is the j-th component of the distance between the contact point and the event centroid. The sum is performed over the surface S, enclosing the event.

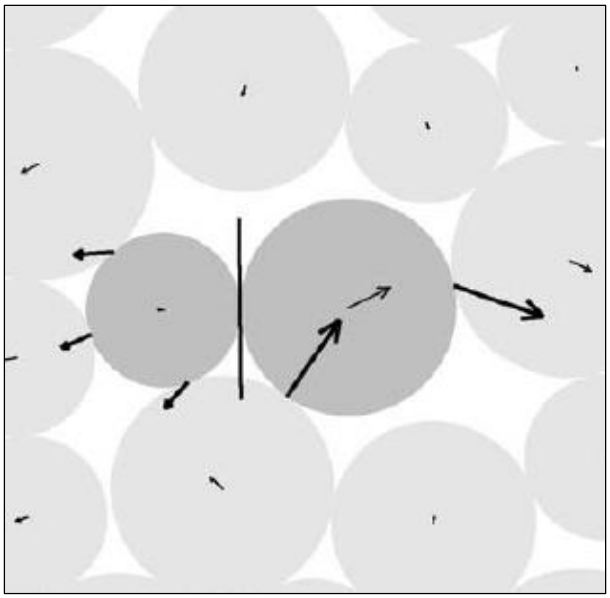

Figure 3-4: An example seismic event composed of a single tensile crack (Fig.1a in Hazzard & Young, 2002). Particle velocity and contact force changes after the bond breakage. The vertical black line is the crack, breakage of bond between the two particles.

It is known that seismic events evolve through time and it is possible to calculate time-dependent moment tensors to reveal information about the nature of rupture initiation and propagation. In the PFC model, the moment tensor can be calculated at each time step after

the initial rupture and the evolution of the source type can be examined. In theory, a full time-dependent moment tensor can be obtained for each event. However, in practice, storing the full time-dependent moment tensors for all events would be very memory intensive. Therefore, in general only a single moment tensor is stored for each event. For particular events of interest, the full time-dependent moment tensor could be examined along with the micromechanics of failure. The single moment tensor that is stored for each event (the time-independent moment tensor) is the moment tensor calculated at the time of maximum scalar moment. The scalar moment can be calculated from the elements of the moment tensor matrix by:

$$M_0 = \sqrt{\frac{\sum_{j=1}^{3} m_j^2}{2}} \qquad (5)$$

Where , m_j is the j-th eigenvalue of the moment tensor matrix (Silver & Jordan, 1982).

As PFC2D runs in dynamic mode, the calculated scalar moment M_0 changes as a function of time. The scalar moment quickly increases to some peak value and then begins to drop.

The single time-independent moment tensor associated with this event is assumed to be the moment tensor calculated at the time of peak scalar moment. The moment magnitude associated with the event is calculated from the peak scalar moment, M_0, by the equation below (Hanks & Kanamori, 1979):

$$M_w = \frac{2}{3}\log M_0 - 6 \qquad (6)$$

It should be noted that the particle size has a significant effect in the calculation of the seismic moment and hence the moment magnitude. As the parameter R_j in equation (4) is directly correlated with the diameter of the particles, the particle size distribution should be chosen carefully. In this study, the Groningen reservoir model is constructed using the particles of which the diameters are chosen from an uniform distribution between 180 m and 260 m (average diameter 210 m). The particle size range chosen also affects the computational efficiency, meaning that with smaller particle size, it requires millions of particles to construct the model, and hence the model simulation takes a very long time.

There is a correlation between the particle size and the simulated seismic magnitude. In Yoon et al. (2012), they simulated a laboratory scaled rock failure test. The average particle size used in the 5 cm x 10 cm rock model was 0.8 mm, and the resulting range of seismic magnitude is Mw -6 to -4 (**Figure 3-5**). In Yoon et al. (2014), they simulated hydraulic fracturing in a few hundreds meter scaled geothermal fracture rock mass. The average particle size used in the model was 20 m, and the resulting range of seismic magnitude is Mw -1 to Mw 1 (**Figure 3-6**).

From this correlation between the particle size and the seismic event magnitude, the particle size chosen in this study, i.e. average particle size of 210 m, was considered to be adequate to simulate seismic event magnitude ranging from Mw 2 to above.

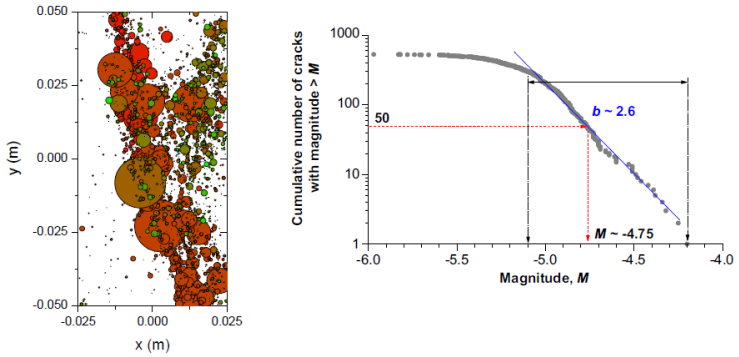

Figure 3-5: Seismic events (acoustic emission) simulated in asymmetric compression rock test and the magnitude frequency distribution of the seismic event moment magnitude (Fig.10 in Yoon et al. 2012).

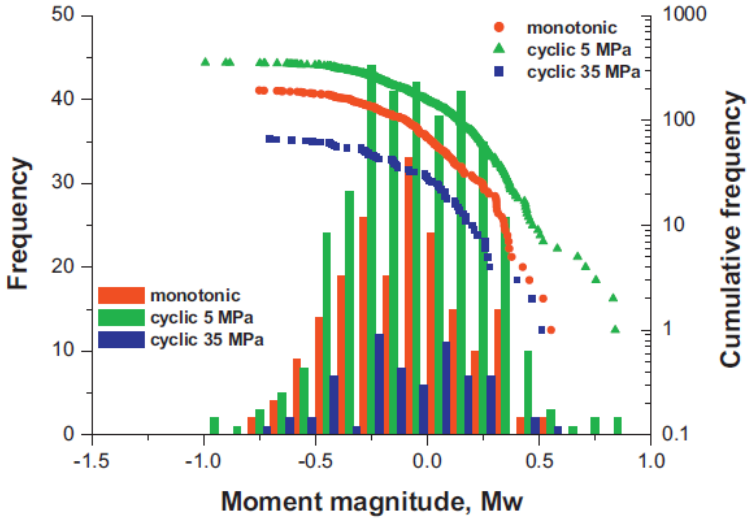

Figure 3-6: Magnitude frequency distribution of the seismic event moment magnitude resulting from hydraulic fracturing – hydraulic stimulation modelling of geothermal reservoir rock mass (Fig.10 in Yoon et al. 2014).

4. Groningen reservoir model

4.1. Model generation in 2D

Generation of a 2D Groningen gas field model using PFC2D was accomplished in several steps. Model generation first started with densely packing the 40 km x 50 km sized model volume with rigid particles, of which the diameters range from 180 m to 260 m, and unit thickness in the out-of-plane direction. The particle size was chosen by considering both computation efficiency and resolution of seismicity modelling. The complex fault system in Groningen region as shown in **Figure 4-1** (from Kortekaas & Jaarsma, 2017) was then overlain onto the particle assembly, and the particle contacts at the locations of the reservoir faults were replaced by the smooth joint contact model. Fault traces were modeled at a consistent depth of 3 km, characteristic of the Groningen reservoir depth. Only faults visualized from literature (i.e., Figure 4b from Buijze et al., 2017) were included in the model. Fault failure (smooth joint failure) was governed by the Mohr-Coulomb failure. In the model, no fault healing was assumed to occur afterwards; that is, once a simulated seismic event occurred on a fault, the broken bonds could not be repaired over time and later experience simulated re-rupturing.

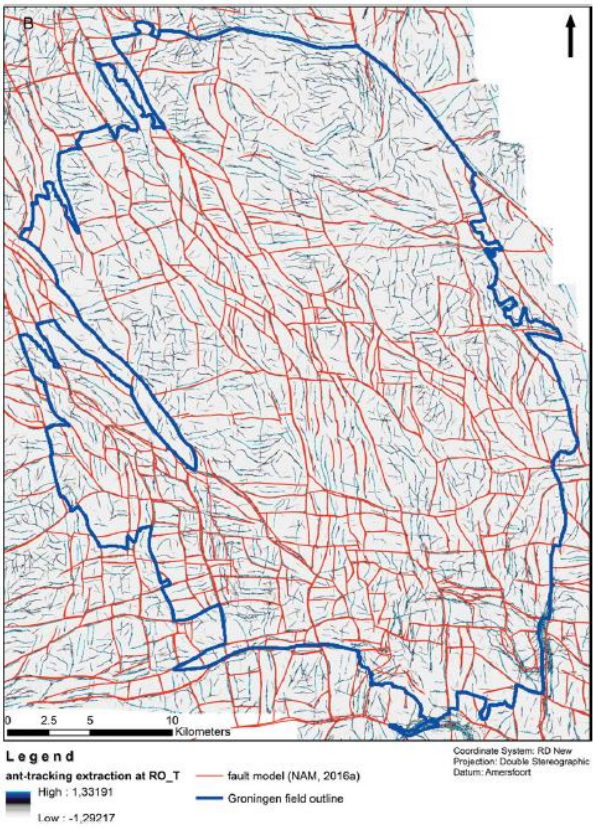

Figure 4-1: Groningen reservoir faults (Fig.3 in Kortekaas & Jaarsma, 2017).

The smooth joint contact model is commonly used in PFC modelling to mimic geological discontinuities (Mas Ivars et al., 2011; Yoon et al. 2017), such as bedding planes, microcracks, joints, discrete fracture network and faults. The mechanical properties of the smooth joint contact model are listed in **Table 4-1**. Some of the parameters were taken from various literatures (Report A, Fugro report) and some were chosen from our best guessing from the literature study. After that, the hydro-mechanical coupling model and pore-network model (described in Section 3) were implemented, and the model was initialized with the reservoir pressure distribution for the year 1960, where the reservoir formation pressure was assumed uniform as shown in **Figure 4-2**.

Table 4-1: Modelling parameters.

Parameters	Value (Unit)	Source
Reservoir gas viscosity	2.5e-5 (Pa.s)	Hettema et al. (2017)
Reservoir gas compressibility	16.7e-6 (1/kPa)	Estimated from temperature and pressure conditions of Groningen gas reservoir
Reservoir matrix permeability	3.4e-14 (m^2)	Jager and Visser (2017), 1-1000 mD
Reservoir matrix porosity	30 (%)	Visser (2012), 10-24%
Fault tensile strength	0.5 (MPa)	Estimated, 1/3 of cohesion
Fault cohesion	1.5 (MPa)	Buijze et al. (2017), 3 MPa
Fault friction angle	30 (degrees)	Estimated
Fault friction coefficient	0.2 (-)	NAM (2015)
Fault dilation angle	3 (degrees)	Estimated
Fault normal stiffness	300e6 (Pa/m)	Estimated
Fault shear stiffness	50e6 (Pa/m)	Estimated
Max horizontal stress	50 (MPa)	NAM (2015), 500-560 bars
Min horizontal stress	40 (MPa)	NAM (2015), 420-520 bars
Orientation of max horizontal stress	N160°E	NAM (2015)

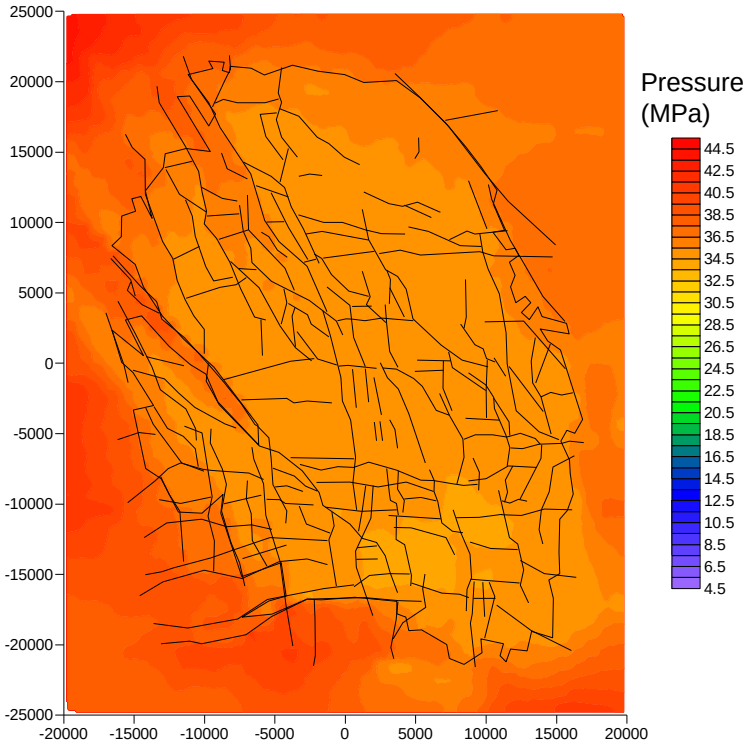

Figure 4-2: PFC2D-generated Groningen geological model, where the reservoir pressure was initialized with the 1960 reservoir pressure distribution, based on numerical modeling assumptions. The axes show the distance (in meters) from the center of the study region.

For the faults within the reservoir, fault permeability was assigned based on the categorization of faults as belonging to one of twelve fault-throw classes as shown in **Figure 4-3**. For example, we programmed that the permeability of those fault with throw 0-25 m (white traces shown in **Figure 4-3**) is same as the reservoir rock matrix. Therefore, the hydraulic apertures assigned to the particle contacts at the locations of white traces of reservoir faults are same as the hydraulic apertures assigned to the reservoir rock matrix. For those faults with throw larger than 276 m are assumed to be almost impermeable and therefore assigned 10^{-6} m for the hydraulic apertures.

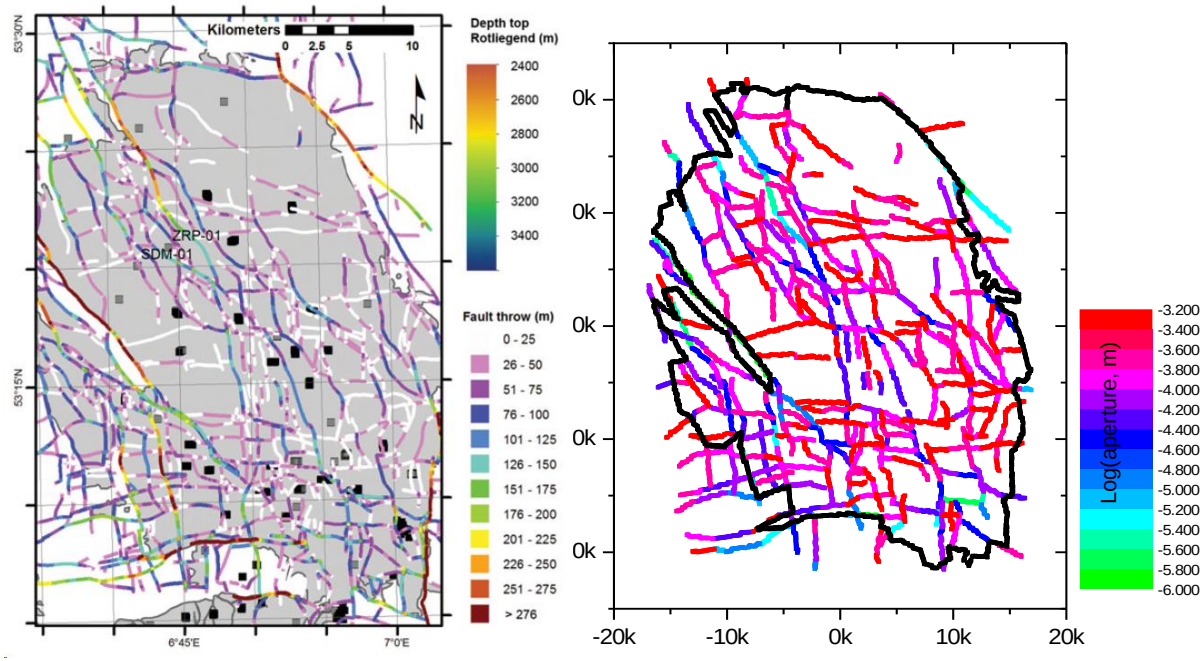

Figure 4-3: (a) Distribution of fault throw (Fig.4 from Buijze et al., 2017) and (b) log(aperture) values assigned to the smooth joint contacts at the location of reservoir fault following the fault throw classes. The reservoir boundary (black) was assigned zero aperture to simulate impermeable boundary.

Next, the model was imposed with in-situ stress field. The assumed orientation of the maximum horizontal stress was N160°E (Guises et al., 2015), and the magnitudes of the maximum and the minimum horizontal stresses were 50 MPa and 40 MPa, respectively. In PFC2D, we used a servo-controlled in-situ stress initialization model, where the velocities of the boundary layer particles were controlled so that the stress field measured inside the model matched the assumed orientation and magnitudes of the maximum and the minimum horizontal stresses.

It should be noted that the magnitudes of stress we used in the model comes from our best guessing after studying various in-situ stress models of the northeast of the Netherlands (Mechelse, 2017), meaning that the stress magnitudes already pose uncertainty. It should also be noted that the stress models in various studies are based on the field measurements conducted long after 1960, and the stress magnitudes may not truly represent the magnitudes of stress prevalent in the Groningen gas reservoir in year 1960 before production started.

To monitor the stress field evolving inside the model, we used five stress measurement circles (Yoon et al., 2012) as shown in **Figure 4-4**. The stress measurement circle logic in PFC was used to calculate the local stress field inside the measurement circles by averaging the stresses at the particle contacts that were confined within the designated measurement circles (black circles shown in **Figure 4-4a**). In PFC2D, we assumed that the reservoir depth was 3 km and the vertical stress is 60 MPa. As the model was initialized with an anisotropic stress field (SH,max = 50 MPa and Sh,min = 40 MPa), there were smooth joint contacts already failing under the anisotropic in-situ stress field as show in **Figure 4-4b**. The mode I tensile failures of the smooth joints are denoted in blue and the mode II shear failures of the smooth joints are denoted in magenta. The model shown in **Figure 4-4b** is the starting model that was applied in depletion modelling.

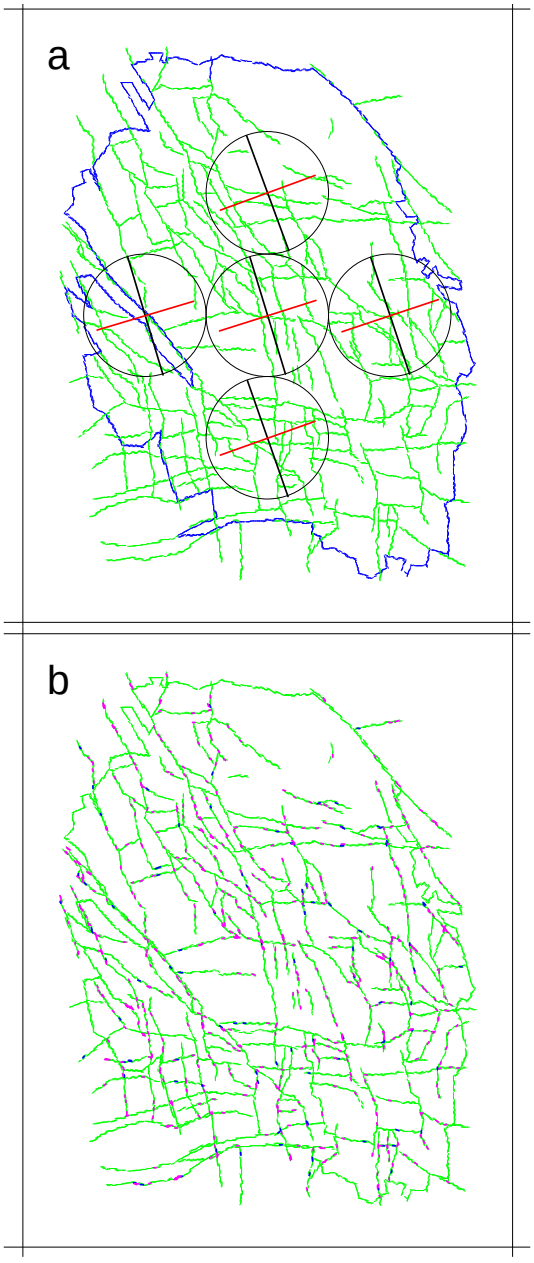

Figure 4-4: (a) PFC2D Groningen gas field model, where the in-situ stress field was initialized: SH,max = 50 MPa, Sh,min = 40 MPa and the orientation of SH,max is N160E. (b) distribution of smooth joint failures (blue: Mode I tensile failure, magenta: Mode II shear failure) resulting from initialization with an anisotropic in-situ stress field.

4.2. Model assumptions

A major assumption in this study is that the use of a 2D model, through PFC2D modeling, is considered valid due to long horizontal extent, 40-50 km, and 200-300 m of net reservoir thickness (**Figure 4-5**), i.e. similar to thin-sheet model. The use of a thin-sheet model to characterize the study region is supported by previous studies such as de Jager and Visser (2017).

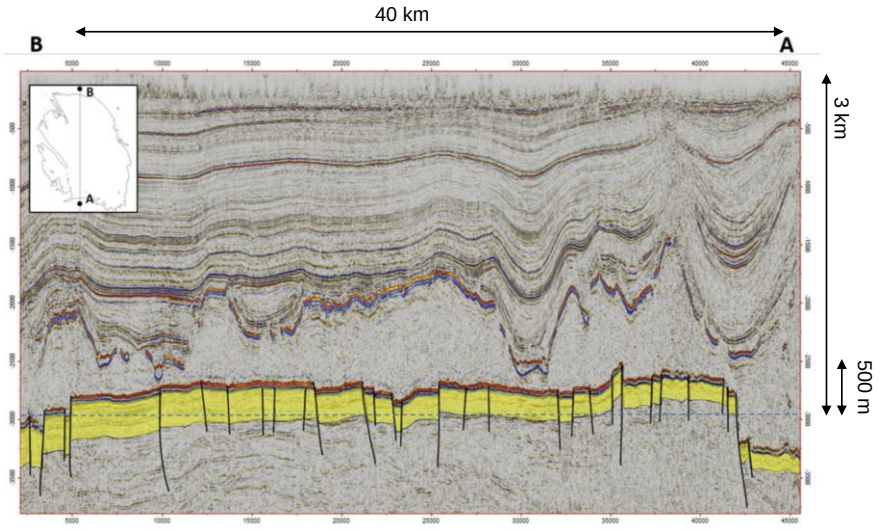

Figure 4-5: Figure 7 from de Jager and Visser (2017), showing a north-south cross section of Groningen stratigraphy. A clearly-delineated layer, shown in yellow, shows that the Groningen reservoir has a long horizontal extent (40-50 km) and 200-300 m of net reservoir thickness.

Spatially-constant mechanical parameters for the Groningen geological model are listed in **Table 4-1**. Some geomechanical parameters were kept consistent for all faults except for those delineating the reservoir boundary, in order to prevent boundary failure. For example, the friction coefficient was assigned values of 0.6 and 0.2 for the reservoir boundary and for the faults, respectively. Likewise, the tensile fault strength and fault cohesion were both assigned values of 1e20 Pa at the reservoir boundary, and 0.5e6 Pa and 1.5e6 Pa everywhere else, respectively. The reservoir boundary was simulated as impermeable, by assigning an aperture of zero to fluid flow channels at the boundary.

The permeability assumed for the reservoir rock matrix is 3.4e-14 m^2, i.e. 34 mili Darcy. The 34 mD permeability is taken from NAM's PETREL model. Using this value, the hydraulic apertures, at the

particle contacts at matrix rock locations are calculated using the equation (8) below:

$$e = \sqrt[3]{\frac{24k\pi\sum_{balls}R^2}{(1-n)\sum_{pipes}L}} \qquad (8)$$

Where, k is the reservoir rock matrix, n is the reservoir rock porosity.

As the model is in 2D with unit thickness in the out-of-plane direction, we further processed the seismicity data in order to calibrate the seismic event magnitudes by taking into account of the reservoir thickness. This calibrating approach was also adopted in the studies of Yoon et al. (204, 2016, 2017).

The moment magnitude (Mw) obtained from PFC2D seismicity computation model, equation (6), is converted to seismic moment (M_0) using:

$$M_0 = 10^{1.5(M_w+6)} \qquad (7)$$

The M0 has unit of Newton meter (Nm). However, due to unit thickness nature of the model, it can be said that the M0 is actually in unit of Nm per meter. To the M0, equation (7), we multiplied the reservoir thickness that corresponds to the location of the seismic event. The reservoir thickness is spatially varied as shown in **Figure 4-6**, which shows that the thickness increases from southeast to northwest of the reservoir.

After multiplying the reservoir thickness to the M0, equation (7), we introduce a calibrating parameter, FRP (Fault Rupture Portion), which describes how much the width of the fault contributed to the rupturing process. Throughout the study, we applied FRP = 0.1, meaning that only 10% of the fault width in the vertical direction ruptured. Combining all the calibrating measure described above results in final seismic moment and hence moment magnitude.

The resulting moment magnitude is then converted to local magnitude, M_L, using the M_L vs. M_w relation adapted for the Groningen region (Dost et al., 2016):

$$M_w - M_L = bM_L + a \qquad (7)$$

Where a = 0.327±0.186, b = -0.169±0.071.

We used combination of a and b parameters that resulted in the largest M_L.

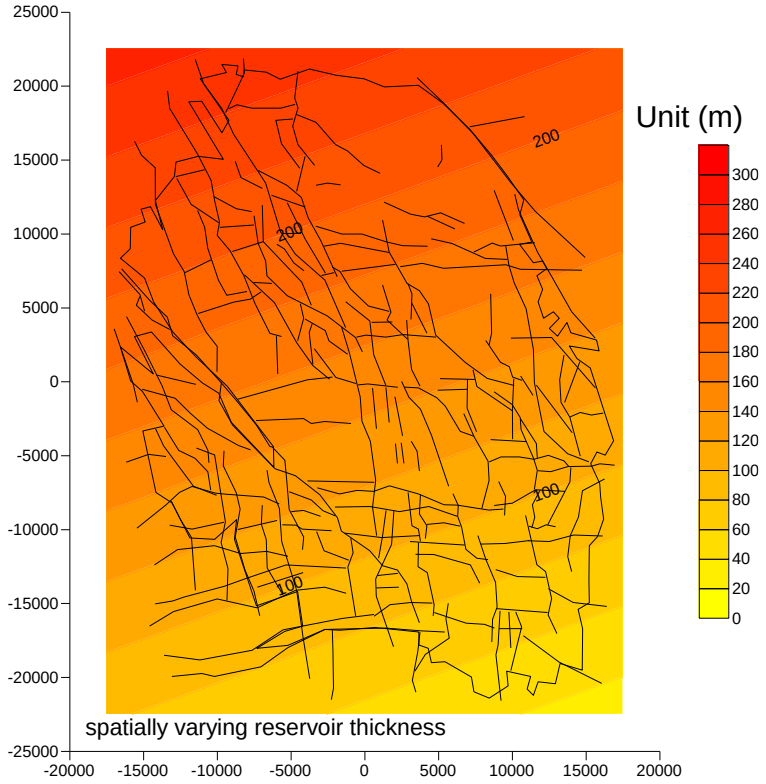

Figure 4-6: Spatially varying net reservoir thickness, showing thinner at southeast part and thicker at northwest part of the reservoir.

5. Depletion modelling

5.1. Distribution of production clusters and pressure depletion

Pressure depletion was imposed on 385 wells, or pressure depletion points shown in **Figure 5-1**. These wells were divided into six groups: East-Central (cyan dots), North (black dots), LOPPZ (Loppersum, red dots), Eemskanaal (orange dots), South-West (blue dots), and South-East (green dots). For each group, pressure decline data from field measurement shown in **Figure 5-2** and **Figure 5-3** were represented by piecewise linear functions as shown in **Figure 5-4** and **Figure 5-5**. The piecewise linear functions were generated by the several selected data points shown in the figure, and then were programmed in the PFC2D to be used as input in the depletion modelling by controlling the pressure at the nodes acting as depletion points. Depletion was simulated in the Groningen study region for 60 years from 1960. In Section 5.2, the simulated spatial evolution of pressure over time is explained in more detail.

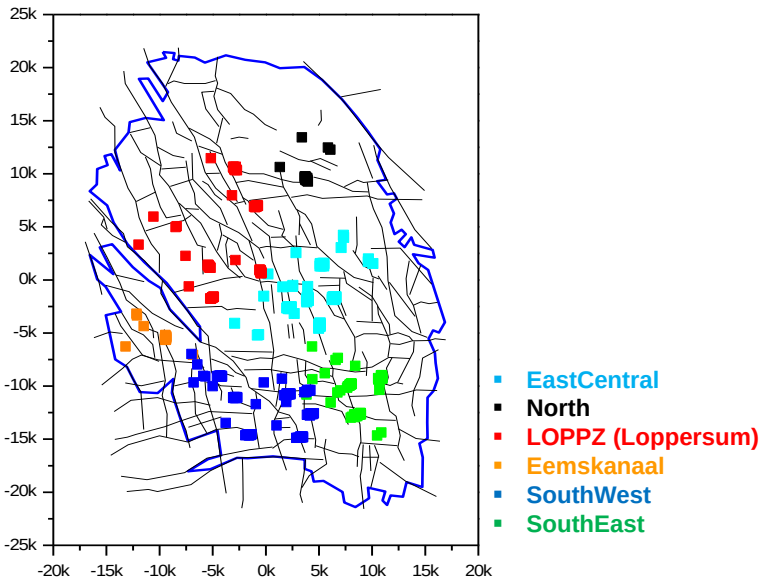

Figure 5-1: Pressure depletion points divided into six groups.

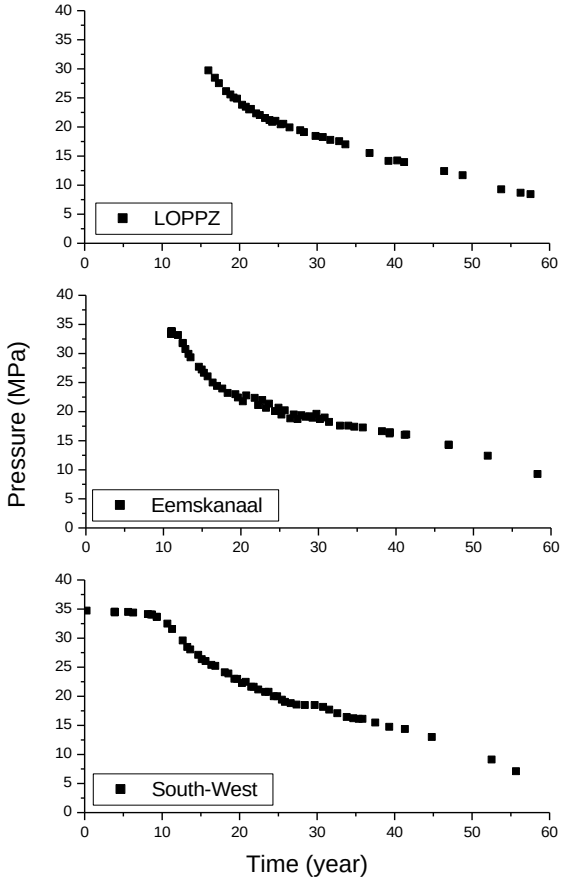

Figure 5-2: Observed changes in well pressure from 1960–2020 for the LOPPZ (Loppersum), Eemskanaal and South-West production well groups.

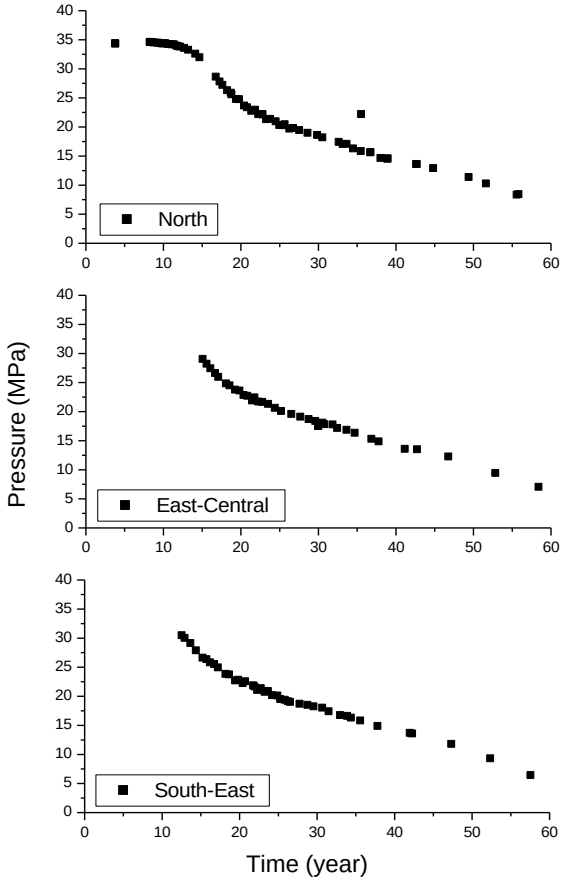

Figure 5-3: Observed changes in well pressure from 1960–2020 for the North, East-Central and South-East production well groups.

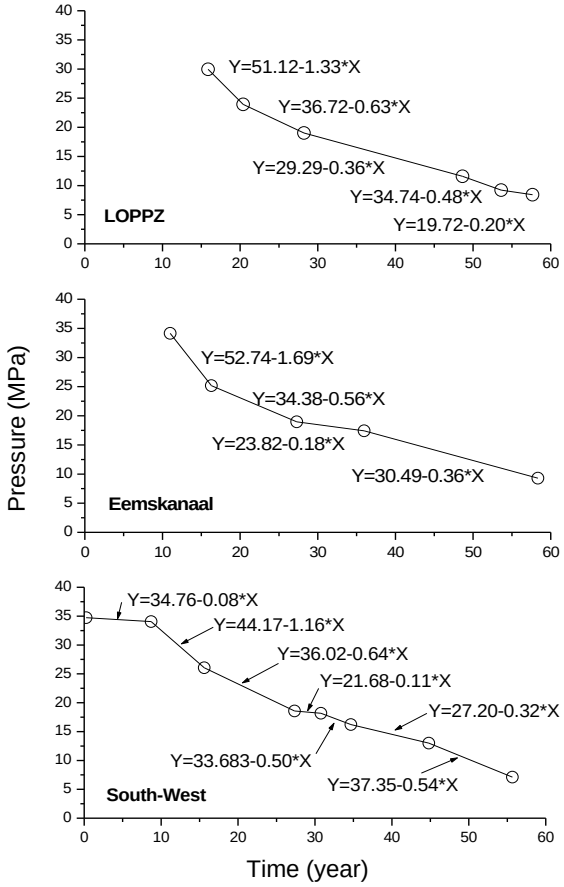

Figure 5-4: Piecewise linear functions used in the simulation of pressure changes at the LOPPZ, Eemskanaal and South-West depletion clusters. Time is displayed on the x-axis; zero corresponds to the year 1960.

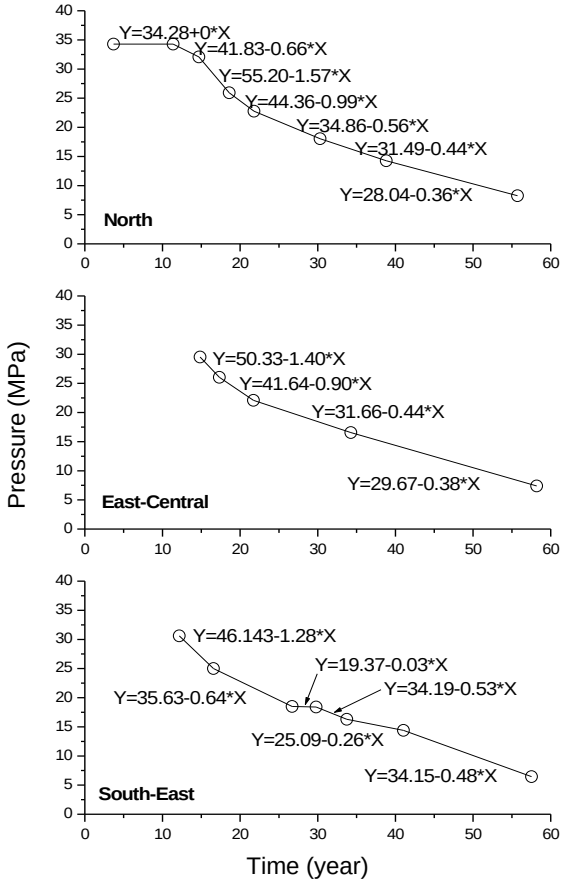

Figure 5-5: Piecewise linear functions used in the simulation of pressure changes at the North, East-Central and South-East depletion clusters. Time is displayed on the x-axis; zero corresponds to the year 1960.

5.2. Evolution of reservoir pressure and seismicity

Simulated pressure and seismic event distributions during depletion are shown in **Figure 5-6**. The figure shows pressure and seismicity evolution with 10 years interval. Pressure minima are generated by the model within the southern and central regions.

Pressure depletion starts first in the south of the reservoir, and the model demonstrates that a good spatial correlation between the seismic events and the area of pressure depletion. In 20 years of simulated depletion, a cluster of seismic events forms in the center of the reservoir. As the simulation progresses, seismicity generated by the model becomes more homogeneous over space, though a majority of events are generated near the eastern and western reservoir boundaries and within the central reservoir area. In total, 72 seismic events were generated during the depletion period. The lowest magnitude of the seismicity is ML 2.0 and the largest magnitude of the seismicity is ML 3.6.

In **Figure 5-7**, we present temporal changes in the statistics of the seismic event magnitudes. For every five years intervals, histograms of the seismic event magnitudes are generated and plotted in **Figure 5-7** with respect to time. This figure can be compared with **Figure 2-2** where the observed seismicity in Groningen gas field is shown in a form of histogram for each year, from 1990 till 2020.

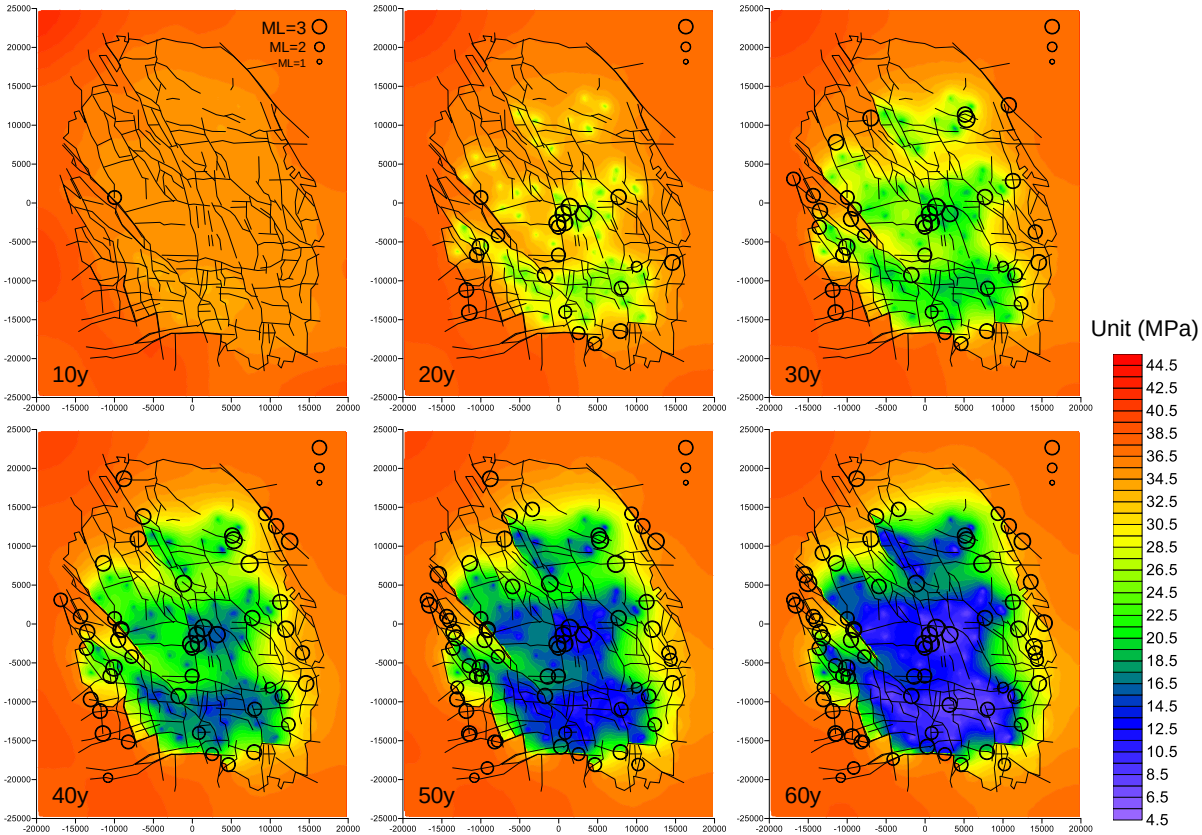

Figure 5-6: Evolution of reservoir pressure and seismicity simulated by the depletion model. Results for every 10 years after the start of simulated depletion are shown. The axes show the distance (in meters) from the center of the study region.

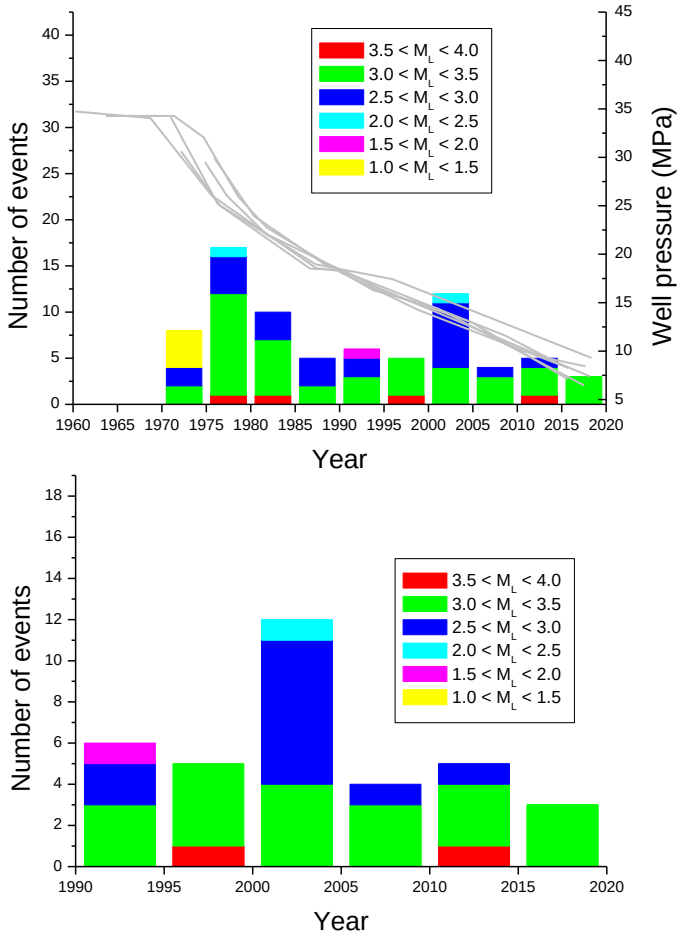

Figure 5-7: Temporal changes in the seismic event magnitude over time.

5.3. Stress analysis

Changes in local maximum and minimum horizontal stresses after 60 years of pressure depletion are shown in **Figure 5-8**.We used the measurement circle technique of PFC2D, where the measurement circle calculates areal averaged stress and strain rate in a measurement circle. In 3D, the measurement sphere calculates volumetric averages stress and strain rate in a measurement sphere. The use of measurement circles (or spheres) enables to calculate the evolution of local stress and strain fields.

Figure 5-8 shows that within the centers of these regions, the maximum horizontal stress increased up to 12–14 MPa, with particularly large areas of increased stress in the south and southeastern regions of the Groningen reservoir. Minimum horizontal stresses increased primarily in the central and southeastern regions of the reservoir for both fault models, by up to 14 MPa. The figure demonstrates that the location of intense seismicity is spatially correlated with the location where the effective stresses show large increase. **Figure 5-9** shows changes in the local stresses represented by Mohr circles. The figure shows that the stresses not only increase but also differential stress (SH,max – Sh,min) increases resulting in a bigger size Mohr circle.

Common understanding of the faulting in the Groningen reservoir is normal faulting type, where the effective vertical stress increase by the amount of reservoir pressure drop is large while the amount of effective horizontal stress increase is smaller than reservoir pressure drop due to confined horizontal reservoir. Such stress change causes enlarged Mohr circle, and eventually satisfies Mohr Coulomb failure criterion of fault.

Although this model is in 2D and does not contain vertical stress component, the Mohr circle transition shown in **Figure 5-9** demonstrates to some extent the mechanism of faulting in a depleting reservoir. One can expect that the location of large horizontal stress increase would show even larger increase in the vertical stress. In such stress evolution scenario, there is a higher chance of faults to fail.

The model being in 2D clearly has limitations, and is not capable of modelling seismicity in normal faulting mode. This may be also the reason for less number of simulated seismicity and smaller magnitudes compared to the field observed seismicity that is mostly concentrated at Loppersum region (see **Figure 2-2**).

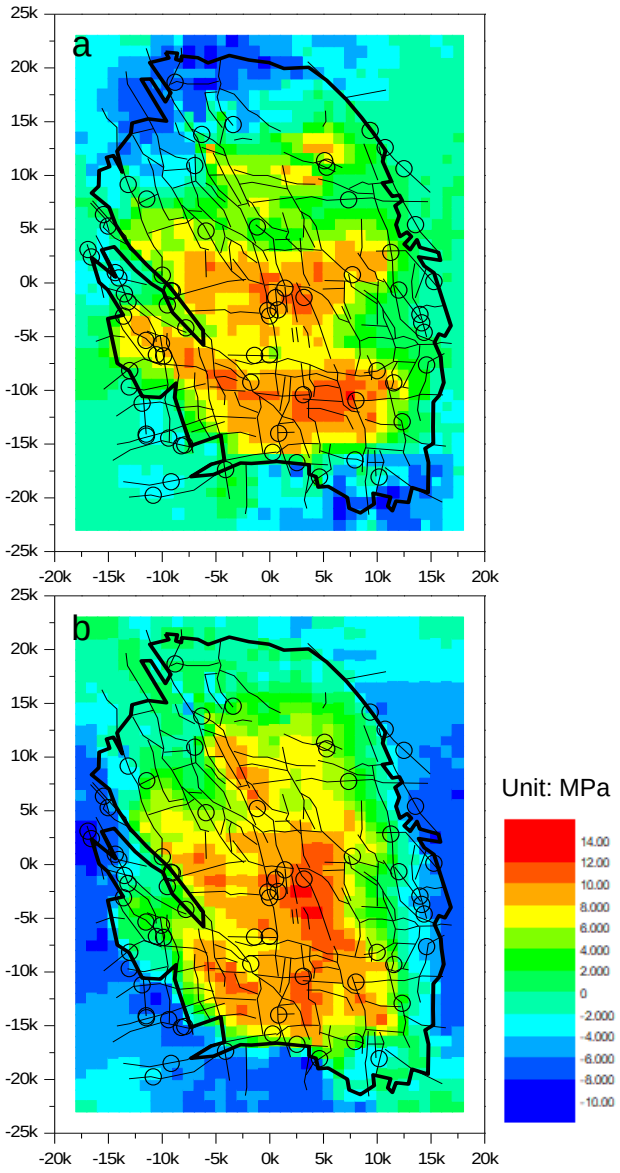

Figure 5-8: Changes in local stresses (a) maximum horizontal stress, (b) minimum horizontal stress. after 60 years of pressure depletion, simulated by the stress measurement technique in PFC2D.

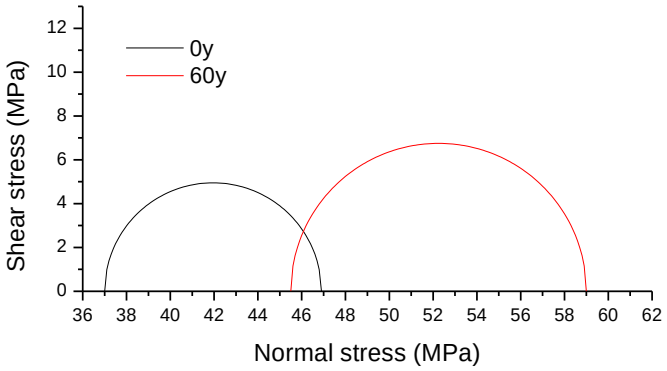

Figure 5-9: Changes in the local stresses (max horizontal and min horizontal) by Mohr stress circles.

5.4. Comparison with field observation: distribution of seismicity

In order to evaluate the consistency between the spatial distributions of the observed seismicity of which the local magnitude is larger than 2.0, as recorded by KNMI (**Figure 5-10**), and the simulated seismicity, the spatial test (S-Test) developed by the Collaboratory for the Study of Earthquake Predictability (CSEP) was applied (Zechar et al., 2010a; 2010b). The S-Test evaluates the consistency between earthquake-catalogue data (in this study, KNMI seismicity catalogue) and a seismicity forecast (in this study, PFC2D simulated seismicity), which is provided as a spatial grid containing the numbers of expected earthquakes exceeding a given magnitude threshold during a given time interval. The S-Test was applied retrospectively; that is, only pre-existing earthquake data during the overlapping time between the depletion modelling time interval (1960-2020, **Figure 5-11**) and time interval during which KNMI earthquake-catalogue data were available (1992-2020, **Figure 5-12**) were considered.

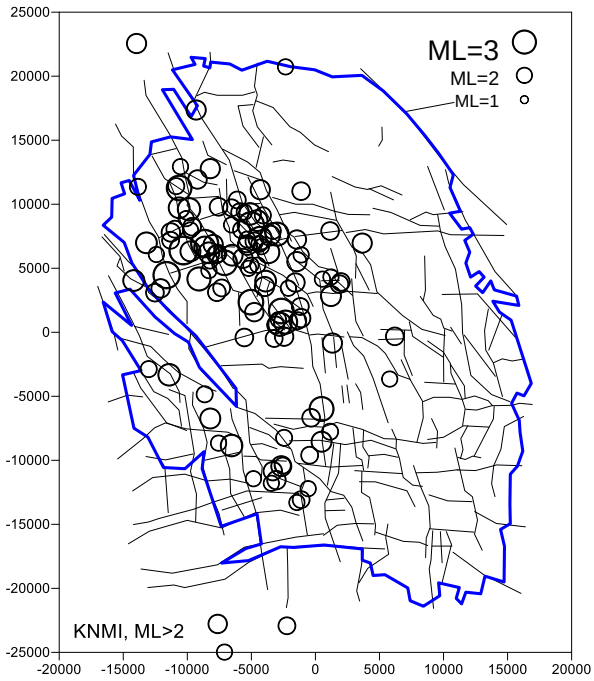

Figure 5-10: Observed seismicity in Groningen, ML ≥ 2.0 seismicity (from KNMI seismicity catalogue, www.knmi.nl).

Two smoothed-seismicity earthquake-forecast models were developed. For each forecast model, one smoothed-seismicity model was developed using PFC-generated seismic event data during the forecast period only (1992–2020), and the other model was

developed using PFC-generated seismic event data during the entire depletion period as described in Section 5.

The two models were considered in order to determine if the spatial distribution of KNMI earthquake data tended to reflect the spatial distribution of seismic events generated by the PFC2D modelling during the forecast (tested) period, the entire distribution of seismic events generated by the PFC2D modelling during the depletion period, or neither. We chose a magnitude threshold of $M_L \geq 2$ in developing both forecast models, to ensure completeness in the KNMI earthquake catalogue during the entire forecast period.

To generate the smoothed-seismicity forecasts, the Groningen study region was divided into a grid with 1 km x 1 km resolution. For each spatial bin, expected numbers of seismic events were calculated as follows:

$$\sum_{i=1}^{n} \frac{C}{r_i^2 + d^2} \quad (9)$$

where for *n* number of seismic events, the contribution from each individual seismic event to the forecasted event rate in each spatial bin was calculated. *C* is a normalization factor, to ensure that the total event rate in the study region equals the number of seismic events used to generate the forecast model. *r* is the distance from event *i* to the center of a given spatial bin, and *d* is the smoothing kernel, which was assigned a value of 5 km.

The algorithm for applying the S-test to each smoothed-seismicity forecast was conducted as follows:

1. A forecast period was defined (01.01.1992–31.12.2019 for each seismicity forecast).

2. The forecast rates are normalized such that the total number of forecasted seismic events in the study region equals the total number of observed earthquakes during the forecast period.

3. A seismicity forecast is generated from the forecast model by calculating the number of expected seismic events during the forecast period in each spatial bin.

4. The number of observed earthquakes during the forecast period (from the KNMI earthquake catalog) in each spatial bin is counted.

5. The log-likelihood for each spatial bin is calculated for the observed KNMI seismicity, based on the Poisson probability distribution:

$$L(\omega|\lambda) = \log\big(\Pr(\omega|\lambda)\big) = -\lambda + \omega\log(\lambda) - \log(\omega!) \qquad (10)$$

6. The joint log-likelihood is then calculated (for *n* spatial bins):

$$L(\Omega|\Lambda) = \sum_{i=1}^{n} L(\omega_i|\lambda_i) \qquad (11)$$

where ω is the number of observed earthquakes (from the KNMI earthquake catalog) in spatial bin *i* during the forecast period, and λ is the number of (normalized) forecasted seismic events in spatial bin *i* during the forecast period.

7. A large number of synthetic seismic event catalogs are simulated from the forecast (here, 1000 simulations were used).

8. The joint log-likelihood is calculated for each of the synthetic seismic event catalogs.

9. The observed joint log-likelihood is compared to the distribution of joint log-likelihood scores from synthetic seismic event catalogs, using the significance level α = 0.05. The quantile score ζ, or the fraction of synthetic seismic event catalogs with joint log-likelihood scores lower than the observed joint log-likelihood, is calculated. If $\zeta < 0.05$, the observed seismic events' spatial distribution is considered inconsistent with that of the forecast; otherwise, if $\zeta \geq 0.05$, the forecast is not rejected.

For the following two seismicity forecasts:

1. Depletion model, forecast developed with PFC-generated seismic events from 1992-2020, and

2. Depletion model, forecast developed with PFC-generated seismic events from 1960-2020, the S-test was applied during the forecast period.

Figure 5-10 and **Figure 5-11** display expected numbers of seismic events for each forecast, based on the respective depletion models and time windows during which simulated seismic event data were used in forecast model development. The pink circles represent PFC-generated seismicity that were used to develop the forecast model, whereas the white circles show locations of observed earthquakes (from the KNMI catalog) during the forecast period.

Both seismicity forecasts passed the S-Test ($\zeta \geq 0.05$), indicating that the spatial distributions of the observed earthquakes and seismic events generated through PFC2D depletion modelling were

consistent at the $M_L \geq 2.0$ threshold with the spatial distribution of KNMI earthquake-catalog data during the forecast time period.

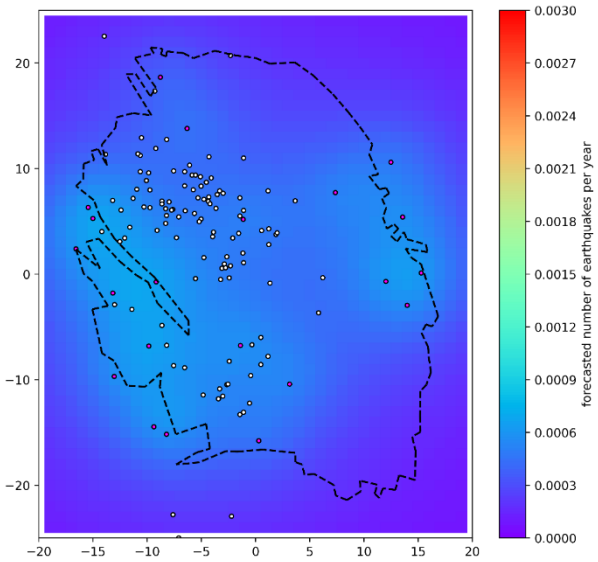

Figure 5-11: Smoothed-seismicity forecast, using the seismicity generated by PFC2D during 1992–2020. The grid shows the expected numbers of forecasted earthquakes. Pink circles display the locations of PFC-generated earthquakes that were used to develop the forecast model, while white circles show locations of observed earthquakes from the KNMI catalog that occurred during the forecast period. The axes show the distance (in kilometers) from the center of the study region.

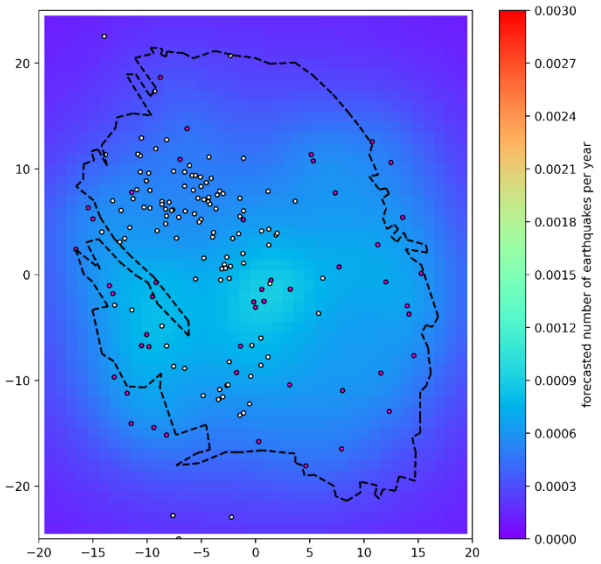

Figure 5-12: Smoothed-seismicity forecast, using seismicity generated by PFC2D during 1960–2020. The grid shows the expected numbers of forecasted earthquakes. Pink circles display the locations of PFC-generated earthquakes that were used to develop the forecast model, while white circles show locations of observed earthquakes from the KNMI catalog that occurred during the forecast period. The axes show the distance (in kilometers) from the center of the study region.

5.5. Comparison with field observation: distribution of reservoir pressure

In addition to the seismicity comparison between the observed and the simulation, we also investigated the spatial correlation between the observed and the simulated reservoir pressure distribution. In **Figure 5-13**, we present two sets of reservoir pressure distribution. The upper figures are from the 3D reservoir model of NAM (constructed from field measurements) at three selected time, year 1980, 2000, 2020. The bottom figures are from the PFC2D depletion modelling at the same three selected time.

There appears a significant discrepancy between the two results, showing that the simulated pressure distribution is highly inhomogeneous and far lower in terms of pressure magnitude. This finding may suggest that the one possible reason for the discrepancy in the seismicity pattern could be the mismatching reservoir pressure distribution. One possible solution for a better matching might be increasing the reservoir permeability by an order of magnitude and making the reservoir fault more conductive to further enhance the pressure diffusion inside the reservoir. However, further calibrating the model for better matching of the seismicity and reservoir pressure is suggested as a follow-up study after having more data for the Groningen reservoir and geological fault structure.

Another discrepancy to note is the reservoir boundary. In the PFC2D modelling, the reservoir boundary (denoted by black polygon) is treated as an impermeable boundary in order to avoid pressure communication between the interior and exterior of the reservoir. Looking at the observed pressure distribution, it seems that the impermeable boundary exists mostly at the west and north ends of the reservoir, whereas the reservoir is open at the east and south ends of the reservoir. This finding may suggest that the Groningen gas reservoir may not be a closed system, but partly an open system. Further modelling work includes this issue, as boundary condition may have significant effect on the instability of such highly complex fault system.

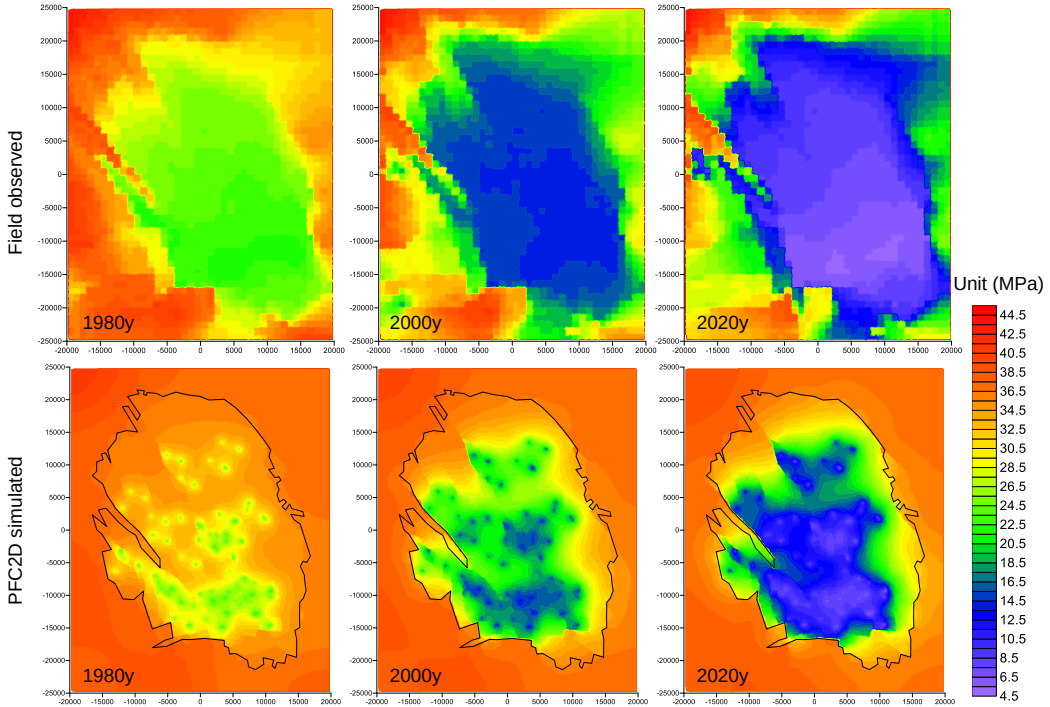

Figure 5-13: Distribution of reservoir pressure, (upper) observed and (bottom) simulated by PFC2D depletion modelling.

5.6. Summary and discussion

Figure 5-14 shows temporal distribution of the seismicity. Black dots are the seismicity data taken from KNMI data set of which the ML is larger than 2. The orange dots are the simulated seismic events by PFC2D depletion modelling. It should be noted that the magnitudes of the simulated seismic events are those further processed by taking into account of the location of the events and the thickness of the reservoir at the corresponding location (see Section 4.2 Model assumption). We plotted only those seismicity after 1990, as KNMI seismicity data set is only available after 1990.

During the time period of 1990-2005, the observed seismicity tends to show relatively lower range of magnitude. However, starting form 2005, the magnitude of the observed seismicity rises to ML larger than 3.0. The figure shows that the time when the max ML seismic event is simulated is reasonably well correlated to the time of max ML observed seismicity. Table 5-1 compares the number of seismicity, maximum ML of the PFC2D simulated and KNMI seismicity.

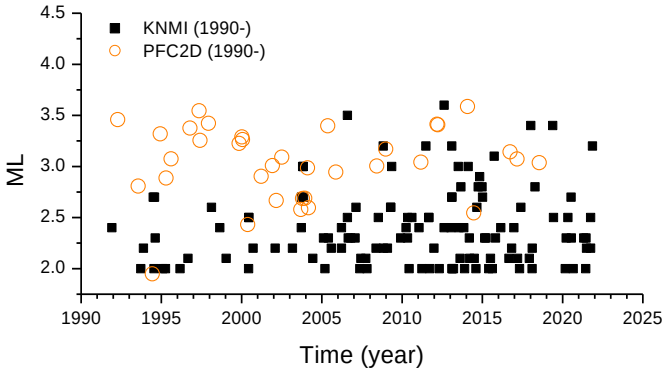

Figure 5-14: Temporal distributions of the observed seismicity (black dots, KNMI data set) and the simulated seismic events (orange dots, PFC2D depletion modelling)

Table 5-1: Numbers of seismic events generated from the depletion model above local magnitude thresholds ML 2.0 and the max ML and its occurrence time in year.

	PFC2D depletion modelled seismicity	KNMI observed seismicity
# seismic events, ML>2	35	123
Max ML	3.6	3.6
Occurrence year	2014	2012

The modelled seismicity, by contrast, includes more events along the west reservoir boundary. This may be due to the large modelled pressure gradient between the interior and exterior of the reservoir. Occurrence of smooth joint failures at this location is interpreted as reasonable from a geomechanics modelling perspective, as large pressure differences would enhance shear stress along the smooth joints, leading to failure, following the Mohr Coulomb failure criterion. Moreover, the faults are lined sub-parallel to the orientation of the maximum horizontal stress, putting the faults into unstable state under the given initial stress field.

The dissimilarity might be mostly due to:

i) the different dimensionality (2D in the model vs. 3D in reality). The 3D stress state in Groningen encourages normal faulting, where the vertical stress is larger than the horizontal stresses. Therefore, many of the observed seismic events show normal faulting. However, focal mechanism studies of the Groningen seismicity demonstrate that there are also seismic events showing strike-slip faulting, especially at fault junctions (Willacy et al., 2019). Focal mechanisms for earthquakes from 2015–2018 indicate a combination of normal and strike-slip faulting. Willacy et al. (2019) performed a full waveform inversion of Groningen seismicity from 2015–2018, finding that normal faulting is most common along faults, though strike-slip faulting is also present at fault junctions. The simulated seismicity, due to the 2D nature of the model, can be treated as strike-slip faulting, and

ii) the fact that the reservoir rock matrix is treated as an elastic medium where the strength of the bonds at the particle contacting points are set high. Only the failure (in

tensile and shear mechanicsms) is allowed at the smooth joint contacts, representing the reservoir fault. If the reservoir rock matrix failure is modelled, those rock failures would be registered as seismic events. As the model runs in fully dynamic mode, meaning that one bond failure radiates seismic wave, it could trigger another bond failure within a close time and space window, which can eventually produce more seismic events.

6. Shut-in modelling

6.1. Description of shut-in scenarios

Each “shut-in” scenario refers to a period of time following depletion where the wells are deactivated, allowing pressure to gradually recover and redistribute over time. In the modelling, this was technically done by freeing the pressure at the node of injection to which the depletion pressure vs. time functions (shown in **Figure 5-4** and **Figure 5-5**) were assigned. In this way, well shut-in was simulated.

The objectives of the shut-in modelling are:

- To see how the reservoir pressure would evolve in time and space in the entire Groningen reservoir field after depletion stopped

- To see if additional seismic events would generate in the entire Groningen reservoir field during pressure redistribution

The following shut-in scenarios are included in this study:

- Shut-in scenario 1: depletion runs for entire 60-year duration (1960–2020); shut-in runs for 30 years (2020–2050)

- Shut-in scenario 2: depletion runs for first 50 years of production period (1960–2010); shut-in runs for 30 years (2010–2040)

The shut-in model results serve also to compare with injection scenarios in Section 8, to see if the seismic events occurring during the 30 years of pressure redistribution could be mitigated by applying injection at specific well clusters, as pressure maintenance scenarios. The injection scenarios are detailed in Sections 8 and 9.

Reservoir pressure evolution during the shut-in model period is shown in **Figure 6-1** (shut-in scenario 1) and **Figure 6-2** (shut-in scenario 2), respectively. Just as in the depletion modelling, the simulated seismicity, i.e., smooth joint contact failure, is shown in the figures.

6.2. Evolution of reservoir pressure and seismicity

6.2.1. Shut-in scenario 1

Figure 6-1 displays in 10-year interval the reservoir pressure and seismicity distributions during 30 years of shut-in, reaching year 2050.

Fewer seismic events were generated by the model during the shut-in period compared to the depletion period; four seismic events were simulated over the 30-year shut-in period, with the largest magnitude being M_L 2.3. This event was generated within the southwestern area of the reservoir.

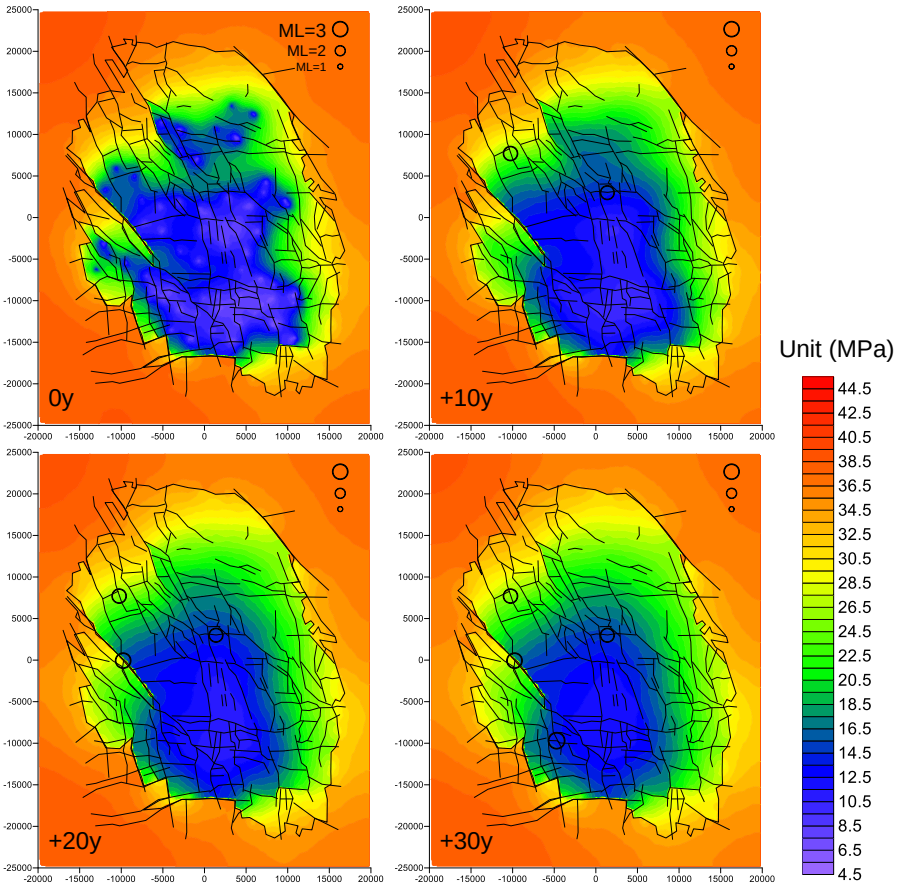

Figure 6-1: Evolution of reservoir pressure and seismicity in shut-in scenario 1. Results for every 10 years after the start of simulated shut-in are shown. The axes show the distance (in meters) from the center of the study region.

6.2.2. Shut-in scenario 2

The evolution of reservoir pressure and seismicity when applying 30 years of shut-in following 50 years of depletion was similar to the previous scenario, in that a gradual, spatially-homogeneous pressure redistribution was modelled (**Figure 6-2**). In total, three seismic events were generated. Of these three events, the largest magnitude was M_L 2.2. This event was generated within the southern area of the reservoir.

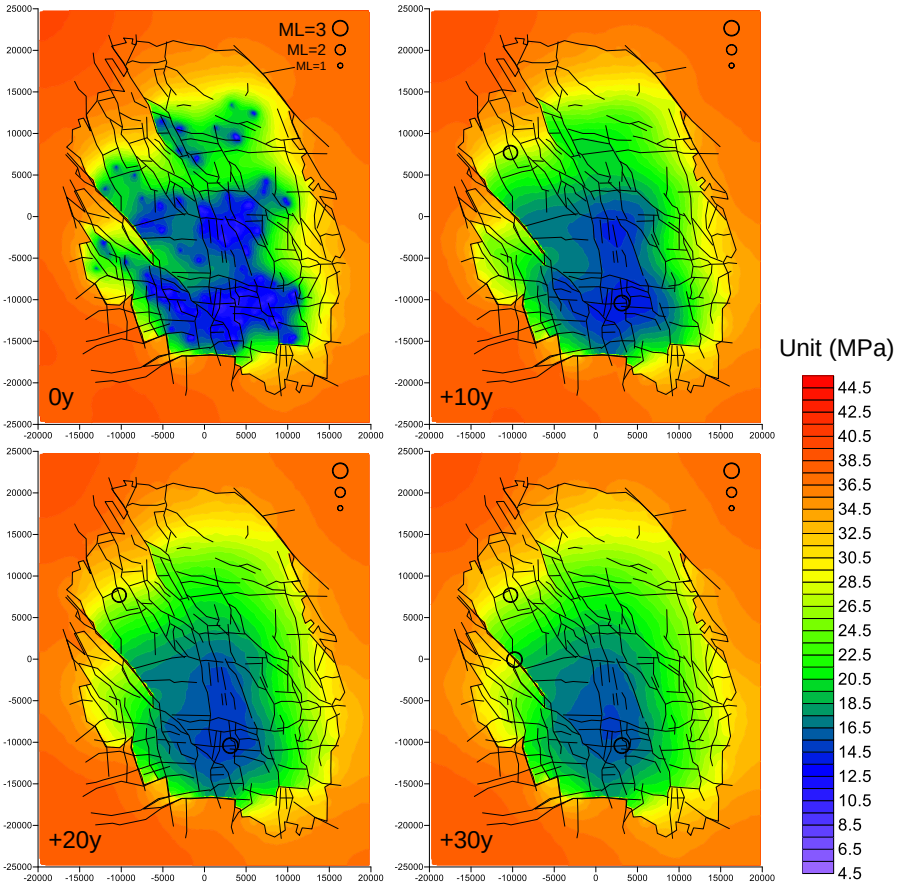

Figure 6-2: Evolution of reservoir pressure and seismicity in shut-in scenario 2. Results for every 10 years after the start of simulated shut-in are shown. The axes show the distance (in meters) from the center of the study region.

6.3. Summary and discussion

Figures 6-3 displays seismicity magnitudes plotted over time during depletion and shut-in for each shut-in scenario. The red lines indicate the times at which shut-in begins. In both plots, considerably fewer seismic events were simulated during the shut-in period, compared to the depletion period. This indicates that the first measure to take to lower the seismicity occurrence is to stop production.

However, the modelling results also indicate that seismic events could occur even after depletion stopped, while the inhomogeneous pressure distribution generated by the long term depletion changes to balance the pressure between the highly depleted and less depleted regions in the reservoir.

Comparing shut-in scenario 2 with scenario 1 demonstrates that seismicity rate could further have been reduced by stopping production earlier than year 2020, before reservoir pressure becomes highly inhomogeneous.

Table 6-1 displays seismic event magnitude statistics for each shut-in scenario.

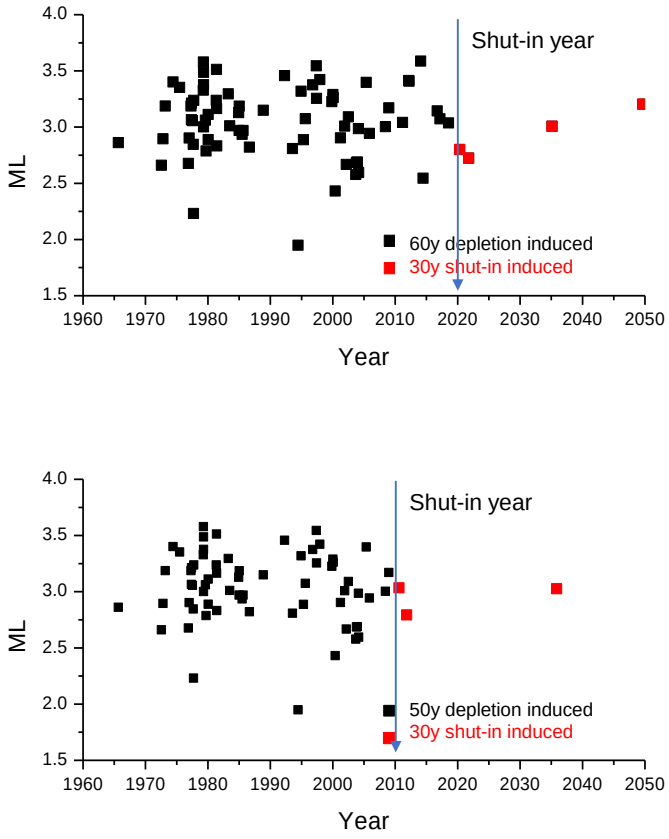

Figure 6-3: ML of simulated seismic events plotted against time, (top) shut-in scenario 1, (bottom) shut-in scenario 2. The vertical line denotes the shut-in year.

Table 6-1: Numbers of seismic events ML larger than 2.0 and the max ML for each shut-in scenario.

	Shut-in scenario 1	Shut-in scenario 2
No. seismic events	4	3
Max ML	3.2	3.0

7. Pressure rise estimation using TOUGH3 modelling

7.1. TOUGH3 model

The numerical tool TOUGH3 (Jung et al., 2018) used in this study is a general purpose numerical solver for multi-component, multi-phase fluid flow in porous media. It leverages on the EOS7C module, **Figure 7-1**, (Oldenburg, 2004), a module developed to solve for the equation of state of five components, namely water, brine, a non-condensable gas (NCG, the gas is either CO_2 or N_2), a tracer component and methane. Each component can exist in both gas and aqueous phase. The non-condensable term refers to the fact that the NCG component cannot condensate to the pure liquid or solid state, but the code evaluates the dissolution of the gas component in the aqueous phase is evaluated.

Density, enthalpy and viscosity are calculated by means of the Peng-Robinson equation of state, while the partitioning of the NCG and CH_4 between the aqueous and gas phases is calculated using a chemical equilibrium approach.

This tool allows to model flow and transport of a gas mixture of NCG and CH_4 (either CO_2 or N_2), with or without the presence of an aqueous phase and H2O vapor, by employing a Darcy's law for multiphase flow and a Fickian diffusion law.

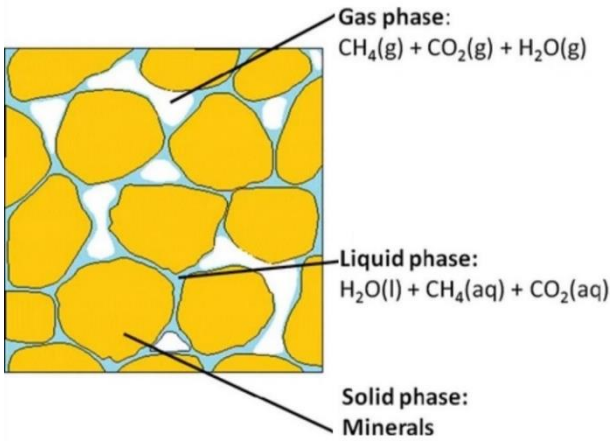

Figure 7-1: EOS7C module representation, considering CO_2 as the NCG gas component (Hou et al., 2012)

7.2. Model description

The grid to represent the depleted CH_4-reservoir composed of two compartments separated by a fault has been set-up with the tool MeshMaker (Moridis, 2016). The numerical model properties have been derived from published reports regarding pressure depletion dynamics (Burkitov, 2015) and pressure maintenance study (NAM 2016). The scenario presented here is the injection of a non-condensable gas in a depleted reservoir composed of two compartments having thickness of 200 meters, being separated by an impermeable fault and with a vertical offset of 100 m (the centers of the compartment is at a depth of 3000 m and of 2900 m). The overburden is assumed to act as a good sealing rock, with low permeability and high gas pressure entry, to avoid leakage of gas. The lateral boundaries are assumed close, therefore the only re-pressurization of the depleted reservoir may come from the injection of fluids. In **Figure 7-2** a sketch of the model is visible. The model has an extension of 2500 m x 1000 m. The model is composed of the 3 main horizontal layers with a vertical offset of 100 m across the fault (with tones of blue), of top and bottom boundaries as well of the units composing the fault core and the fault damage zone (orange colors). Properties of the model are provided in Appendix B of this report.

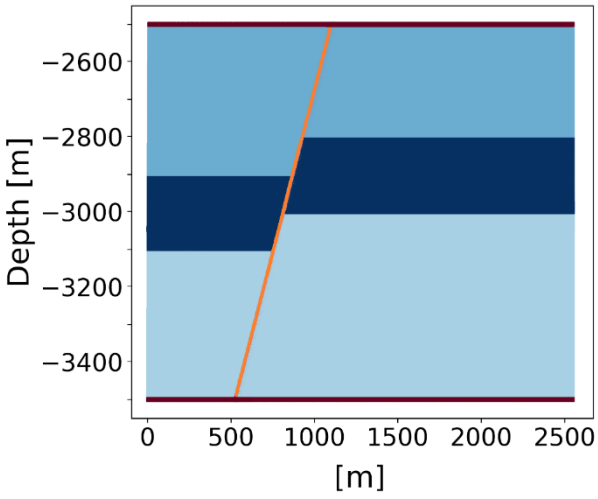

Figure 7-2: Sketch of the computational domain (not to scale). Colors refers to different logical groups defined. The orange line represents the fault, from top to bottom different colors corresponds respectively to: top boundary condition, overburden, reservoir underburden, Bottom boundary connection.

The model is initialized as water saturated. An initial run is then performed, to achieve conditions similar to the reservoir conditions before the start of the production. To achieve these conditions, the damage zone of the fault has been set to higher permeability values (up to a depth corresponding to the top of the corresponding reservoir) and a constant concentration source of CH_4 has been initialized at the bottom boundary of the model. In this way, the CH4 migrates from the source to the reservoir. The model has been run to reach the target saturation and pressure in the reservoir (**Figure 7-3**).

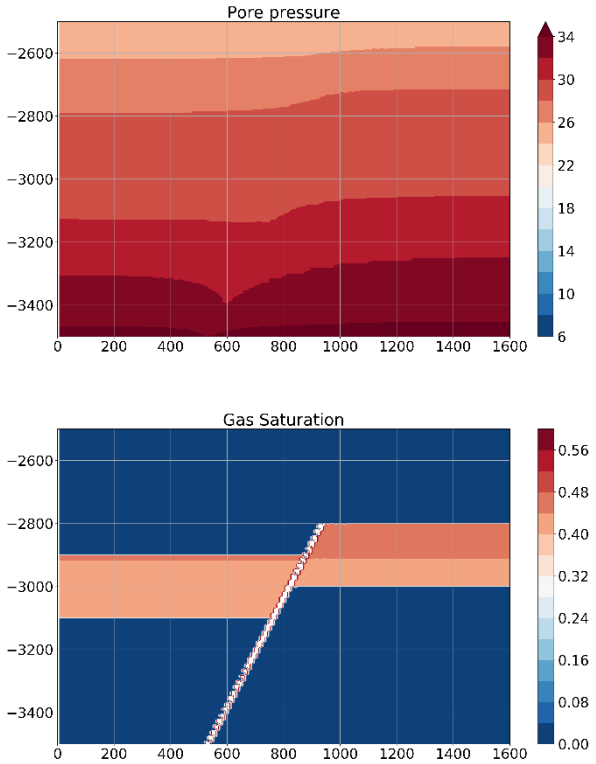

Figure 7-3: Initial condition of the reservoir. Thin crossed lines are guidelines for visual reference.

7.2. Model results

After reaching the initial condition shown in **Figure 7-3**, the CH4 source term has been removed, the fault damage zone has been reinitialized as water saturated and with hydrostatic condition. A new steady state is then computed. A pair of wells is then set-up, to reproduce the gas production phase. The goal of this phase was to achieve realistic initial conditions for the successive reinjection phase. The gas production is simulated until the pressure drop in the reservoir is seemed representative of the real, post gas-production, reservoir conditions, reaching a pressure in the reservoir of 60 bar. **Figure 7-4** shows the pore pressure and gas saturation at this state.

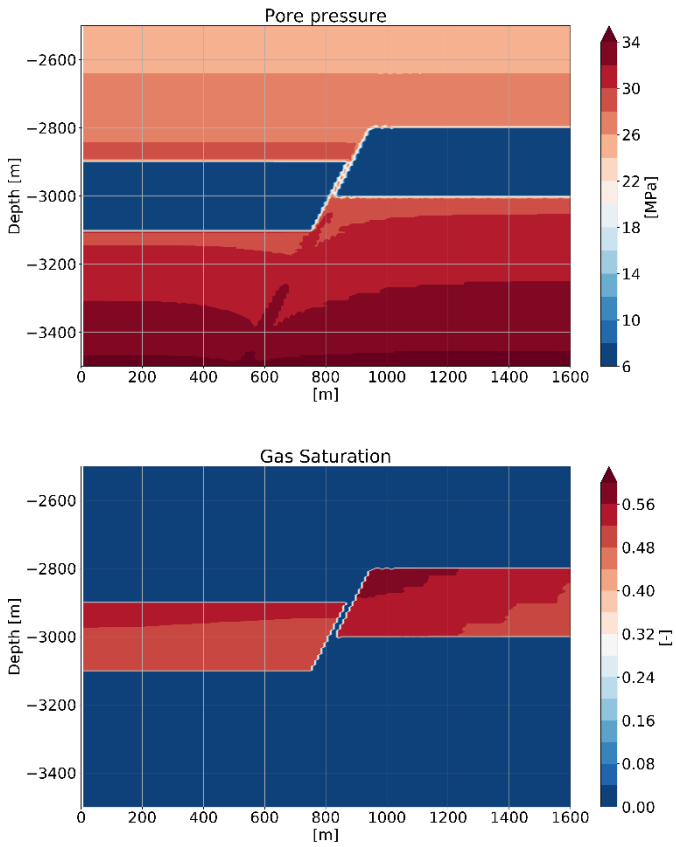

Figure 7-4: Pressure (MPa) and gas saturation distribution at the end of the production phase.

The last step is the injection of gas to reestablish the pressure to a target pressure of 300 bar. The injection is modelled as a constant mass rate injection at the left compartment (231 m, -3025 m). The injection points are denoted by dots in **Figure 7-5** and Figure 7-6. The

injection rate in the left compartment is 2365 ton/year/m (the injection must be scaled with respect to the third dimension, therefore the meter unit).

Two independent scenarios have been modelled, with the injected non-condensable gas being N2 or CO2.

7.2.1. N2 injection

Pressure re-equilibration with the injection of N2 takes place rapidly, see **Figure 7-5** for the evolution after respectively 7.5 and 15 years. The injection of NCG raise the pressure in the compartments, while at the same time perturbating the saturation in different parts of the compartments. The complex pattern of the pressure in the proximity of the bottom of the model, along the fault, is not affecting the results since the permeability is eight order of magnitude smaller with respect to the reservoir permeability, therefore there are no changes for the time span of few decades here analyzed.

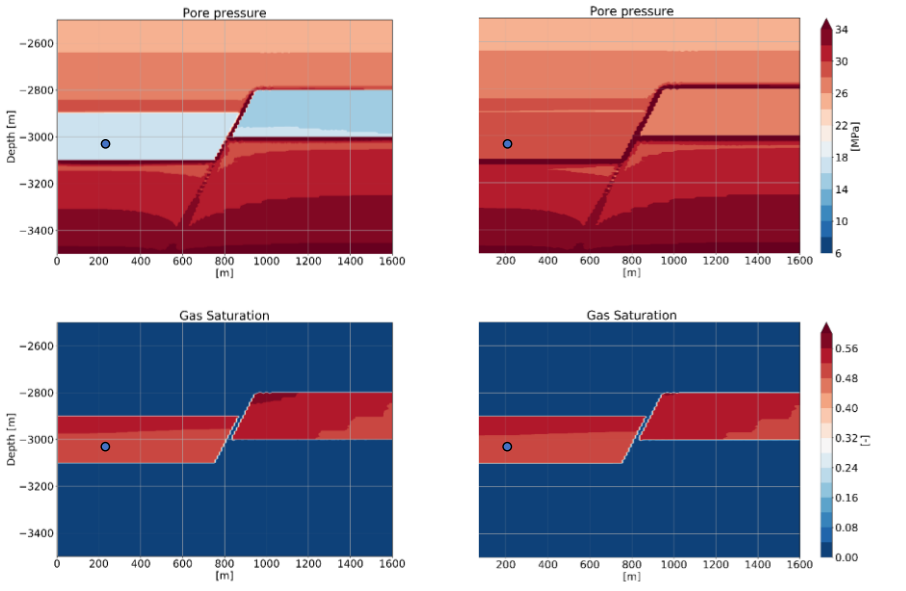

Figure 7-5: State after 7.5 years and 15 years of N2 injection. Dots are injection points.

7.2.2. CO2 injection

For CO2 injection case, **Figure 7-6** shows the state after 7.5 and 47 years of CO2 injection. The figures are qualitative similar to the figures representing the injection of N2. The difference is in the time: the smaller compressibility of N2 and the dissolution into liquid water of part of the injected CO2 slow down the pressure recovery in case of injection with CO2.

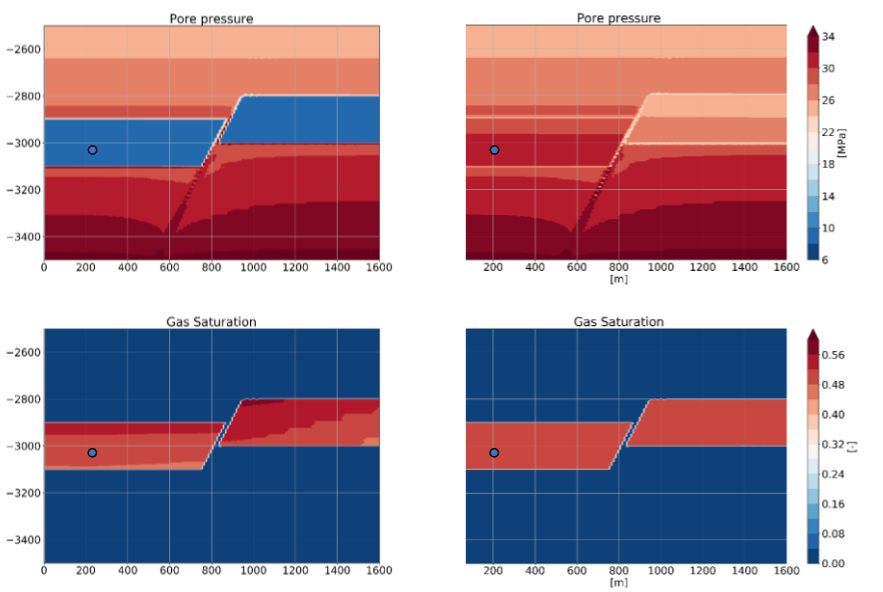

Figure 7-6: State after 7.5 years and 47 years injection of CO2. Dots are injection points.

7.3. Summary

The two injection scenarios resulted in a markedly different time evolution of pressure inside the reservoir. A comparison of pressure evolution for a point located in the left reservoir is presented in **Figure 7-7**. In this figure, the pressure evolutions due to different NCG injected are compared. For the injection of N2, the slope is almost constant or slightly steeper after 10 years, while the pressure during injection of CO2 at constant rate shows more variability. The target pressure of 300 bars in the reservoir is reached after 15 years of N2 injection and after 47 years of CO2 injection. Since the amount of mass injected is constant and the pressure perturbation takes on the order of days/weeks to equilibrate, the variations depend on the different compressibility at different pressure.

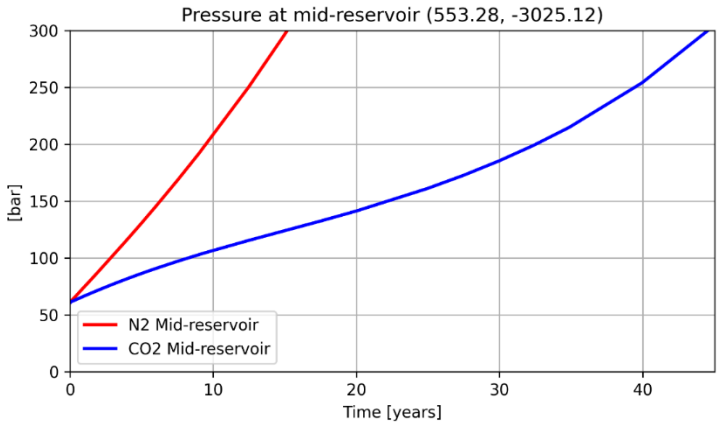

Figure 7-7: Pressure evolution comparison, until the pressure reaches 300 bar.

The dissolved mass ratio of N2 and CO2 in the liquid phase is plotted in **Figure 7-8**. The mass fraction of NCG gas dissolved in the liquid phase is about 4% in case of CO2 injection (blue broken curve) after 5 years, while for the injection of N2 it is less than 0.5% (red broken curve). This means that a relatively large mass of CO2 is readily dissolved in the liquid, not contributing to the pressure re-equilibration of the reservoir.

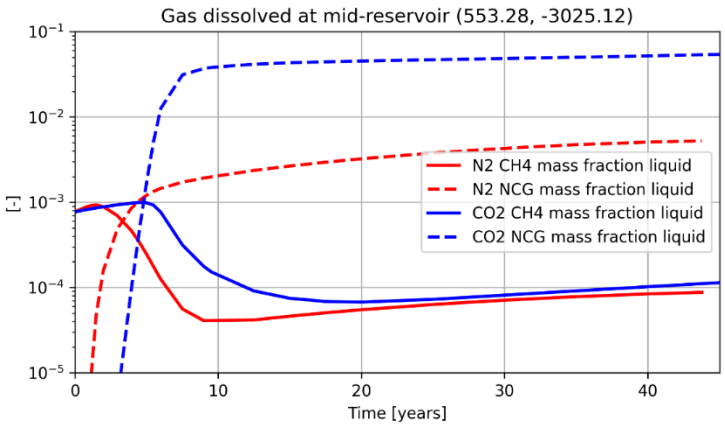

Figure 7-8: Liquid mass fraction of dissolved gas. Logarithmic scale.

The mass rate injection is the same for the two scenarios, but the pressure re-equilibration with CO2 is markedly slower with respect to N2 injection. Although N2 has a higher viscosity than CO2 at in-situ conditions, the permeability of the reservoir is high enough to guarantee that pressure redistribution is taking place in a relatively short time (in the order of days to months, being quicker for the less viscous and less dense N2) and pressure difference between CO2 and N2 injections are not due to local hydraulic effects. The discrepancy in pressure evolution can be attributed to N2 being stiffer (less compressible) than CO2. Additionally, a larger mass of CO2 is dissolved into the liquid phase, with respect to N2.

The same mass of gas will lead to different pressure changes due to reservoir conditions and due to its capability of dissolving or displacing water. Different injected gas will produce different pressurization rates. Even if the same volume (at in-situ conditions) of a substance in gas form is injected in the reservoir, the easier the dissolution of the substance in water, the smaller the pressurization rate will be.

The pressure increasing rates obtained in the TOUGH3 modelling and presented in **Figure 7-7** were mathematically formulated and programmed in the PFC2D modelling for simulation of CO_2 and N_2 injection induced seismicity. This is presented in Section 8.

8. Injection modelling

8.1. Description of injection scenarios

In this section, we demonstrate how the seismicity simulated in the shut-in scenarios could change and possibly be mitigated by controlling the pressure evolution at certain cluster locations under two assumed injection scenarios: CO_2 injection and N_2 injection, in a depleted gas reservoir after 60 years of depletion.

For demonstrative purposes, we chose the East-Central (EC) cluster to control the pressure evolution by means of simulated injection of CO_2 and N_2. The EC cluster was chosen because of the limited distance to the center of the reservoir; it is distant from the most critical region (Loppersum); it is distant from the south of the reservoir where gas production continued.

The following injection scenarios are simulated:

- Scenario 1: CO_2 injection at EC cluster for 15 years followed by 15 years of shut-in, after 60 years of pressure depletion, while shut-in maintains at all other clusters

- Scenario 2: N_2 injection at EC cluster for 15 years followed by 15 years of shut-in, after 60 years of pressure depletion, while shut-in maintains at all other clusters

8.2. Evolution of reservoir pressure and seismicity by CO_2 injection

In injection scenario 1, simulated CO_2 injection was applied to the EC well cluster for 15 years following 60 years of simulated depletion. 15 years of simulated shut-in was applied to the EC cluster after injection (see **Figure 5-1** for well cluster locations); simulated shut-in was applied to all other well clusters following depletion.

Figure 8-1 shows modelled pressure and seismicity distributions after the combined injection and shut-in periods.

Four seismic events occurred during the injection period, and one seismic event occurred during shut-in. The largest simulated seismic event had a magnitude of ML 3.2.

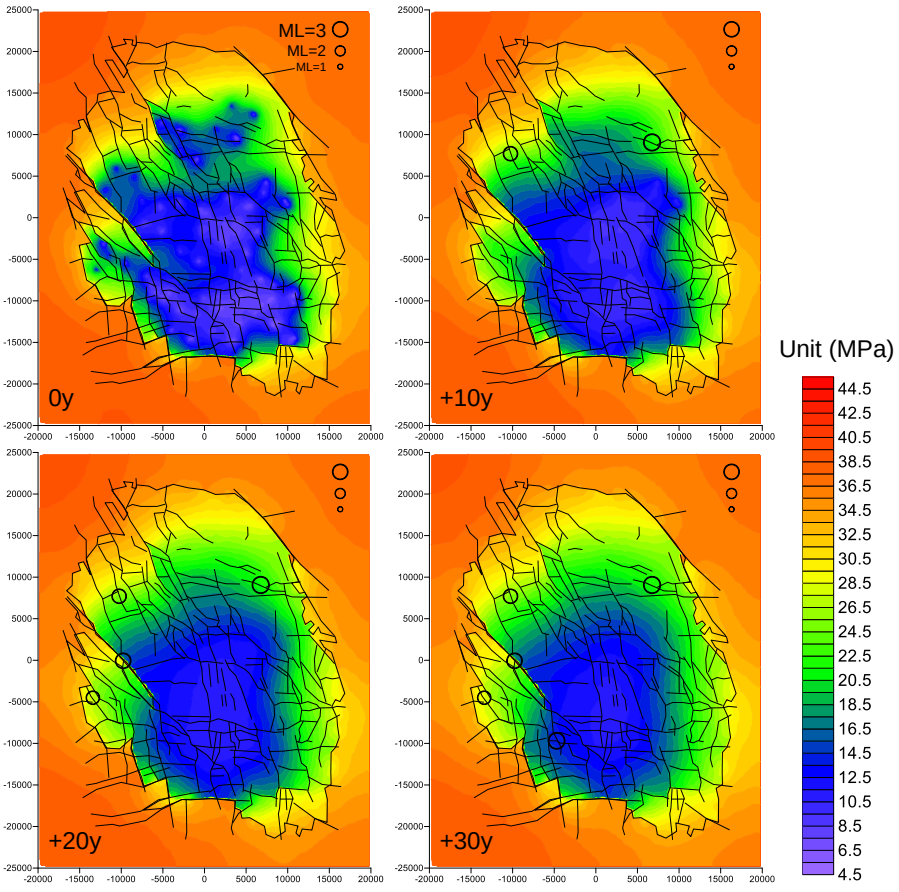

Figure 8-1: Evolution of reservoir pressure and seismicity generated by injection scenario 1. Results for every 10 years after the start of simulated injection are shown.

8.3. Evolution of reservoir pressure and seismicity by N_2 injection

In injection scenario 2, N_2 was injected into the EC well cluster for 15 years following 60 years of depletion. All other well clusters immediately entered shut-in following depletion; 15 years of shut-in were applied to the EC cluster following N_2 injection. **Figure 8-2** displays the pressure and seismicity distribution after the combined injection and shut-in periods. Unlike in scenario 1 where the pressure rise is very small, in scenario 2, pressure increased rapidly within the east-central area of the reservoir.

Five seismic events were generated during injection, while two seismic events were generated during shut-in. All of these events were located in the northern half of the reservoir, and all but one was located near the low-pressure depletion zone border to the northwest. The largest seismic event simulated had a magnitude ML 3.7.

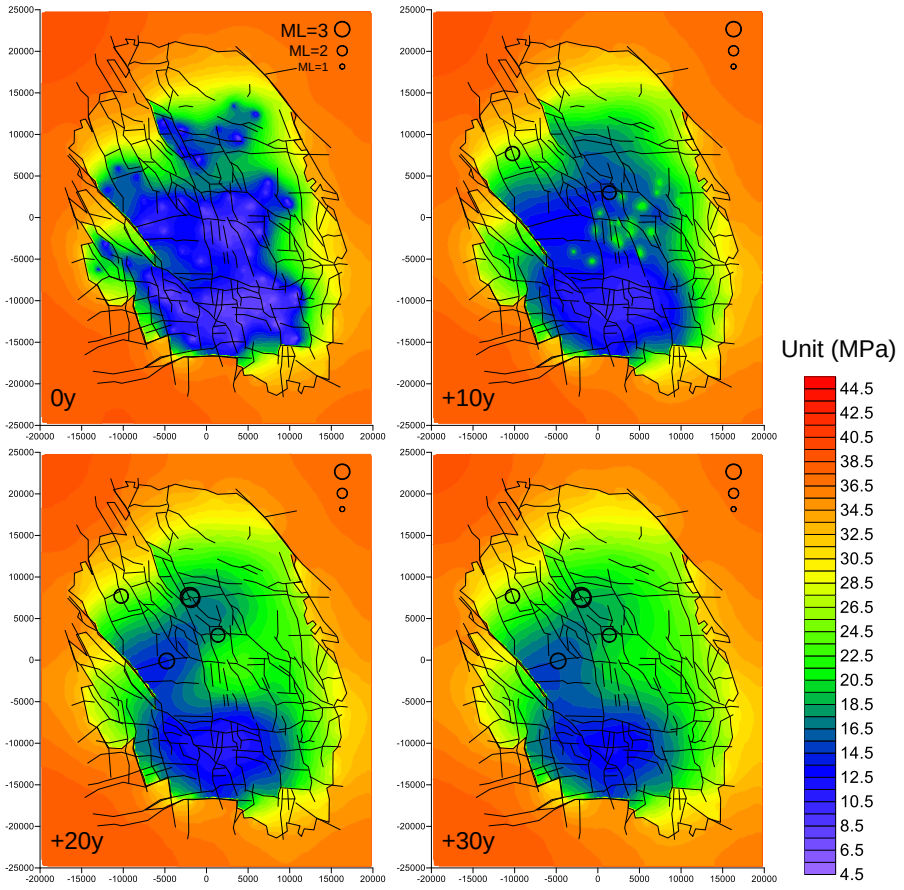

Figure 8-2: Evolution of reservoir pressure and seismicity generated by injection scenario 2. Results for every 10 years after the start of simulated injection are shown.

8.4. Discussion and summary

Figure 8-3 compares simulated pressure and seismicity distributions at the end of the combined injection and shut-in periods. Same number of seismic events were generated for both injection scenarios 1 and 2 (see **Table 8-1**). However, the maximum magnitude of the induced seismic events is different. For CO2 injection the max ML is 3.2 and for N2 injection the max ML is 3.7. Another significant difference is that, in case of CO2 injection the pressure rise due to injection is negligible due to the fact that CO2 dissolves more into the reservoir fluid, and the pressure distribution during injection is homogeneous, and the seismic events tends to occur at relatively at far-field from the injection. In case of N2 injection, the pressure rise is relatively fast due to the nature of N2 that it does not dissolve in the reservoir fluid. During injection, there appears highly concentrated pressure increase, and the seismic events tends to occur at relatively at near-field from the injection.

Table 8-1: Comparison between the shut-in model, and the two injection (CO2 and N2) models.

	Shut-in model* (30 years)	CO2 injection (15y injection + 15y shut-in)	N2 injection (15y injection + 15y shut-in)
No. seismic events	4	5	5
Max ML	3.2	3.2	3.7

* Shut-in scenario 1 (see Section 6)

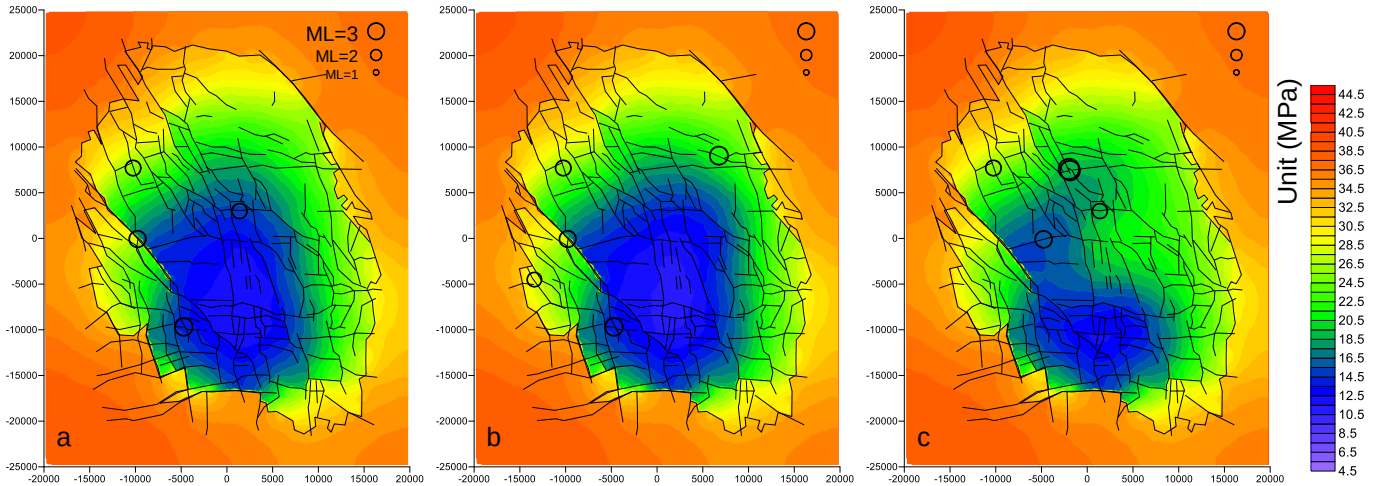

Figure 8-3: Reservoir pressure and seismic events (a) after 30 years of shut-in of all clusters, (b) after 15 years of CO2 injection and 15 years of shut-in at EC cluster, (c) after 15 years of N2 injection and 15 years of shut-in at EC cluster.

9. “What-if” injection modelling

9.1. Description of “what-if” injection scenarios

Simulated N2 injection is applied from the results of Section 8, showing that N2 injection is more efficient compared to $CO2_2$ injection for the purpose of pressure maintenance.

In this section, we simulated four “what-if” injection scenarios. **Figure 9-1** displays the schematics of the four tested “what-if” injection scenarios.

- Scenario 1: After 50 years of depletion (assuming that gas production ended at year 2010), depletion at EC (East Central) cluster is replaced by N_2 injection and maintained for 15 years and followed by 15 years of shut-in. After 50 years of depletion, shut-in is applied to all other clusters and maintained for 30 years. The total duration of simulation time is 80 years.

- Scenario 2: After 50 years of depletion (assuming that gas production ended at year 2010), depletion at EC (East Central) cluster is replaced by N_2 injection and maintained for 15 years and followed by 15 years of shut-in. For all other clusters, depletion further continued for another 10 years, followed by 20 years of shut-in. The total duration of simulation time is 80 years.

- Scenario 3: After 40 years of depletion (assuming that gas production ended at year 2000), depletion at EC (East Central) cluster is replaced by N_2 injection and maintained for 15 years and followed by 15 years of shut-in. After 40 years of depletion, shut-in is applied to all other cluster and maintained for 30 years. The total duration of simulation time is 70 years.

- Scenario 4: After 40 years of depletion (assuming that gas production ended at year 2000), depletion at EC (East Central) cluster is replaced by N_2 injection and maintained for 15 years and followed by 15 years of shut-in. For all other clusters, depletion further continued for another 20 years, followed by 10 years of shut-in. The total duration of simulation time is 70 years.

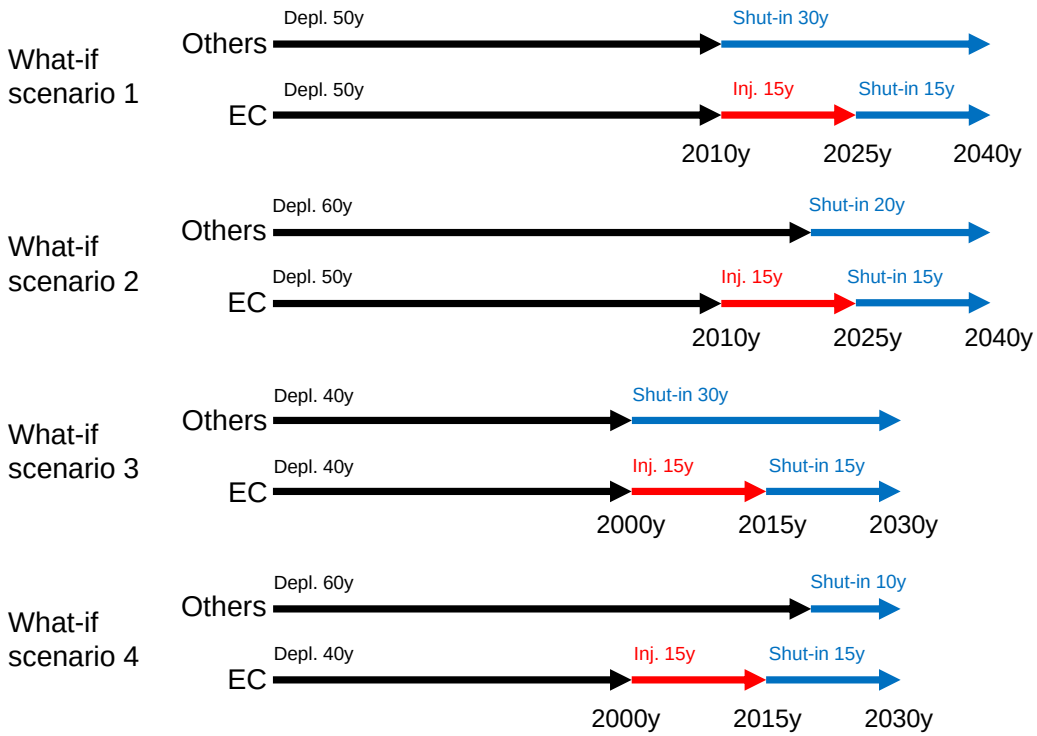

Figure 9-1: Schematic representation of four what-if injection scenarios. Black arrow denotes depletion modelling, red arrow denotes injection modelling, blue arrow denotes shut-in modelling.

9.2. Evolution of reservoir pressure and seismicity – "what-if" injection scenario 1

Figure 9-2 shows evolution of reservoir pressure and seismicity for what-if injection scenario 1. During the 15 years of injection period, five seismic events were simulated. These seismic events were generated at the northwest region. The max ML seismic event (ML 3.7) occurred at Loppersum region. During 15 years of shut-in period, no seismic events occurred. The absence of seismic events during the shut-in period may be due to relatively homogeneous pressure distribution in the entire reservoir field. Table below lists the number of seismic events and the maximum magnitude during injection and shut-in periods.

	Injection (15y)	Shut-in (15y)
No. seismic events	5	0
Max ML	3.7	NA

In **Figure 9-3**, we present temporal changes in the average well pressure for each cluster. Black arrow denotes depletion time period, red arrow denotes injection time period, blue arrow denotes shut-in time period. Well pressure at five clusters (LOPPZ, North, SouthEast, SouthWest, Eemskanall), except EastCentral cluster, declined for 50 years. Right after start of shut-in, the well pressure suddenly increased, and gradually increased over time for 30 years of shut-in period. Sudden increase in the well pressure is simulated because of the high pressure gradient formed during the depletion between the depletion points and the surrounding area. After start of shut-in, flow back is simulated from relatively high pressure area to the depletion point. However, after a few years, the pressure monitored at the wells stabilizes, and showed gradual increase over long time period. The curve also shows that there exists pressure difference between north and south of the reservoir which can be seen from the red curve (North) and the blue curve (SouthWest). The amount of pressure difference between north and south is approximately less than 10 MPa.

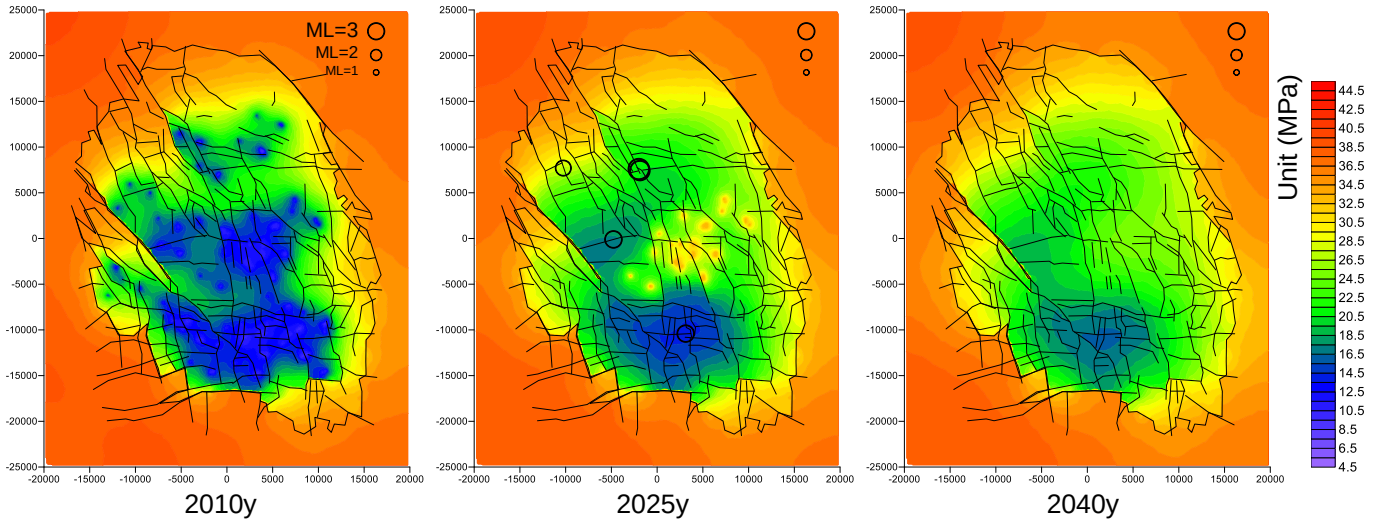

Figure 9-2: Evolution of reservoir pressure and seismicity for what-if injection scenario 1. At year 2025 (after 15 years of N2 injection at East Central cluster) the injection pressure reaches the maximum. At year 2040 (after 15 years of shut-in), the reservoir pressure distribution becomes homogeneous. All other clusters went shut-in for 30 years after 50 years of depletion which ended at year 2010.

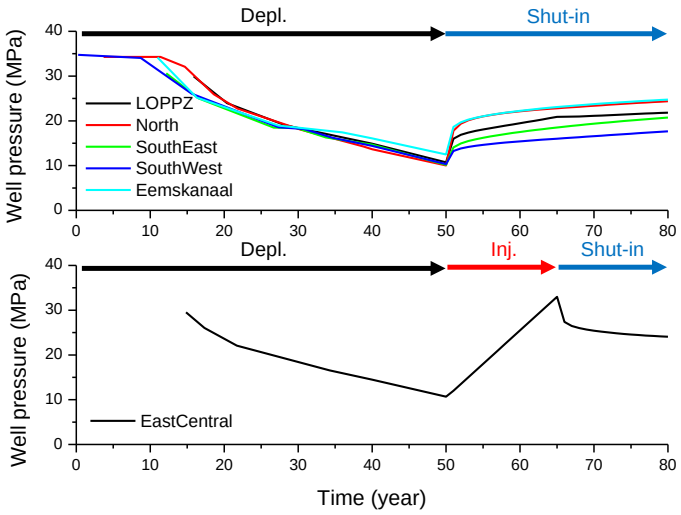

Figure 9-3: Evolution of average pressure of well clusters over time for what-if injection scenario 1. Black arrow denotes depletion time period, red arrow denotes injection time period, blue arrow denotes shut-in time period.

9.3. Evolution of reservoir pressure and seismicity – "what-if" injection scenario 2

Figure 9-4 shows evolution of reservoir pressure and seismicity for what-if injection scenario 2. During the 15 years of injection period, 15 seismic events were simulated. These seismic events were mostly generated at Loppersum region, and the max ML seismic event (ML 3.9) occurred. During 15 years of shut-in period, one seismic events occurred.

	Injection (15y)	Shut-in (15y)
No. seismic events	15	1
Max ML	3.9	2.8

In **Figure 9-5**, we present temporal changes in the average well pressure for each cluster. Black arrow denotes depletion time period, red arrow denotes injection time period, blue arrow denotes shut-in time period. Well pressure at five clusters (LOPPZ, North, SouthEast, SouthWest, Eemskanall), except EastCentral cluster, declined for 60 years. Right after start of shut-in, the well pressure suddenly increased, and gradually increased over time for 20 years of shut-in period. Increase in the well pressure is simulated because of the high pressure gradient formed during the depletion between the depletion points and the surrounding area. After start of shut-in, flow back is simulated from the relatively high pressure area to the depletion point. However, after a few years, the pressure monitored at the wells stabilizes, and showed gradual increase over long time period. The curve also shows that there exists pressure difference between north and south of the reservoir which can be seen from the red curve (North) and the blue curve (SouthWest). The amount of pressure difference between north and south is approximately less than 10 MPa.

The location of the max ML seismic event in scenario 1 and in scenario 2 is identical, whereas the magnitude is slightly different (ML 3.7 vs. ML 3.9). The difference is due to further depletion in the north part of the reservoir, which resulted in elevated stress on the fault due to depletion as explained in Section 5.3 Stress analysis. The overpressure zone formed at east central region then triggers fault failure under elevated stress level, and resulted in slightly higher magnitude. This finding demonstrates that when combining depletion and injection at the same time, the injection location and pressure rate should be chosen carefully not to trigger fault instability at the region of pressure depletion. We speculate that if the overpressure zone was mitigated by slower increase of injection applied to EC cluster, the magnitude of the seismicity at Loppersum region could have been lowered than ML 3.9.

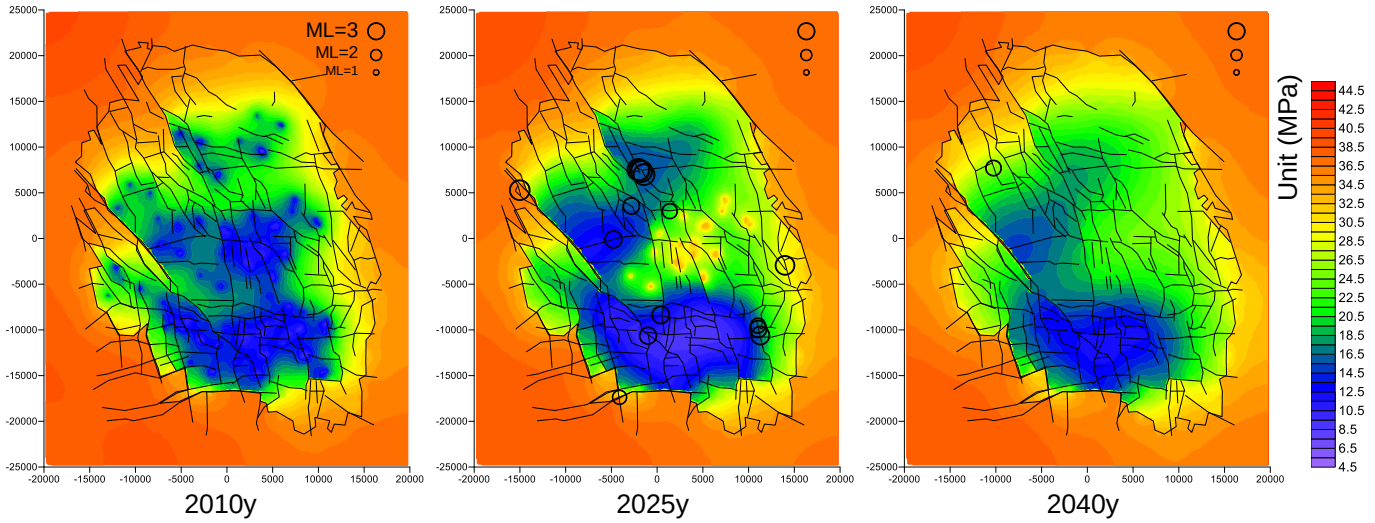

Figure 9-4: Evolution of reservoir pressure and seismicity for what-if injection scenario 2. At year 2025 (15 years after start of N2 injection at East Central cluster) the injection pressure reaches the maximum. At year 2040 (15 years after start of shut-in at East Central cluster), the reservoir pressure distribution becomes homogeneous. All other clusters were shut-in for 20 years after 60 years of depletion ended at year 2020.

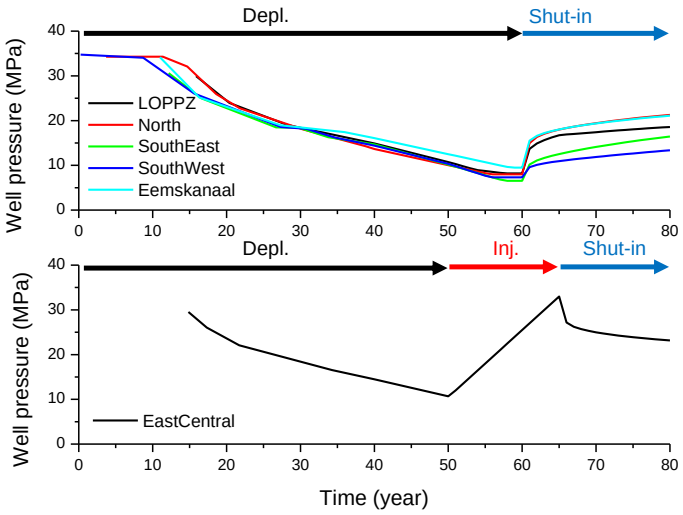

Figure 9-5: Evolution of average pressure of well clusters over time for what-if injection scenario 2. Black arrow denotes depletion time period, red arrow denotes injection time period, blue arrow denotes shut-in time period.

9.4. Evolution of reservoir pressure and seismicity – "what-if" injection scenario 3

Figure 9-6 shows evolution of reservoir pressure and seismicity for what-if injection scenario 3. During the 15 years of injection period, seven seismic events were simulated. These seismic events were generated at the northwest region. The max ML seismic event (ML 3.6) occurred at Loppersum region. During 15 years of shut-in period, one seismic event occurred. Table below lists the number of seismic events and the maximum magnitude during injection and shut-in periods.

	Injection (15y)	Shut-in (15y)
No. seismic events	7	1
Max ML	3.6	4.2

In **Figure 9-7**, we present temporal changes in the average well pressure for each cluster. Black arrow denotes depletion time period, red arrow denotes injection time period, blue arrow denotes shut-in time period. Well pressure at five clusters (LOPPZ, North, SouthEast, SouthWest, Eemskanall), except EastCentral cluster, declined for 40 years. Right after start of shut-in, the well pressure suddenly increased, and gradually increased over time for 30 years of shut-in period. Increase in the well pressure is simulated because of the high pressure gradient formed during the depletion between the depletion points and the surrounding area. After start of shut-in, flow back is simulated from the relatively high pressure area to the depletion point. However, after a few years, the pressure monitored at the wells stabilizes, and showed gradual increase over long time period. The curve also shows that there exists pressure difference between north and south of the reservoir which can be seen from the red curve (North) and the blue curve (SouthWest). The amount of pressure difference between north and south is approximately less than 10 MPa.

In this scenario, the max ML seismic event occurred during the shut-in period with magnitude ML 4.2. The location of this seismic event is at Loppersum region. The possible reason for this seismic event occurrence during shut-in is that, 40 years of depletion period was not long enough to release the strain energy accumulated at the fault at Loppersum region, and occurrence of this large magnitude event was delayed.

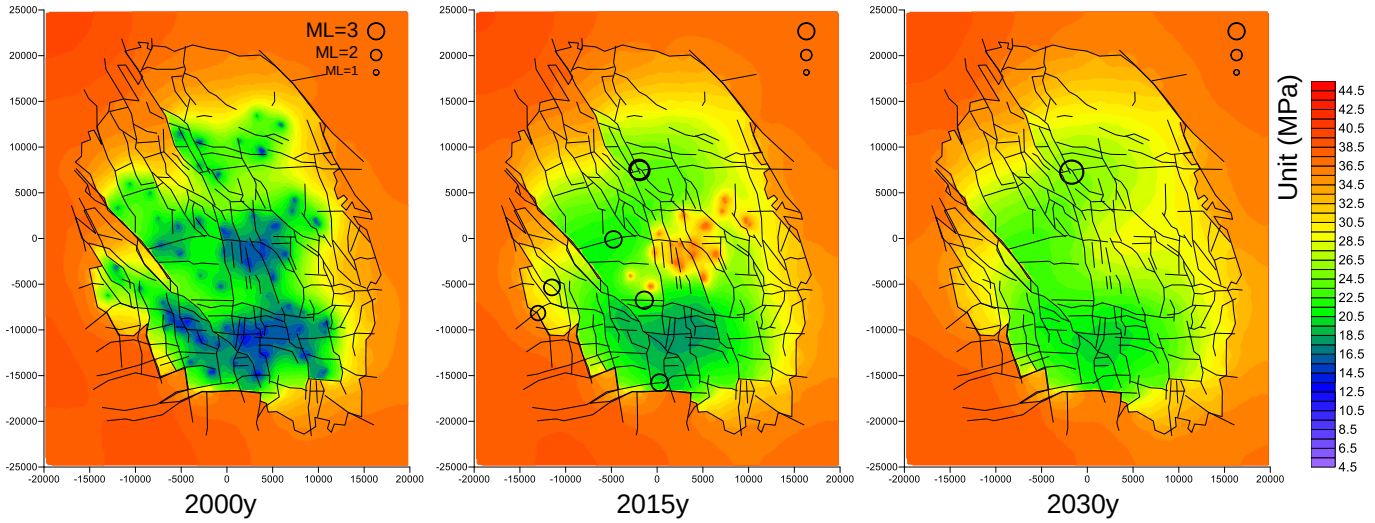

Figure 9-6: Evolution of reservoir pressure and seismicity for what-if injection scenario 3. At year 2015 (15 years after start of N2 injection at East Central cluster) the injection pressure reaches the maximum. At year 2030 (15 years after start of shut-in at East Central cluster), the reservoir pressure distribution becomes homogeneous. All other clusters were shut-in for 30 years after 40 years of depletion ended at year 2000.

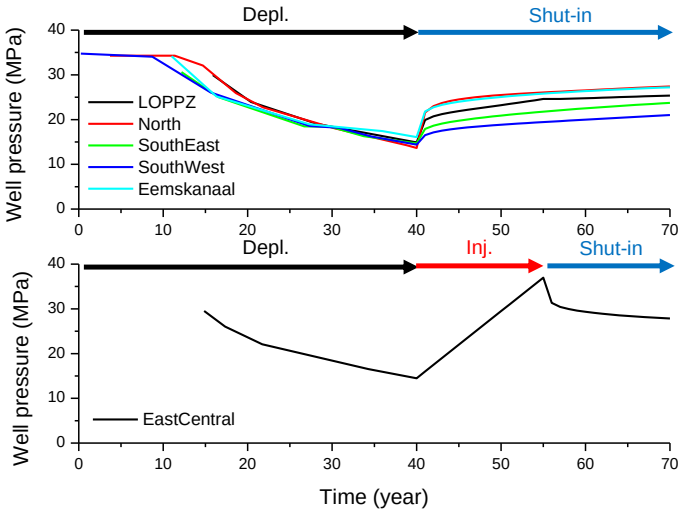

Figure 9-7: Evolution of average pressure of well clusters over time for what-if injection scenario 3. Black arrow denotes depletion time period, red arrow denotes injection time period, blue arrow denotes shut-in time period.

9.5. Evolution of reservoir pressure and seismicity – "what-if" injection scenario 4

Figure 9-8 shows evolution of reservoir pressure and seismicity for what-if injection scenario 4. This scenario also resulted in the highest seismicity rate, as a total of 28 seismic events were generated during the combined injection and shut-in periods. 24 seismic events were generated during injection, while four seismic events were generated during shut-in. Notably, none of the seismicity was generated within the east-central region where injection was simulated; however, seismic events generated by the model were present throughout the rest of the reservoir. In the northern area, seismicity rates increased during the last five years of simulated injection, with a cluster forming within one of the local modelled low-pressure zones. The largest seismic event generated by the model had a magnitude of ML 4.1 and was located at Loppersum region.

	Injection	Shut-in
No. seismic events	24	4
Max ML	4.1	3.3

In **Figure 9-9**, we present temporal changes in the average well pressure for each cluster. Black arrow denotes depletion time period, red arrow denotes injection time period, blue arrow denotes shut-in time period. Well pressure at five clusters (LOPPZ, North, SouthEast, SouthWest, Eemskanall), except EastCentral cluster, declined for 40 years. Right after start of shut-in, the well pressure suddenly increased, and gradually increased over time for 30 years of shut-in period. Increase in the well pressure is simulated because of the high pressure gradient formed during the depletion between the depletion points and the surrounding area. After start of shut-in, flow back is simulated from the relatively high pressure area to the depletion point. However, after a few years, the pressure monitored at the wells stabilizes, and showed gradual increase over long time period. The curve also shows that there exists pressure difference between north and south of the reservoir which can be seen from the red curve (North) and the blue curve (SouthWest). The amount of pressure difference between north and south is approximately less than 10 MPa.

Out of the four "what-if" scenarios, what-if scenario 4 resulted in the most spatial heterogeneity in modelled pressure, particularly at the end of the injection period, where numerous local minima and maxima were simulated within the depletion and injection zones, respectively. As pressure migrated during shut-in, the distribution became more homogeneous within the east-central area, and three

distinct modelled low-pressure zones within the depletion area were identified.

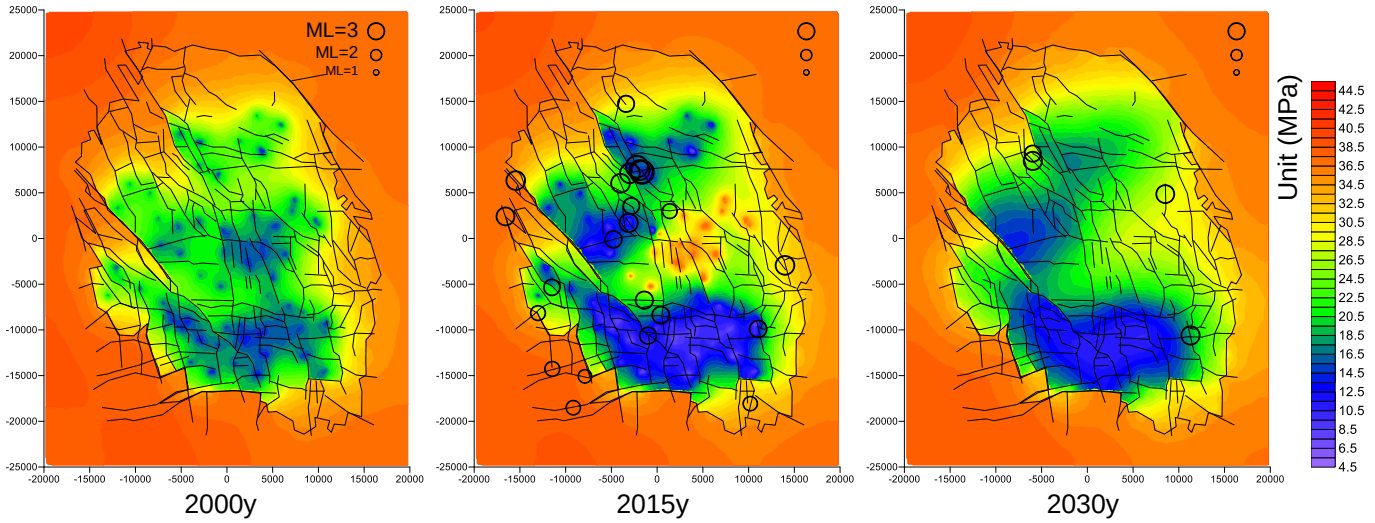

Figure 9-8: Evolution of reservoir pressure and seismicity for what-if injection scenario 4. At year 2025 (15 years after start of N2 injection at East Central cluster) the injection pressure reaches the maximum. At year 2040 (15 years after start of shut-in at East Central cluster), the reservoir pressure distribution becomes homogeneous. All other clusters were shut-in for 30 years after 50 years of depletion ended at year 2010.

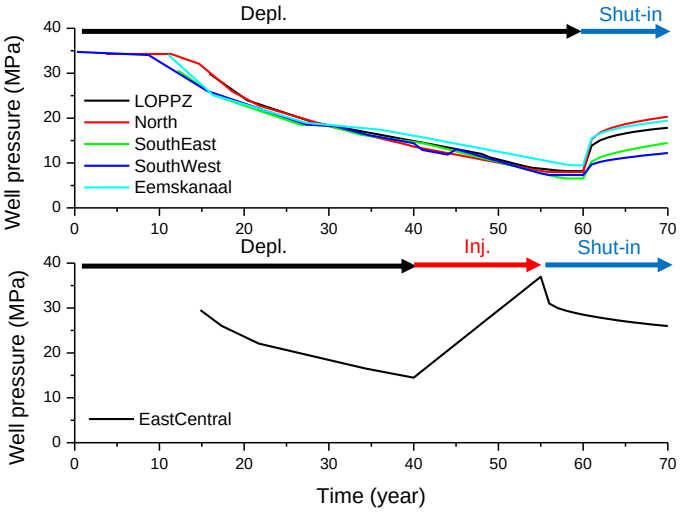

Figure 9-9: Evolution of average pressure of well clusters over time for what-if injection scenario 4. Black arrow denotes depletion time period, red arrow denotes injection time period, blue arrow denotes shut-in time period.

9.6. Summary and discussion

We tested four hypothetical (what-if) injection scenarios, combining shut-in and injection (what-if injection scenarios 1 and 3) and combining shut-in, depletion and injection (what-if injection scenarios 2 and 4). Two major hypotheses are: 1) gas production ended in year 2010 (50 years of gas production), and 2) gas production ended even earlier in year 2000 (40 years of gas production).

In all tested what-if injection scenarios, the largest magnitude seismic event occurred at Loppersum region. This implies that the fault stability at Loppersum region is very sensitive and injection at EC clusters easily triggers seismicity of the faults at Loppersum region. This implies that production/injection at or near Loppersum region should be avoided as they may easily trigger seismicity at Loppersum region.

Continuing depletion at all well clusters except for EC while applying injection within the EC cluster resulted in inhomogeneous pressure distribution (what-if injection scenarios 2 and 4). The overpressure at east central cluster region resulted in triggering of seismic events at Loppersum region. When compared with shut-in scenarios (see Section 6), the comparison demonstrates that homogeneously distributed reservoir pressure did not generate seismic events at Loppersum. This supports the hypothesis that increased homogeneity in pressure distribution throughout the reservoir may help to mitigate seismic hazard through decreasing seismicity rates, and emphasizes that the goal of an injection scenario should be to reduce spatially inhomogeneous pressure distribution.

What-if injection scenarios 2 and 4 resulted in larger number of seismic events than scenarios 1 and 3. This finding implies that combining injection in depleting reservoir may have negative effect on mitigating seismicity, as stresses on faults may have increased due to pressure depletion, leading to higher level of stress criticality, and injection may trigger fault failure, leading to higher seismic magnitude.

In all tested what-if injection scenarios, the pressure rise at the injection clusters was programmed to rise approximately 25 MPa in 15 years. This pressure rise is the result of TOUGH3 modelling (see **Figure 7-7**). Such high rate of pressure increase is considered too aggressive. We suggest a series of additional modelling with reduced injection rate, i.e. 25% of the estimated injection rate, in order to see if slower pressure rise due to reduced rate injection could mitigate the occurrence of seismicity, especially at Loppersum region.

The total number of seismic events generated in the what-if scenarios 2 and 4 are larger than the scenarios 1 and 3 by a factor of 3-5, as shown in **Figure 9-10**. This result demonstrates that combined

injection at east central clusters and continued production at south clusters could result in higher level of seismic hazard as the overall reservoir pressure distribution becomes highly inhomogeneous.

The reason for choosing EC cluster for injection is because EC cluster is located at the central part of the reservoir where the pressure depletion was the largest and distant from the south clusters so that mixing of injected N2 with Groningen gas can be avoided (not to deteriorate the gas quality). However, locating the N2 injection near to the gas production or combining N2 injection among the production wells may not be the worst case. The Groningen gas is known to be low-calorific with about 15% of N2 contained.

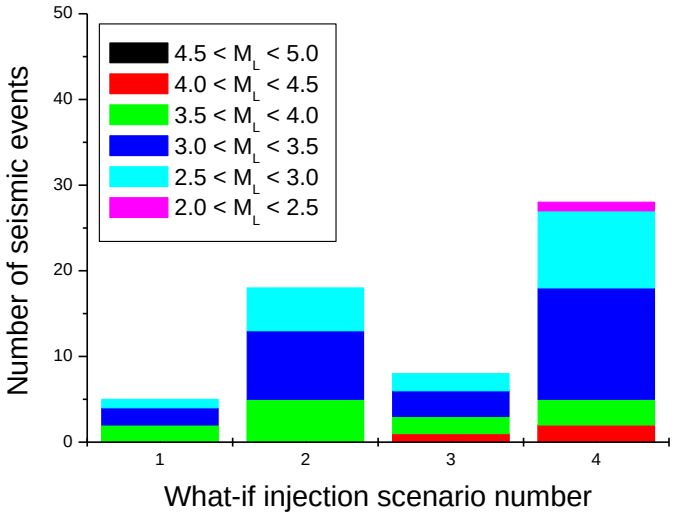

Figure 9-10: Comparison of the numbers and the magnitudes of seismic events in four what-if injection scenarios.

10. Discussion

In this study, we built a model to test the potential benefit of fluid injection on seismicity in the Groningen gas field. Extensive information and data about the reservoir, the pressure and production history, as well as the induced seismicity and subsidence were available. This enabled us to build and calibrate a new detailed model which can combine fluid flow and pressure changes with stresses and resulting earthquakes (not done before for the Groningen reservoir). However, there are several types of limitations, which are not explored and/or solved enough. Originally, the study was designed as a proof of concept, not as a preliminary design of a possible injection in the Groningen reservoir. The limitations of the model can be divided in the following sub-section.

10.1. Limitations of the modelling method

- The characterisation of the reservoir, geological model.
- The values and spatial variation of relevant parameters are not taken into account in the model.
- Pressure and production history (pressure data is simplified, annual variation ignored, pressure data not available for all locations and years, especially further from production wells, production per well was not available and is not used as input into the model).
- The modelling method (2D instead of 3D will not be able to include the vertical pressure and stress variation properly.
- Constraint on the particle size of the model limits the range of magnitudes that can be generated.
- Inconsistencies of the results with the observations
    - Reservoir pressure: Average pressure after 60 years of production is still too high, also after increasing number of wells and sealing the outer boundary of the reservoir.
    - Seismicity: The model does not match well enough to observations regarding seismicity history, magnitude and spatial distribution, especially the large seismic event clusters at Loppersum region.

10.2. Suggestions for further study

Sensitivity and uncertainty analysis

There are several parameters used in the modelling with various levels of uncertainty about magnitude and spatial variation, as listed below.

- Fault mechanical properties
- Fault permeability
- Fault sealing
- Reservoir matrix permeability
- In-situ stress magnitude
- Orientation of maximum horizontal stress
- Pressure depletion profiles of production clusters

The model parameters that can have the largest impacts on the modelling seismicity are fault mechanical properties, fault permeability, fault sealing and in-situ stress magnitudes. As they are all judged to have high level of uncertainty, we suggest as further study, involving a systematic sensitivity analysis and investigating the effects of parameter uncertainties on the overall induced seismic hazard profiles.

Additional (realistic) injection scenarios

In this study, we conducted two injection scenarios to assess differences in modelled seismicity patterns caused by simulation injection with CO2 vs. N2. For additional work, we suggest sensitivity modelling of various injection parameters, such as rate, additional durations and locations, style of injection (constant rate, cyclically varied rate, e.g. Yoon et al., 2015), and investigation of their impacts on overall induced seismic hazard profiles.

Also, if realistic injection scenarios should be explored, then preliminary design should be adapted to availability of wells and other conditions such as possibility of contamination/dilution of produced gas by injected gas.

11. Conclusions

This numerical modelling study aims at investigating and quantify the effect of fluid injection on the seismicity in the depleted Groningen gas reservoir. The objective is to assess whether the fluid injection has a positive effect in mitigating the seismic events that have occurred due to pressure decline and to give recommendations for pressure maintenance.

Previous studies by TNO and NAM concluded that injection can maintain reservoir pressure in depleting reservoirs, such as the Groningen gas field, and the fluid injection is technically feasible. However, the overall net effect of large-scale fluid injection on the seismic risk profile was not quantified and the seismic risk associated with different fluid injection scenarios was only studied in a qualitative way. Therefore, it is unknown whether fluid injection can be used to minimize the risk of induced seismicity in depleting gas fields.

The modelling code used in this study is PFC2D (Particle Flow Code 2D), a commercial code of ITASCA, with in-house developed hydro-mechanical coupled and seismicity computing models. We modelled the entire field of Groningen gas reservoir with 40 km by 50 km in size with the complex reservoir faults. The model is in 2D which we considered valid due to its long horizontal extent (40-50 km) compared to the net thickness of the reservoir (200-300 m). We built the model with highly complex geometry of the reservoir fault using the smooth joint contact model in PFC2D. Model parameters used were taken from various literatures related to the Groningen reservoir and seismicity studies.

First, we simulated the past 60 years of depletion induced seismicity that covers the time range from year 1960 to 2020 (Section 5). Second, we simulated future seismicity, assuming that the gas production stopped in year 2020 (or in year 2010) and all the production wells are shut-in (Section 6). Third, we simulated future seismicity after year 2020, assuming that injection took place in some of the well clusters with CO_2 and N_2 as injection gas (Section 8). Fourth, we simulated future seismicity after year 2020, when N_2 injection took place in some of the well clusters while all other clusters are shut-in or are in continued production (Section 9).

We obtained the following results.

(Section 5) During the 60-year depletion periods, the greatest pressure decline was simulated at the east and south parts of the reservoir. The evolution of reservoir pressure did not match well with the field observed pressure distribution. However, in terms of seismicity, comparison between the simulated and the observed (KNMI seismicity) matched fairly well, for the time period between 1990 and 2020. Ultimately, the depletion model adequately captured the spatial distribution of observed earthquakes above local

magnitude ML 2.0, rendering their spatial seismicity distributions consistent with that of KNMI earthquake-catalog data.

(Section 6) Two hypothetical shut-in scenarios were tested. In the first case, shut-in of all wells in all clusters occurred in year 2020, meaning that pressure depletion took place over the past 60 years. In the second case, shut-in of all wells in all clusters occurred in year 2010, meaning that pressure depletion took place over the past 50 years. In both shut-in scenarios, we confirmed that the seismicity rate decreased significantly during the two shut-in periods. This finding implies that the very first measure to take to lower the level of seismic hazard is to stop gas production and to let the reservoir pressure go into equilibrium. Based on these results, the injection scenarios were designed with the intention to increase spatial homogeneity in pressure recovery, to reduce the number and magnitude of seismic events triggered by inhomogeneous reservoir pressure distribution.

(Section 7) We tested injection of two different gas, CO2 and N2, into a depleted reservoir with partly saturated with CH4 and water. We used TOUGH3 code to simulate mixture of different gases that are in two phases. With same mass amount of gas injection, the results indicated that the reservoir pressure increase is limited when CO2 is injected, as CO2 dissolves more into the water that is remaining in the reservoir. The results indicated that the reservoir pressure increases as intended for pressure maintenance purpose when N2 is injected, as N2 does not dissolve in the remaining water. The key results in Section 7 is the pressure increase over time monitored at the center of the reservoir, which we formulated mathematically and programmed for inputs in the PFC2D modelling.

(Section 8) Using the results of Section 7, the two injection scenarios were tested. In the first case, CO2 is injected at east central cluster for 15 years and followed by 15 years of shut-in, whereas all the other clusters were shut-in. In the second case, N2 is injected at east central cluster for 15 years and followed by 15 years of shut-in, whereas all the other clusters were shut-in for 30 years. The results demonstrated a significant difference between the two tested scenarios. The difference is that, in case of CO2 injection the pressure rise due to injection is negligible, the injection did not generate overpressure zone at east central region. In case of N2 injection, the pressure rise is relatively fast, and resulted in overpressure zone at east central region, and triggered seismic events at Loppersum region. This implies that overpressure zone formed by N2 injection could trigger unwanted seismic events at regions of stress criticality, e.g. Loppersum region. This finding also implies that N2 injection seems to be an effective measure to increase the reservoir pressure, but one has to be careful in choosing the location and the rate of injection, as not to trigger seismic events at far-field due to poro-elastic stress triggering mechanism.

(Section 9) We tested four hypothetical (what-if) injection scenarios, combining shut-in and injection (what-if injection scenarios 1 and 3)

and combining shut-in, depletion and injection (what-if injection scenarios 2 and 4). In all tested what-if injection scenarios, the largest magnitude seismic event occurred at Loppersum region. This implies that the fault stability at Loppersum region is very sensitive and injection at EC clusters easily triggers seismicity of the faults at Loppersum region. This implies that production/injection at or near Loppersum region should be avoided as they may easily trigger seismicity at Loppersum region. Continuing depletion at all well clusters except for EC while applying injection within the EC cluster resulted in inhomogeneous pressure distribution (what-if injection scenarios 2 and 4). The overpressure at east central cluster region resulted in triggering of seismic events at Loppersum region. When compared with shut-in scenarios (see Section 6), the comparison demonstrates that homogeneously distributed reservoir pressure did not generate seismic events at Loppersum. This supports the hypothesis that increased homogeneity in pressure distribution throughout the reservoir may help to mitigate seismic hazard through decreasing seismicity rates, and emphasizes that the goal of an injection scenario should be to reduce spatially inhomogeneous pressure distribution. What-if injection scenarios 2 and 4 resulted in larger number of seismic events than scenarios 1 and 3. This finding implies that combining injection in depleting reservoir may have negative effect on mitigating seismicity, as stresses on faults may have increased due to pressure depletion, leading to higher level of stress criticality, and injection may trigger fault failure, leading to higher seismic magnitude.

We make the following recommendations for mitigating depletion induced seismicity and for pressure maintenance purpose by fluid injection in Groningen gas field.

1) The first measure to take to lower the seismicity rate is to stop gas production and to shut-in the wells.

2) During significant production in the Groningen gas field, no injection should be carried out in the Loppersum region because of critical stresses and fault locations.

3) To compensate for the pressure loss at those regions, the rate and duration of injection should be low and long, respectively, to prevent instability of near-field faults by pressure increase effect and to prevent instability of far-field faults due to the poro-elastic triggering effect.

4) Based on the increased rate of modelled pressure increase, without a substantial increase in the number or magnitude of simulated seismic events, injection should be carried out using N2 instead of CO2, as CO2 dissolves more effectively in water than N2.

5) Combining injection in a depleting reservoir may have negative effect on mitigating seismicity, as stresses on faults

may have increased due to pressure depletion, leading to higher level of stress criticality, and injection may trigger fault failure, leading to higher seismic magnitude.

As of now, there is no conclusive evidence that the injection rate can be adapted to result in minimal seismicity. In the case of significant additional production within the Groningen gas field, additional study, including sensitivity tests, will be necessary in order to determine whether fluid injection is beneficial and/or necessary.

12. References

Al-Busaidi, A., Hazzard, J.F., Young, R.P. (2005). Distinct element modelling of hydraulically fractured Lac du Bonnet granite. J Geophy Res 110, B06302.

Bentz, S., Kwiatek, G., Martínez-Garzón, P., Bohnhoff, M., & Dresen, G. (2020). Seismic moment evolution during hydraulic stimulations. Geophysical Research Letters 47, e2019GL086185.

Bourne, S.J., Oates, S.J., and van Elk, J. (2018). The exponential rise of induced seismicity with increasing stress levels in the Groningen gas field and its implications for controlling seismic risk, Geophysical Journal International 213, 1693-1700.

Bourne., S. and Oates, S. (2019). Evolution of induced earthquake magnitude distributions with increasing stress in the Groningen gas field. NAM, November 2019.

Buijze, L., van den Bogert, P.A J., Wassing, B.B.T., and Orlic, B. (2019). Nucleation and arrest of dynamic rupture induced by reservoir depletion. Journal of Geophysical Research: Solid Earth 124, 3620-3645.

Buijze, L., van den Bogert, P.A J., Wassing, B.B.T., Orlic, B., and ten Veen, J. (2017). Fault reactivation mechanisms and dynamic rupture modelling of depletion-induced seismic events in a Rotliegend gas reservoir. Netherlands Journal of Geosciences 96(5), 131-148.

Burkitov, U., Van Oeveren, H., Valvatne, P. (2016): Groningen Field Review 2015 Subsurface Dynamic Modelling Report.

de Jager, J., and Visser, C. (2017). Geology of the Groningen field – An overview, Netherlands Journal of Geosciences 96(5), 3-15.

Dost, B., Goutbeek, F., Eck, T.V., and Kraaijpoel, D. (2012). Monitoring induced seismicity in the North of the Netherlands: status report 2010, Tech. Rep., Koninklijk Nederlands Meteorologisch, de Bilt, The Netherlands.

Dost, B., Edwards, B., and Bommer, J.J. (2016). Local and moment magnitudes in the Groningen field. NAM, June 2016.

Graupner, Bastian, Rutqvist, Jonny, Guglielmi, Yves, Nguyen, Thanh Son, Yoon, Jeoung Seok, Maßmann, Jobst, Ziefle, Gesa, Shiu, Wenjie, Kim, Taehyun, Park, Jung-Wook, and Urpi, Luca. DECOVALEX-2019 (Task B Final Report). United States: N. p., 2020. Web. doi:10.2172/1762802.

Guises, R., Embry, J.-M., and Barton, C. (2015). Dynamic geomechanical modelling to assess and minimize the risk for fault

slip during reservoir depletion of the Groningen field. NAM, June 2015.

Hanks, T.C., Kanamori, H. (1979). A moment magnitude scale. Journal of Geophysical Research 84, 2348–2350.

Hazzard, J.F., Young,R.P., Oates,S.J. (2002). Numerical modelling of seismicity induced by fluid injection in a fractured reservoir. In: Proceedings of the 5th North American Rock Mechanics Symposium, Mining and Tunnel Innovation and Opportunity, Toronto, Canada, 7–10 July 2002, pp.1023–1030.

Hazzard, J.F., Young, R.P. (2002). Moment tensors and micromechanical models. Tectonophysics 356, 181–197.

Hazzard, J.F., Young, R.P. (2004). Dynamic modelling of induced seismicity. Int J Rock Mech & Min Sci 41, 1365–1370.

Hettema, M. (2020). Analysis of mechanics of fault reactivation in depleting reservoirs, International Journal of Rock Mechanics & Mining Sciences 129, 104290.

Hunfeld, L.B., Niemeijer, A.R., and Spiers, C.J. (2017). Frictional properties of simulated fault gouges from the seismogenic Groningen gas field under in situ P-T -chemical conditions, Journal of Geophysical Research: Solid Earth 122, 8969-8989.

Hofmann, R., and team (2016). Groningen Pressure Maintenance (GPM) study – progress report February 2016. NAM, February 2016.

Hökmark, H., Lönnqvist, M., Fälth, B. (2010). Technical Report TR-10-23 THM-issues in repository rock – thermal, mechanical, thermo-mechanical and hydro-mechanical evolution of the rock at the Forsmark and Laxemar sites. SKB-Swedish Nuclear Fuel and Waste Management Co., 26–27.

Hou, Z., Gou, Y., Taron, J. (2012): Thermo-hydro-mechanical modeling of carbon dioxide injection for enhanced gas-recovery (CO2-EGR): a benchmarking study for code comparison. Environ Earth Sci 67, 549–561.

Itasca Consulting Group Inc. (2012). Technical Memorandum—5.0 parallel bond enhancement, Minneapolis.

Itasca Consulting Group Inc. (2008). PFC2D—Particle Flow Code in 2 Dimensions, Version 4.0, Minneapolis.

Itasca Consulting Group Inc. (1999). UDEC/3DEC (Universal Distinct Element Code in 2/3 Dimensions), version 5.0, Minneapolis, MN.

Jung, Y., Pau, G. S. H., Finsterle, S., Doughty, C. (2018). “TOUGH3 User’s Guide Version 1.0”, Energy Geosciences Division, Lawrence Berkeley National Laboratory, University of California, Berkeley, California.

Kortekaas, M. & Jaarsma, B. (2017). Improved definition of faults in the Groningen field using seismic attributes. Netherlands Journal of Geosciences 96-5, s71-s85.

Luckner, L., van Genuchten, M. T., Nielsen, D. R. (1989). A consistent set of parametric models for the two-phase flow of immiscible fluids in the subsurface. Water Resour. Res., 25 (10) (1989), 2187–2193.

Madariaga, R. (1976). Dynamics of an expanding circular fault. Bulletin of the Seismological Society of America 66, 639-666.

Marone, C. (1998). Laboratory-derived friction laws and their application to seismic faulting. Annual Review of Earth and Planetary Sciences 26, 643–696.

Mas Ivars, D., Pierce M.E., Darcel, C., Reyes-Montes, J., Potyondy, D., Young, R.P., Cundall, P.A. (2011). The synthetic rock mass approach for jointed rock mass modelling. International Journal of Rock Mechanics & Mining Sciences 48, 219-244.

Moridis, G. (2016). User’s manual of the MeshMaker v1.5 code: a mesh generator for domain discretization in simulations of the TOUGH+ and TOUGH2 families of codes. LBNL 1005134, Berkeley, California, USA: Lawrence Berkeley National Laboratory.

Muntendam-Bos, A. G., Hoedeman, G., Polychronopoulou, K., Draganov, D., Weemstra, C., van der Zee, W., Bakker, R. R., and Roest, H. (2022). An overview of induced seismicity in the Netherlands. Netherlands Journal of Geosciences, Vol. 101, No. 1, doi:10.1017/njg.2021.14.

NAM (2016). Groningen Pressure Maintenance (GPM) Study – Progress Report February 2016. Assen: NAM B.V.

NAM (2013). Technical Addendum to the Winningsplan Groningen 2013: Subsidence, Induced Earthquakes and Seismic Hazard Analysis in the Groningen Field. November 2013.

Nepveu, M., van Thienen-Visser, K., and Sijacic, D. (2016). Statistics of seismic events at the Groningen field. Bull Earthquake Eng 14, 3343-3362.

Oldenburg, C. M., Webb, S. W., Pruess, K., Moridis, G. J. (2004): Mixing of stably stratified gases in subsurface reservoirs: a comparison of diffusion models. Transp. Porous Med. 54, 323–334.

Potyondy, D.O., and Cundall, P.A. (2004). A bonded-particle model for rock. Int J Rock Mech & Min Sci 41, 1329-1364.

Scholz, C. (1990). The Mechanics of Earthquakes and Faulting. Cambridge University Press, Cambridge, UK, 439 pp.

Silver, P.G., Jordan, T.H. (1982). Optimal estimation of scalar moment. Geophysical Journal of the Royal Astronomical Society 70, 755– 787.

van den Bogert, P.A.J. (2018). Depletion-induced fault slip and seismic rupture. NAM, December 2018.

van Elk, J., and Doornhof, D. (2019). Special report on the Westerwijtwerd earthquake 22nd May 2019. NAM, May 2019.

van Elk, J., Doornhof, D., Bommer, J. J., Bourne, S. J., Oates, S. J., Pinho, R., and Crowley, H. (2017). Hazard and risk assessments for induced seismicity in Groningen. Netherlands Journal of Geosciences, Vol. 96, No. 5, 259–269.

van Thienen-Visser, K., Pruiksma, J.P., and Breunese, J.N. (2015). Compaction and subsidence of the Groningen gas field in the Netherlands, Proc. IAHS 372, 367-373.

van Thienen-Visser, K., Sijacic, D., van Wees, J.-D., Kraaijpoel, D., and Roholl, J. (2016). Groningen field 2013 to present: gas production and induced seismicity. TNO 2016 R10425.

Wentinck, R. H. (2015). Induced seismicity in the Groningen field—statistical assessment of tremors along faults in a compacting reservoir. Report No. SR.15.11335. Shell Global Solutions International B.V. (Rijswijk).

Willacy, C., van Dedem, E., Minisini, S., Li, J., Blokland, J.-W., Das, I., and Droujinine, A. (2019). Full-Waveform Event Location and Moment Tensor Inversion for Induced Seismicity. Geophysics 84(2), 39-57.

Worden, C. B., Thompson, E. M., Hearne, M., and D. J. Wald (2020). ShakeMap Manual Online: technical manual, user's guide, and software guide, U. S. Geological Survey. http://usgs.github.io/shakemap/. DOI: https://doi.org/10.5066/F7D21VPQ.

Yoon, J.S., Zang, A., Stephansson, O. (2012). Simulating fracture and friction of Aue granite under confined asymmetric compressive test using clumped particle model. International Journal of Rock Mechanics & Mining Sciences 49, 68-83.

Yoon, J.S., Zang, A., and Stephansson, O. (2014). Numerical investigation on optimized stimulation of intact and naturally

fractured deep geothermal reservoirs using hydro-mechanical coupled discrete particles joints model. Geothermics 52, 165-184.

Yoon, J.S., Zimmermann, G., and Zang, A. (2015). Discrete element modeling of cyclic rate fluid injection at multiple locations in naturally fractured reservoirs, International Journal of Rock Mechanics & Mining Sciences 74, 15-23.

Yoon, J.S., Stephansson, O., Zang, A., Min, K.B., Lanaro, F. (2017). Discrete bonded particle modelling of fault activation near a nuclear waste repository site and comparison to static rupture earthquake scaling laws, International Journal of Rock Mechanics & Mining Sciences 98, 1-9.

Yoon, J.S., Stephansson, O., Min, K.B. (2014). Relation between earthquake magnitude, fracture length and fracture shear displacement in the KBS-3 repository at Forsmark Main Review Phase. Technical Note 2014:59, SSM Swedish Radiation Safety Authority.

Yoon, J.S., Stephansson, O., Min, K.B. (2016). Modelling of the thermal evolution of the KBS-3 repository at Forsmark and associated induced seismic activity Main Review Phase. Technical Note 2016:23, SSM Swedish Radiation Safety Authority.

Zechar J.D., Schorlemmer D, Liukis M, Yu, J., Euchner F., Maechling P.J., Jordan, T.H. (2010a). The Collaboratory for the Study of Earthquake Predictability perspective on computational earthquake science. Concurrency and Computation: Practice and Experience 22, 1836-1847.

Zechar, J. D., Gerstenberger, M. C., Rhoades, D. A. (2010b). Likelihood-Based Tests for Evaluating Space-Rate-Magnitude Earthquake Forecasts. Bulletin of the Seismological Society of America 100, 1184–1195.

Zhao, X., Young, R.P. (2011). Numerical modelling of seismicity induced by fluid injection in naturally fractured reservoirs. Geophysics 76(6), WC167–WC170.

Appendix A – Injection induced seismicity model used in the hazard analysis in Report C

The Report C (KEM-24 WP5 Effect of pressure maintenance by fluid injection on seismic risk Hazard analysis) provides assessment of injection induced seismic hazard. The injection induced seismicity catalogue used in the assessment is provided in this Appendix. It should be noted that the seismicity catalogues are from a preliminary PFC2D modelling (presented at KEM-24 panel meeting, dated 2021 November 24).

The tested model contains: 1) closed reservoir boundary, 2) 123 depletion points, and 3) sealing+conductive reservoir faults. Pressure depletion for 60 years was simulated by applying pressure vs. time curves for six groups of wells, and the evolution of reservoir pressure and seismicity is shown in Figure A-1.

Figure A-2 is the schematics of the four testes injection scenarios.

- Scenario 3: Injection at nine locations with rate of 1e-3 m3/s and duration of 10 years.
- Scenario 4: Injection at nine locations with rate of 10e-3 m3/s and duration of 1 year
- Scenario 5: Injection at nine locations, after the reservoir has gone through 30 years of shut-in period, with rate of 1e-3 m3/s and duration of 10 years
- Scenario 6: Injection at nine locations, after the reservoir has gone through 30 years of shut-in period, with rate of 5e-3 m3/s and duration of 5 years

Figure A-3 displays the temporal distribution of the seismicity in the tested injection scenarios. Figures A-4 displays the injection induced seismic events, and the reservoir pressure distribution after 30 years since the start of injection. The seismic event magnitudes that were taken into account in the hazard analysis in Report C by Fugro.

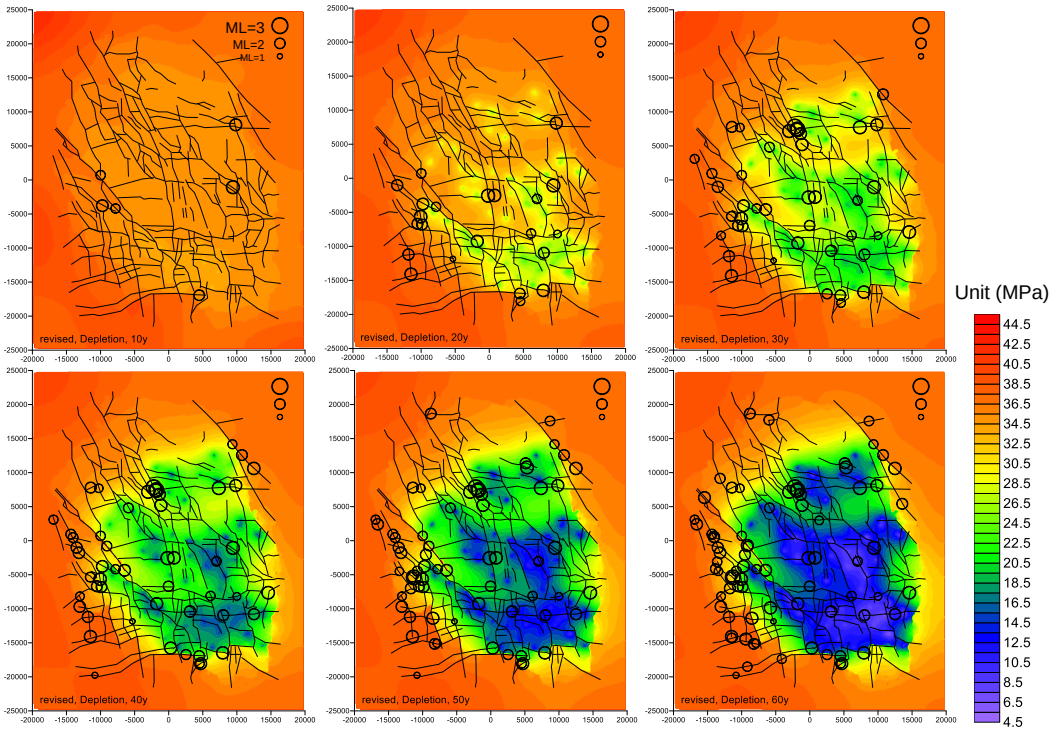

Figure A-1: Evolution of reservoir pressure and seismicity simulated by the depletion model (date 2021 November 24). Results for every 10 years after the start of simulated depletion are shown. The axes show the distance (in meters) from the center of the study region.

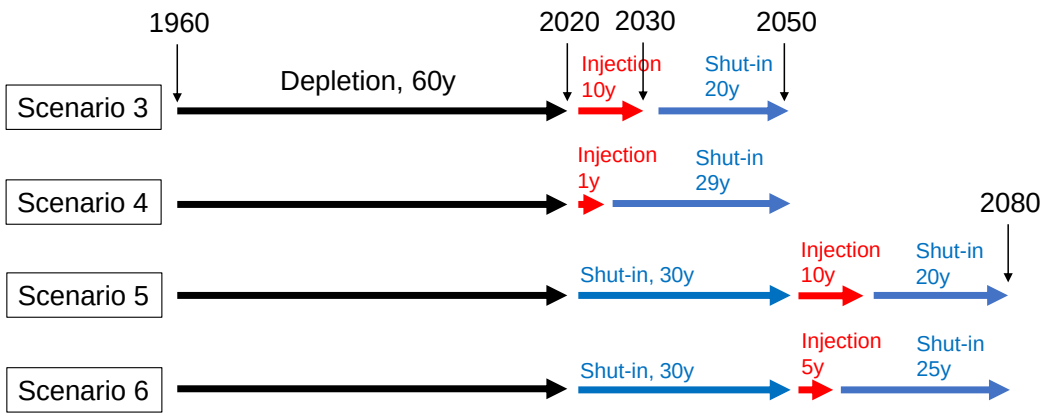

Figure A-2: Schematics of the four tested injection scenarios for the model date 2021 November 24.

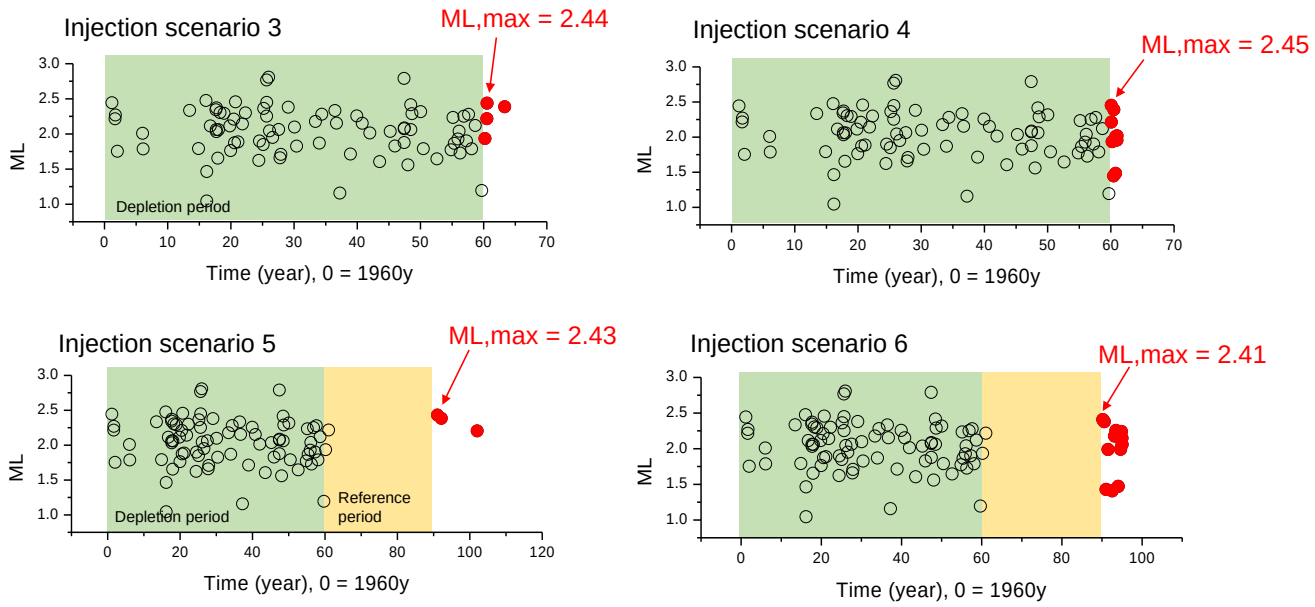

Figure A-3: Temporal distribution of the seismic events simulated in the four tested injection scenarios.

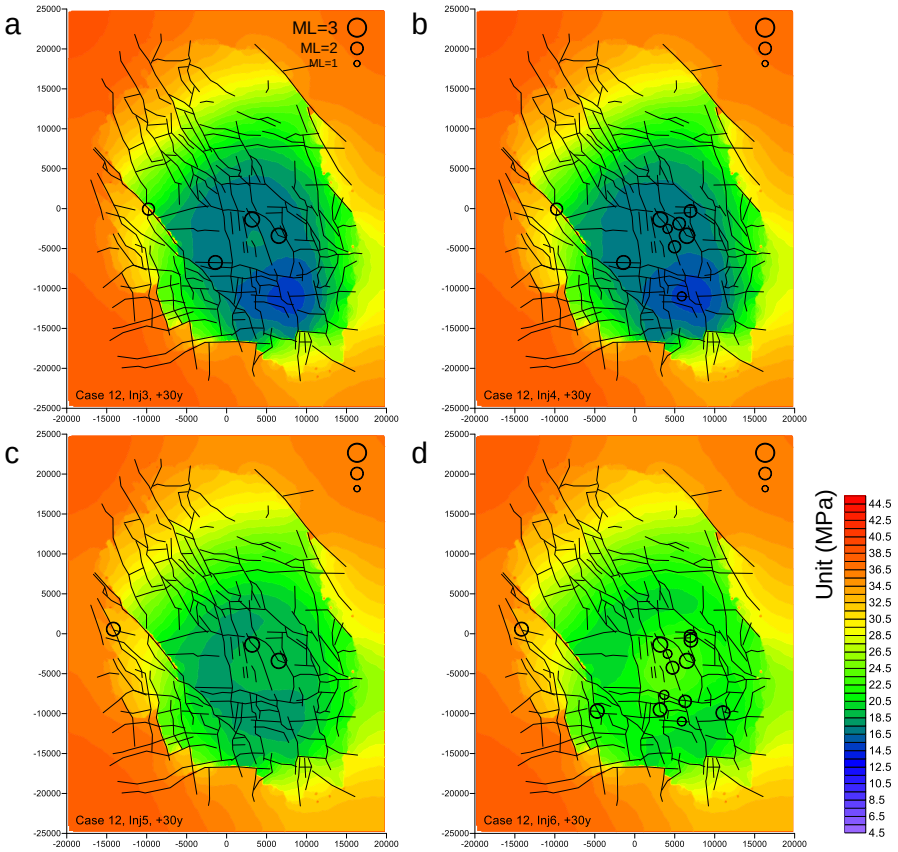

Figure A-4: Spatial distribution of the seismic events simulated in the four tested injection scenarios, 30 years after start of injection, a) injection scenario 3, b) injection scenario 4, c) injection scenario 5, d) injection scenario 6..

Appendix B – Model parameters for TOUGH3 modelling

Properties of the TOUGH3 model are reported in this Appendix, Table B-1. In **Table B-2** and **Table B-3** there are parameters relating to the definition of capillary pressures and of the relative permeabilities.

Table B-1: Hydraulic model parameters, modified van Genuchen as in Luckner et al. (1989) (OB: Overburden, RE: Reservoir, UB: Underburden, FT: Fault, BD: Boundary).

	OB	RE	UB	FT	BD
Porosity	0.2	0.2	0.2	0.05	0.3
Permeability	1e-21	1.5e-13	1e-21	1e-21	1e-21
Gas saturation	0.01	0.5	0.01	0.01	0.01
Capillary pressure model	Modified van Genuchten				No capillary pressure
Relative permeability model	Modified van Genuchten				Both phases perfectly mobile

The multiphase flow is considered in the framework of the Van Genuchten modified model (Luckner et al., 1989). The Van Genuchten modified model is described by the following set of equations (Jung et al., 2018) to define the relative permeabilities k_{rl} (liquid phase relative permeability) and k_{rg} (gas phase relative permeability) and the capillary pressure p_c, as functions of the degree of saturation:

$$S_{ec} = \frac{S_l - S_{lrc}}{1 - S_{lrc}}$$

$$S_{ekl} = \frac{S_l - S_{lrk}}{1 - S_{lrk}}$$

$$S_{ekg} = \frac{S_l}{1 - S_{gr}}$$

$$S_{ec*} = \frac{\varepsilon}{1 - S_{lrc}}$$

$$p_c = -\frac{1}{\alpha}\left[\left(S_{ec}\right)^{(\gamma-1)/m} - 1\right]^{1/n} \quad \text{for} \quad S_l \geq (S_{lrc} + \varepsilon)$$

$$p_c = -\frac{1}{\alpha}\left[S_{ec*}^{(\gamma-1)/m} - 1\right]^{1/n} - \beta \cdot \left(S_l - S_{lrc} - \varepsilon\right) \quad \text{for} \quad S_l < (S_{lrc} + \varepsilon)$$

$$k_{rl} = S_{ekl}^{\gamma} \cdot S_{ekl}^{(1-\gamma)\eta} \cdot \left[1 - \left(1 - S_{ekl}^{(1-\gamma)/m}\right)^m\right]^2$$

$$k_{rg} = \left(1 - S_{ekg}\right)^{\xi}\left[1 - S_{ekg}^{1/m}\right]^{2m}$$

The symbols are presented in Table B-2.

Table B-2: Parameters of the modified van Genuchten model.

Parameter	Description
Sl	Liquid saturation
Slrc	Residual liquid saturation
Sgr	Residual gas saturation
ε, εk, Slrk	Model parameters/threshold
α	Parameter related to gas entry pressure
γ	Fracture surface area reduction (here 0, no fractures)
n, m	Parameters related to pore size distribution
Pc,max	Maximum capillary pressure
β	Model parameter, curve definition

An example for the computed values of relative permeabilities and capillary pressure for different saturation degree is presented in Figure B-1.

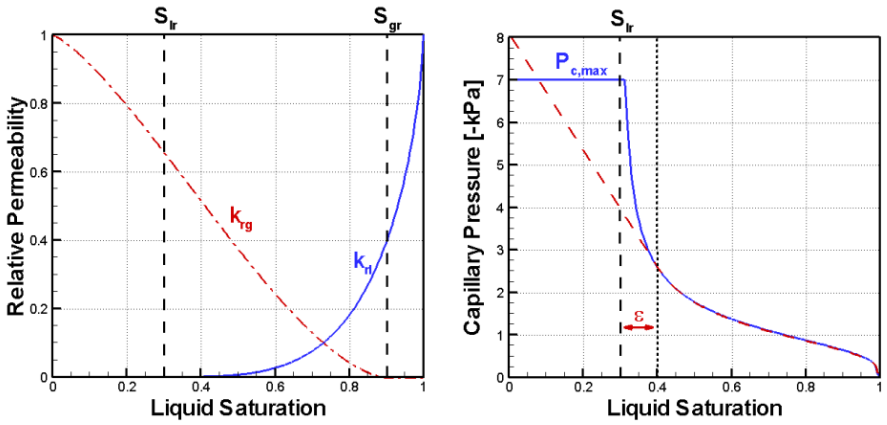

Figure B-1: Relative permeabilities and capillary pressure as functions of liquid saturation. Example figure, after (Jung et al., 2018).

In Table B-2 and Table B-4 there are parameters relating to the definition of capillary pressures and of the relative permeabilities.

Table B-3: Relative capillary pressure parameters.

	OB	RE	UB	FT	BD
N	2	2	2	2	
1/a (Pa)	1e8	1e6	1e8	1e8	
Pc,max (Pa)	1e10	1e10	1e10	1e10	
m	0.5	0.5	0.5	0.5	

Table B-4: Relative permeability parameters.

	OB	RE	UB	FT	BD
Slrk	0.25	0.25	0.25	0.25	0.25
Sgr	1e-3	1e-3	1e-3	1e-3	1e-3
η	0.01	0.5	0.01	0.01	
εk					

Water properties are computed internally by TOUGH3 according to the Industrial Formulation 1997 for the Thermodynamic Properties of Water and Steam (IAPWS-IF97), while real gas properties module are obtained via Peng-Robinson equations of state.

Appendix C – Review comments

In this Appendix, two review reports are provided. One review is done by Dr. [redacted] (an independent reservoir engineering consultant) who participated in the study during the early phase of the model development and calibration. The other review is done by Prof. [redacted] (Department of Energy Resources Engineering, Seoul National University, Korea) whom we invited to provide an external independent review.

Comments by Dr. [redacted] (dated 2021.11.17.)

1. Reservoir Engineering Observations

Fugro has conducted a seismic hazard and risk assessment of pressure maintenance by fluid injection for the Groningen gas field. For this purpose, they have made use of hydro-mechanical coupled modelling of the reservoir by Dynafrax UG. Internal Reservoir Engineering consultancy and reviews were provided in relation to the six work packages of the project.

In the area of fluid flow and reservoir dynamics the team required more time than foreseen to adapt the hydro-mechanical model to the very specific and detailed Groningen field conditions.

In the end the full benefit of integrating geomechanics and fluid flow modelling along the proposed lines came in sight, but has not been fully realized. Observations and conclusions from reservoir engineering reviews, based on results reported as of October 2021 are as follows:

1.1. Observations

1) The 2-D model does not seem to capture all relevant geomechanical processes. This seems in particular the case for vertical movements along the fracture planes. This may be the reason that it underestimates the frequency of seismic events.

2) Compaction of the reservoir is not modelled. Differential compaction may be a source of seismicity. This effect cannot be represented in the current 2D model.

3) A single layer model is used, consisting of a slice with a thickness of 1 m. This causes many scaling problems, including on volumes of gas in the reservoir, cumulative production and on production/injection volumes.

4) History matching is based on the pressure distribution delivered by NAM studies. Pressure depletion is not simulated but imposed on 123 well locations.

5) Description of injected fluids is schematic, e.g. gas expansion is not explicitly handled.

6) Flow modelling in the reservoir requires a work around to represent matrix porosity and permeability in the discrete element model. Overall reservoir permeability derived from the history match seems low.

7) Production and injection scenarios were defined without proper input to reflect current field development.

8) Study limitations

a. The project has a strong research character and estimates for manpower and computing resources proved to be optimistic.

b. The models had extremely long running times (days to weeks) on the available IT systems, which did not allow for quick scouting runs.

c. Communication across disciplines was hampered by the requirement to have virtual meetings only.

1.2. Conclusions and Recommendations

1) The current 2-D model does not capture major processes, in particular vertical movements along the fracture planes. Since it only represents a layer of 1 m uniform thickness. It does not represent realistic fluid volumes and distributions across the field.

2) The study concludes that fluid injection does not reduce seismic hazard. Although the model does not capture all geomechanical mechanisms, there is little reason to doubt this high level result, because inevitably injection will introduce further local pressure imbalances in the reservoir.

3) A 3-D model along the lines investigated in this study may merit serious investigation. It will certainly require more time and integration with other disciplines (reservoir engineering, well engineering, field development planning). For such a 3-D model one of the small gas (storage) fields in the Netherlands may be a good candidate. Size of these fields is two orders of magnitude smaller than the Groningen field.

Comments by Prof. [redacted] (dated 2022.7.6.)

Forecasting earthquake is a formidable task with a great deal of uncertainties in boundary stress (in situ stress), and physical parameters of faults. The current practice largely relies on earthquake statistics in the past with given fault information. Fuller understanding of earthquake mechanism is much needed in particular for manmade earthquakes, e.g., due to injection or production of fluid. The report is a unique study that investigated the impact of various scenarios of fluid production, shut-in and injection on induced seismicity.

The approach taken by the report is mostly particle based discrete element method modeling in which interactions of assemblies of circular (or spherical in 3D) particles mimics rock deformation, damage and resulting seismicity. The seismicity results when bonds break under high local stresses and stored strain energy is released as kinetic energy. The Particle Flow Code (PFC) used in this report has been successfully used for the induced seismicity in the past (Hazzard and Young, 2004) mostly in the lab and mine-by experiments due to mechanical loading or excavations. The PFC code was also used for fluid injection induced seismicity for various sensitivity studies as shown by highly cited, hence acknowledged, papers (Zao and Young, 2011; Yoon et al., 2014). The greatest merit of chosen approach by this report is the unique capability of modeling rupturing process and, therefore, the study can greatly enhance the understanding on the induced seismicity. On the other hand, no existing numerical tool has a ‘predictive’ capability of earthquake occurrence. In applying this and other tools, one need to be very clear on the limitations, and assumptions associated with the modeling approach. Application of numerical study has to be carried out in a progress and diagnostic manner with combinations of step-wise calibration with extensive past and future monitoring.

The work in the report is nearly the first study that aims to mimic production induced seismicity, and ‘predict’ the future earthquake occurrence in large reservoir scale (40 km x 50 km) by using Particle Flow Code (PFC). The following aspects has to be considered in evaluating this report.

The production induced seismicity mostly occur in normal faulting stress regime where vertical stress is the largest. With decreased reservoir pressure due to depletion, effective vertical stress increase by the amount of reservoir pressure drop while the amount of effective horizontal stress increase is smaller than reservoir pressure drop due to confined horizontal reservoir. This causes enlarged Mohr circle eventually satisfying Mohr Coulomb failure criterion of fault even with decreased reservoir pressure. It is very important to note that the two dimensional horizontal plane model used in this study is not capable of modeling production induced seismicity in normal faulting stress regime. The focal

mechanism at Groningen site does indicate the most common form was normal faulting as shown by Willacy et al. (2019). All the seismicity observed during modeling exercise in this report is strike slip faulting reflecting only some fraction at fault junctions observed at Groningen. This was duly acknowledged in the report but need to be clearly stated as a main limitation of the current study.

As production induced seismicity is closely related to the change of minimum and maximum horizontal stress, evolution of measured horizontal stresses - stress path - are often utilized to analyze the production induced seismicity (Zoback and Zinke, 2002). Measured horizontal stresses together with the reservoir pressure enables us to draw Mohr Circle (a graphical representation of stress state) relative to failure criterion of fault and useful characteristics often categorized as 'stress path parameters' are obtained that is a useful quantitative measure to evaluate the production induced seismicity. The current report only attempted to mimic the reservoir pressure evolution by inserting the monitored pressure into the numerical model, and it did not offer the comparison of modeled stress and monitored stress. This reviewer does not have knowledge whether and how much monitored data is available for horizontal stress evolution obtained from leak off test, borehole breakout or focal mechanisms. The reviewer would like to emphasize that utilizing the evolution of measured horizontal stresses are vital in preproducing and predicting production induced seismicity.

Associated with the above comment is the relative lack of key mechanism explicitly pursued in the current report. It appears that the differences in reservoir pressure is identified as one of the reasons for production induced seismicity. The reviewer would like to mention that the key mechanism should be more clarified as noted in the previous paragraph. Horizontal stress changes coupled with reservoir pressure decrease, and reservoir subsidence should be the key mechanisms and it would be very much worthwhile to reproduce these mechanisms through Particle Flow Code (PFC).

The report simulated the production and injection by passing on the measured reservoir pressure through interpolation, and simulated reservoir pressure by a separate numerical code, TOUGH3, respectively. This practical approach can help in dealing with large reservoir scale and less-efficient flow logic in Particle Flow Code(PFC). Nevertheless, the reviewer would like to note that the reservoir pressure modeled by TOUGH3 are based on 'vertical' two-dimensional section and there are uncertainties associated with two-dimensional approximation of reservoir model.

Extensive plan of further study was listed and the reviewer strongly supports the further extended study given the consequences of future actions. In this sense, numerical model is an intellectual tool, and the model is a simplification of reality rather than an imitation of

reality. In addition to the variation of parameters used in the current study, change of the scale needs to be seriously considered. What is lacking in the current stage is the lack of the most critical mechanism at Groningen, and further study might be executed in two lines of scales; smaller scale with only a few faults and larger scale with much simplified fault geometries focusing on overall reservoir pressure and horizontal stress variations.

One of the conclusions of the current study is that the depletion model did not adequately capture the observed earthquake clusters, e.g., in the northwestern region. In reviewers' opinion, reproducing overall earthquakes due to depletion was already a meaningful step and one should not worry about the precise location of the earthquake. Matching spatial location of earthquake may not be a tractable goal at this stage.

Another conclusion of the current study is the very little seismicity observed during the shut-in periods considered in this study. In fact, induced seismicity during shut-in is commonly observed after injection caused by stress transfer and delayed fluid migration. One mitigation measure suggested for the case of injection-induced seismicity is 'bleed off' of the injected fluid in order to accelerate the reservoir pressure reduction. For the production induced seismicity, comparable mitigation action would be 'injection' to compensate decreased reservoir pressure due to production. However, occurrence of production-induced seismicity implies that neighboring faults are critically stressed. Therefore, it would not be prudent to immediately consider injection as counter-measure. In the current study, shut-in was considered for up to 30 years, and obtained little seismicity during shut-in is reasonable given the long period considered and this is comparable to most of previous induced seismicity during shut-in which only occurred in a matter of days or months with very few exceptions of a few years after shut-in. Nevertheless, the effect of shut-in and injection would be best tackled in a few selected locations of Groningen with explicit modeling of the sequence of 'shut-in' or 'injection' preceded by fluid 'production (depletion)'.

References

Hazzard, J. F. and R. P. Young, 2004. Dynamic modelling of induced seismicity, International Journal of Rock Mechanics and Mining Sciences 41(8): 1365-1376.

Zhao, X. and R. P. Young, 2011. Numerical modeling of seismicity induced by fluid injection in naturally fractured reservoirs, Geophysics 76(6): WC167-WC180.

Yoon, J. S., et al., 2014. Numerical investigation on optimized stimulation of intact and naturally fractured deep geothermal

reservoirs using hydro-mechanical coupled discrete particles joints model, Geothermics 52: 165-184.

Zoback MD, Zinke JC, 2002. Production induced normal faulting in the Valhall and Ekofisk oil fields, Pure & Applied Geophysics, 159:403-420

Appendix D – KEM-24 WP0 Literature review and compilation of input data/parameters for Groningen gas field modelling, 30 September 2022